Title
Venom-derived toxins as biochemical and pharmacological probes of pain pathway

Author
Bohlen, Christopher

Publication Date
2012

Peer reviewed|Thesis/dissertation

Venom-derived toxins as biochemical and pharmacological probes of pain pathways

by

Christopher J Bohlen

DISSERTATION

Submitted in partial satisfaction of the requirements for the degree of

DOCTOR OF PHILOSOPHY

in

Neuroscience

in the

GRADUATE DIVISION

of the

UNIVERSITY OF CALIFORNIA, SAN FRANCISCO

ACKNOWLEDGEMENTS

Graduate education has been a time of great growth for me due, in large part, to the many people who have played a mentoring role. Foremost, I would like to thank my advisor, David Julius, who has constantly pushed me to transcend my comfort zone and strive to execute challenging but beautiful experiments. David has a penetrating analytical mind coupled to an unbridled creativity and is a continuing inspiration. Likewise, my committee members, Roger Nicoll, Dan Minor, Yuriy Kirichok, and Diana Bautista, all possess unique perspectives and strengths, and I thank them for giving me so many different intellectual and scientific models to attempt to emulate. All of the members of the Julius lab have been wonderful colleagues and teachers, but I would particularly like to thank Ben Myers, whose inexhaustible knowledge and aphoristic wisdom set me on the right track early on, Avi Priel, whose sense of the big picture opened my eyes to many aspects of life and science, and Erhu Cao, whose tenacity and independence have been a constant encouragement. I'll also be forever grateful to Mark Foster and Ross Wilson for introducing me to science in the laboratory despite my exceptional cluelessness as an undergraduate.

Thank you to my loving parents, brother, and sister, who have shaped and continue to shape who I am. And, of course, Robin; you're the best.

This work includes two published manuscripts. Their full citations are included here.

Bohlen, C.J., Chesler, A.T., Sharif-Naeini, R., Medzihradszky, K.F., Zhou, S., King, D., Sanchez, E.E., Burlingame, A.L., Basbaum, A.I., and Julius, D. (2011). A heteromeric Texas coral snake toxin targets acid-sensing ion channels to produce pain. Nature *479*, 410-414.

Bohlen, C.J., Priel, A., Zhou, S., King, D., Siemens, J., and Julius, D. (2010). A bivalent tarantula toxin activates the capsaicin receptor, TRPV1, by targeting the outer pore domain. Cell *141*, 834-845.

VENOM-DERIVED TOXINS AS BIOCHEMICAL AND PHYSIOLOGICAL PROBES OF PAIN PATHWAYS

by Christopher J. Bohlen

ABSTRACT

Venoms often target vital processes to cause paralysis or death, but many types of venom also elicit notoriously intense pain. While these pain-producing effects can result as a byproduct of generalized tissue trauma, some venom-derived toxins target somatosensory nerve terminals in order to activate nociceptive (pain-sensing) neural pathways. In my thesis work, I have discovered two novel toxins that contribute to the exceptionally painful bites of the Earth Tiger tarantula (*Ornithoctonus huwena*) and the Texas coral snake (*Micrurus tener tener*) respectively. The Earth Tiger tarantula produces a novel tandem-repeated toxin that activates the capsaicin receptor, TRPV1, through a long-lasting, bivalent binding event. I have further employed this toxin to explore the structure-function relationships of its target, TRPV1. The Texas coral snake produces an unusual heteromeric toxin that activates members of the acid sensing ion channel family, and we have utilized it to explore the physiological contribution of the ASIC1 member of this family to pain sensation.

TABLE OF CONTENTS

LIST OF FIGURES

Chapter 2

Chapter 3

CHAPTER 1

Introduction

Venom and pain sensation

Venoms represent pharmacopeias of evolutionarily-honed and sophisticated toxin proteins. Through duplication and rapid divergence of toxin-encoding genes, venomous organisms have come to produce toxins that adroitly manipulate the physiology of predator and prey organisms. By virtue of the fact that they target central receptors of critical physiological processes, toxins have been useful for identifying and manipulating important signaling molecules in synaptic transmission, action potential propagation, and haemostasis (Caleo and Schiavo, 2009; Chang, 1999; Dutton and Craik, 2001; French et al., 2010; Sajevic et al., 2011; Schmidtko et al., 2010). In addition, toxins highlight portions of these receptors that define their unique properties, including ion conduction pathway of ion channels, ligand binding sites for ligand-gated receptors, and voltage-sensing domains of voltage-gated channels (Alabi et al., 2007; MacKinnon et al., 1990; Swartz and MacKinnon, 1997; Tsetlin et al., 2009). Finally, toxins sometimes also display secondary characteristics that enhance their potency and efficacy through unexpected mechanisms, such as an affinity for lipids (localizing the toxin in close proximity to transmembrane receptors), a state-dependence of binding (favoring a particular conformation), or the ability to interact synergistically with other toxins (Cestele et al., 1998; Doley and Kini, 2009; Lee and MacKinnon, 2004; Milescu et al., 2007). Thus, toxins continue to reveal novel pharmacological strategies for manipulating specific receptors and controlling cellular function.

Somatosensory nerve endings express a battery of receptors and ion channels that serve to transduce physical and chemical stimuli from the environment into an electrical signal of the nervous system. Individual receptors are activated by changes in temperature, oxidation state, pH, or concentrations of inflammatory signaling molecules, and thereby alert the nervous system of environmental challenge by triggering a pain

response (Basbaum et al., 2009). It is not surprising, then, that these specialized receptors can become activated in the context of envenomation. Ubiquitous venom components such as phospholipases, proteases and porins (Fry et al., 2009) can damage sensory nerve endings directly, and they can also trigger the release of intracellular agents (e.g. ATP) from nearby cells undergoing lysis. Similarly, paralytic toxins and anticoagulant toxins can produce pain as a sequela of muscle rigidification or hemorrhagic shock, respectively. Kallikreins from cobra venom, proteases that disrupt blood pressure regulation, release the key inflammatory mediator, bradykinin, and in fact played a central role in its discovery (Hawgood, 1997).

Pain often results as a downstream consequence of more dire physiological disruptions, but some organisms produce toxins that elicit a profound pain response in the absence of other deleterious symptoms (Mebs, 2002; Schmidt, 1990). Presumably, these pain-producing toxins serve to discourage threatening predators by triggering a disorienting and memorable sensory experience. Ion channels and receptors that would normally become activated under conditions of injury or pathology become essentially hijacked by venom components, leading to a robust perception of injury despite relatively minor tissue damage. Aside from the adaptive advantage they provide in nature, such toxins represent invaluable tools for understanding the molecular underpinnings of pain sensation. This utility is well-documented with regard to plant-derived irritants, which have been used to help identify ion channels that normally detect changes in temperature and/or inflammatory cues (Bautista et al., 2005; Caterina et al., 1997; McKemy et al., 2002). My thesis work has focused, instead, on venom-derived proteinaceous toxins that produce pain by activating nociceptive pathways. I have identified two toxins that activate the capsaicin receptor, TRPV1, or the acid-sensing ion channels (ASICs) respectively. How these pain-producing toxins produce their effects

cannot be appreciated without considering their molecular compositions, which exemplify two distinct biochemical strategies that venom proteins employ to potently activate their targets.

TRPV1 toxins

TRPV1, a member of the transient receptor potential (TRP) superfamily of excitatory ion channels, was initially identified based on its sensitivity to capsaicin, the active ingredient of chili peppers (Caterina et al., 1997). TRPV1 has since been found to be expressed predominantly by nociceptors (peripheral sensory neurons that respond to painful stimuli) and to be activated by a variety of noxious signals including high temperature and acidic pH (Cavanaugh et al., 2011; Tominaga et al., 1998). Knockout mice lacking TRPV1 show dramatically reduced hypersensitivity to heat during inflammation (Caterina et al., 2000; Davis et al., 2000), and TRPV1 has become a major focus in pharmaceutical efforts to attenuate inflammatory pain.

TRPV1 is a key downstream effector of inflammatory second-messenger cascades, becoming activated or sensitized during injury. As such, TRPV1 can be sensitized by a variety of toxins that have no direct interaction with the receptor. Kallikreins, phospholipases, and proteases typically found in venoms can indirectly alter TRPV1's phosphorylation state or lipid surroundings (e.g. prostaglandin or PIP_2 concentration) and potentiate the receptor (Tominaga and Tominaga, 2005), but the multitudinous effects of these molecules need not be considered from a TRPV1-centric viewpoint. However, in some cases, TRPV1 is necessary for the pro-nociceptive effects despite being an indirect target. A protein toxin from frog (*Bombina variegata*) skin, Bv8, for example, produces hyperalgesia by activating PKCε-coupled prokineticin receptors, which leads to phosphorylation and sensitization of TRPV1 (Vellani et al., 2006); mice

lacking TRPV1 require 100-fold higher doses of toxin to achieve the hyperalgesia observed in wild-type animals (Negri et al., 2006). Homologues of Bv8 have been found in other frog, fish, and monitor lizard species, suggesting that many venoms may sensitize nociceptors through this mechanism (Fry et al., 2006; Negri et al., 2007; Schweitz et al., 1990).

TRPV1-inhibiting toxins have been identified in two venoms, although the physiological significance of these compounds in the context of envenomation remains enigmatic. APHC1, a peptide isolated from nematocyst extract of the sea anemone *Heteractis crispa*, partially inhibits capsaicin-evoked TRPV1 responses and reduces pain-related behaviors in mice challenged with heat or capsaicin (Andreev et al., 2008). Two small molecule compounds from *Agelenopsis aperta* venom were also found to inhibit TRPV1, but they had been previously identified as non-specific ion channel blockers, and their interaction with TRPV1 may represent an off-target effect (Kitaguchi and Swartz, 2005). Still, several venom toxins are known to produce analgesic effects, and these may play a non-intuitive adaptive role for the organisms in which they are found (Beeton et al., 2006).

In addition to members of the *capsicum* genus (i.e. chili peppers), a variety of species have evolved toxins that directly activate or potentiate TRPV1. The succulent *Euphorbia resinifera* and some other species of spurge produce the small molecule resiniferatoxin, which is a more potent and longer-lasting TRPV1 agonist than capsaicin itself (Appendino and Szallasi, 1997; Caterina et al., 1997). The tentacle extracts of several cnidarian species (the box jellyfish *Chironex fleckeri*, the lion’s mane jellyfish, *Cyanea capillata*, the anemone *Aiptasia pulchella*, and the Portuguese Man o' War, *Physalia physalis*) as well as the polyether toxins gambierol and brevetoxin (the central toxins of ciguatera poisoning) all potentiate activation of TRPV1 by capsaicin, perhaps

contributing the noxious consequences of cnidarians stings and ciguatera/shellfish poisoning respectively (Cuypers et al., 2006; Cuypers et al., 2007). Proteinaceous toxins that activate TRPV1 have arisen independently in two distantly-related tarantula species: the Trinidad chevron tarantula, *Psalmopoeus cambridgei*, and the Chinese bird spider, *Ornithoctonus huwena* (Bohlen et al., 2010; Siemens et al., 2006). These last tarantula toxins, in addition to their usefulness in studying TRPV1, present unique insights into venom evolution and diversification, which will be discussed in the following sections.

The two-faced vanillotoxins

A screen for venom-derived TRPV1 agonists revealed three homologous toxins from the venom of *Psalmopoeus cambridgei*, which were named 'vanillotoxins' (VaTx1-3) due to their ability to activate TRPV1 with similar efficacy as the vanilloid compounds capsaicin and resiniferatoxin (Siemens et al., 2006). The presence and spacing of six cysteine residues in each VaTx sequence characterizes them as members of the inhibitor cysteine knot (ICK) family of toxins. One of the most commonly found scaffolds in venom toxins, the disulfide-rich ICK motif allows relatively short toxin sequences (typically 25-45 amino acids) to adopt well-defined and stable tertiary structures (Daly and Craik, 2011). The vanillotoxins present an interesting case study into how such ICK toxins can attain novel pharmacologies.

ICK toxins fulfill a broad range of different functions, which have been acquired through a process of gene duplication and rapid diversification (Conticello et al., 2001; Kordis and Gubensek, 2000; Liang, 2004). VaTx1-3, although they are 53-82% identical to one another, embody distinct stages of functional specificity: VaTx1 activates TRPV1 and inhibits the voltage-gated potassium channel $K_v2.1$ within the same concentration range, whereas VaTx2 and VaTx3 exhibit progressively lower potency against $K_v2.1$ as well as

higher potency for activating TRPV1 (Siemens et al., 2006). This apparent progression of functionality is also reflected in toxin sequence alignments, which show that VaTx1 is most similar to K_v inhibitor toxins from related tarantulas(such as HmTx1), and that VaTx1 and 3 share less similarity with one another than either shares with VaTx2 (Escoubas et al., 2002; Siemens et al., 2006).

Interestingly, VaTx1 recognizes distinct regions of K_v and TRP channels, despite the fact that these two channel families share a similar overall architecture. Both K_v and TRP functional channels are likely tetrameric and contain six transmembrane helices per monomer, with the fifth and sixth transmembrane helices comprising the core pore-forming domain of the tetrameric complex (Hoenderop et al., 2003; Kedei et al., 2001; Long et al., 2005a; Voets et al., 2002). This pore-forming domain is the region that specifies TRPV1 sensitivity to vanillotoxins (Bohlen et al., 2010). In contrast, VaTx1 inhibits K_v2.1 through interactions with the voltage-sensing domain (the third and fourth transmembrane helices), much like the well-studied gating-modulator toxins of the voltage-gated channel family (Bohlen et al., 2010; Catterall et al., 2007; Swartz, 2007). Thus, VaTx1 must present two distinct (although perhaps overlapping) pharmacophores to manipulate its two target channels, while VaTx2 and VaTx3 demonstrate a waning functionality of the K_v2.1 pharmacophore in favor of refining the TRPV1-binding surface. Many toxins have acquired fundamentally different roles over evolutionary time, such as the Kunitz family of toxins, which were originally recruited to venoms as protease inhibitors, but have since acquired the capacity to block voltage-gated potassium channels (Fry et al., 2009). The transition between these functionalities can be appreciated in the bifunctional huwentoxin-XI, in which both a trypsin-inhibiting surface and a K_v channel-inhibiting surface are displayed on opposite faces of the toxin (Yuan et al., 2008). In line with this theme, the vanillotoxins present preserved transition state

intermediates of a progression between paralyzing and pain-inducing toxin functionalities, although the binding surfaces that dictate their graded specificity remain to be identified.

Multivalent toxins

While the vanillotoxins present an interesting case-study of a well-known phenomenon (the conversion of a toxin's activity profile from one function to another), the TRPV1-activating toxin that I identified from *Ornithoctonus huwena* venom (described in Chapter 2) exemplifies a perhaps less-appreciated venom strategy. While this toxin contains the ICK motif described for the vanillotoxins, the full-length toxin sequence actually consists of two ICK motifs in tandem. The two ICK 'domains' are highly homologous to one another, apparently the product of a gene duplication event that placed the copy in the same open reading frame as the original. The resulting toxin can be separated into two separately-folded ICK toxins, each of which activates TRPV1 when applied on its own, inspiring the name double-knot toxin (DkTx). However, the tandemly-conjoined full-length toxin has higher potency and a dramatically longer-lasting association with TRPV1 than either of the separated ICK domains has on its own, far beyond what would result from their additive contributions (Bohlen et al., 2010).

Combining multiple copies of a molecule into a single compound to heighten its effectiveness is a well-known strategy in pharmaceutical chemistry (Choi, 2004). Whether targeting many receptors across a viral or cellular surface (polyvalency), targeting multiple distinct binding sites on a receptor (hetero-multivalency), or targeting identical binding sites on multiple subunits of a multimeric complex (homo-multivalency), this approach relies on tethering multiple ligands together such that they bind to multiple receptor sites simultaneously. In theory, physically connecting monovalent ligands can

strengthen binding affinity enormously. A trivalent derivative of the antibiotic vancomycin approaches ideality in this regard; it binds to a trivalent ligand (a molecule displaying three D-Ala-D-Ala dipeptides) with over 10^{10} higher affinity than monovalent vancomycin (Rao et al., 1998). The enthalpic contribution to monomer binding is nearly tripled in the trivalent vancomycin, and this additive contribution to binding energy (ΔH^{mono} = -50.2 kJ mol^{-1}, ΔH^{tri} = -167 kJ mol^{-1}) results in a multiplicative improvement in binding affinity (K_d^{mono} = 1.6 × 10^{-6} M, K_d^{tri} = 4 × 10^{-17} M) (Rao et al., 1998). The measured dissociation constant for the trivalent vancomycin falls short of the theoretical prediction (the K_d of the monomer taken to the third power) due to an entropic penalty associated with conformational constraint. More generally, the energetic effects of multivalent molecule binding events are difficult to predict due to restricted access to binding sites and steric effects, but multivalent ligands commonly exhibit 10- to 1000-fold increases in binding affinity compared to their monovalent counterparts (Choi, 2004).

Multivalent ligands also typically out-perform their monovalent counterparts in persistence of action. The long-lasting nature of multivalent ligands is well-illustrated by a synthetic cGMP dimer (two cGMP molecules tethered by a PEG-spacer) that was designed as a bivalent agonist for the homotetrameric CNG channel (Kramer and Karpen, 1998). Once one cGMP moiety (one half of the bivalent ligand) has bound, the second is restricted to a very small volume prescribed by the linker length. Because the second cGMP moiety is restricted to so small of a volume (on the order of femtoliters), even a single molecule represents an extremely high effective concentration, driving its very rapid association to a second nearby subunit of the tetrameric channel. A quantitative model predicts that, since both cGMP moieties must dissociate for the full bivalent molecule to be liberated from its channel target, the dissociation rate of the bivalent ligand (k_{off}^{bi}) is proportional to the dissociation rate of the monomer (k_{off}^{mono})

multiplied by the probability that the second monomer is unbound, and a statistical factor of two: $k_{off}^{bi} = 2k_{off}^{mono} K_d^{mono}/(K_d^{mono} + C_{eff})$. The effective concentration of the tethered second cGMP molecule, C_{eff}, can be estimated by assuming it is restricted to an evenly-populated hemisphere with radius equal to the bivalent ligand's linker length: $C_{eff} = 1/(N_A) \times 1/(2/3\pi r^3)$ where r is the linker length in decimeters and N_A is Avogadro's number (Kramer and Karpen, 1998). More refined models have been developed to incorporate random walk statistics for specific polymer chains and non-hemispheric excluded volume effects (Gargano et al., 2001; Krishnamurthy et al., 2007). Although the extremely slow dissociation rate observed with multivalent ligands typically excludes meaningful measures of k_{off}^{bi}, the theory illustrates the extreme kinetic enhancements of multivalent ligands over their monovalent counterparts. Notably, multivalent interactions undergo accelerated dissociation in the presence of very high concentrations (approaching C_{eff}) of monovalent ligand, which competes for occupancy of the second (or third, or fourth, etc.) binding site (Kramer and Karpen, 1998; Smith et al., 2006).

Multivalent (non-toxin) ligand design has been explored for numerous receptors of pharmaceutical interest, including cholinergic receptors (Christopoulos et al., 2001; Rosini et al., 1999), adrenergic receptors (Kizuka and Hanson, 1987), opioid receptors (Portoghese et al., 1988), serotonin receptors (Leboulluec et al., 1995), voltage-gated calcium channels, voltage-gated sodium channels (Joslyn et al., 1988; Smith et al., 2006), and a diversity of surface receptors from infectious viruses and bacteria (Choi, 2004). Natural toxins target a broad spectrum of multimeric receptors and have been of great use in basic research as well as therapeutic endeavors, where their pharmacological profiles have occasionally made them useful pharmaceuticals (Lewis and Garcia, 2003; Terlau and Olivera, 2004). Although some toxins have been extensively modified to improve specificity, potency, and/or bioavailability (Craik and

Adams, 2007), multivalent strategies for improving toxin effectiveness remain almost entirely untapped. One exception is the utilization of a thrombopoieten receptor-binding peptide that has been incorporated into an ICK-toxin-like scaffold. When two of the 'miniproteins' are covalently crosslinked together, they produce a bivalent ligand that promotes dimerization and consequent activation of the thrombopoieten receptor (Krause et al., 2007). Considering the abundance multimeric receptors that are targeted by natural toxins, however, there is substantial potential for designing more potent and specific multivalent ligands for these receptors. Some targets (for example the voltage gated sodium channel family) contain several distinct toxin binding sites that alter channel gating, which could potentially be targeted simultaneously with hetero-multivalent ligands (Catterall et al., 2007; Smith et al., 2006). The advantage of subtype specificity found in other toxins, for example K_v channel inhibitor toxins (Mouhat et al., 2008), could in principle be exploited to generate novel hetero-multivalent ligands that are specific for hetero-multimeric receptor complexes.

Outside of pharmaceutical science, multivalency can be readily observed throughout biology, most familiarly in the form of immunoglobulins, surface-exposed lectins, and DNA-binding proteins (Choi, 2004). It is likely that venomous creatures also employ multivalency in the toxins they produce, as they stand to benefit from the high affinity and slow dissociation rates of multivalent toxins and contain gene-duplication machinery to promote construction of these molecules (Kordis and Gubensek, 2000). The extreme case of sarafotoxin highlights this potential for multivalent toxin production in venom glands: the burrowing asp *Atractaspis engaddensis* produces a sarafotoxin precursor peptide that contains twelve repeats of the toxin sequence in tandem (Ducancel et al., 1993).

While in the case of sarafotoxin (and several other tandemly-repeated toxin precursors) the active toxin is proteolytically liberated from its precursor post-translationally, other venoms contain intact, functional multi-domain toxins that may engage in multivalent interactions. DkTx presents a clear case where multiple TRPV1-binding toxins are tethered to produce a ligand that is more potent and longer-lasting than its monovalent peers (VaTx1-3 and the separated ICK domains of DkTx), presumably resulting in a heightened pain response in envenomated victims (Bohlen et al., 2010). Additionally, a toxin containing two tandem ICK motifs was recently discovered in venom from the yellow sac spider (*Cheiracanthium punctorium*) (Vassilevski et al., 2010). The cytolytic function of this *C. punctorium* toxin likely contributes to the local pain and erythema that results from envenomation, but whether this occurs by a bivalent mechanism is unknown. Transcriptomic analysis of the banded Gila monster (*Heloderma suspectum cinctum*) venom gland identified a toxin, helofensin, that contains four tandem β-defensin repeats with no apparent protease cleavage site in the short linkers connecting them and may function as a multivalent toxin (Fry et al., 2010). Finally, venomous secretions from ticks contain toxins that are comprised of multiple Kunitz-type domains (Mans et al., 2008; van de Locht et al., 1996), although these tandem domains likely serve to simultaneously inhibit multiple coagulatory proteases locally, as in the case of the mammalian multi-Kunitz domain tissue factor pathway inhibitor, TFPI (Lwaleed and Bass, 2006). Interestingly, the anticoagulant rhodnin from the kissing bug, *Rhodnius prolixus*, is also formed by two tandemly-repeated Kazal-type domains (Friedrich et al., 1993). While the toxins described above are examples of tandemly-repeated motifs on a single peptide chain, other noncovalently- or disulfide-linked toxin multimers have been identified with properties that point to a multivalent interaction with their receptors. Such multi-protein toxin complexes will be discussed below.

Toxins targeting acid-sensing ion channels

Members of the ASIC family of ion channels play a major role in the responsiveness of nociceptive nerve fibers to acidosis. Acidic pH activates subsets of neurons found in somatosensory ganglia (Krishtal and Pidoplichko, 1980), and the response profile depends on the severity of acidification. While TRPV1 is chiefly responsible for slowly-desensitizing currents elicited by extreme acidification (pH < 6) (Davis et al., 2000), ASIC channels produce relatively rapidly-desensitizing excitatory currents that result from milder acidic insults (Drew et al., 2004; Poirot et al., 2006), within a pH range that is typical of tissue acidosis during inflammation. The large extracellular domain of ASICs allow them to respond to extracellular protons with high sensitivity and cooperativity, presumably through multiple acidic amino acids whose pKa has been tuned by neighboring residues. Functional channels are made-up of homotrimer or heterotrimer assemblies of the ASIC family members (ASIC1-4), with distinct trimeric combinations being associated with different pH-sensitivities and desensitization rates (Hesselager et al., 2004; Jasti et al., 2007).

While ASICs may be activated briefly during envenomation due to the venom's acidic pH or as a consequence of tissue inflammation, three toxins have been identified that directly inhibit or activate members of the ASIC family. Two of the three act as potent and effective ASIC inhibitors. APETx2 from the sea anemone *Anthopleura elegantissim* inhibits ASIC3 homomeric channels as well as ASIC3-containing heteromers (Diochot et al., 2004). The same tarantula that produces the TRPV1-activating toxins VaTx1-3 (*P. cambridgei*), also expresses an ASIC inhibitor, PcTx1, which exhibits high specificity for homomeric channels formed by the ASIC1a splice variant (Escoubas et al., 2000). While ASIC transcripts have been detected in a range of tissues other than somatosensory ganglia, including brain, bone, bladder, retina, inner-ear, tongue, testis, and lung

(Lingueglia, 2007), it is not clear what selective advantage these inhibitory peptide toxins confer, which may reflect our limited understanding of the physiological impact of ASICs. Nevertheless, APETx2 and PcTx1 toxins have been useful in pharmacological isolation and characterization of ASIC3-containing channels at sensory nerve-endings, as well as the ASIC1a subtype in spinal cord and brain, supporting a role for these channels in pain sensation or fear and ischemia, respectively (Deval et al., 2010; Deval et al., 2011; Mazzuca et al., 2007; Pignataro et al., 2007; Ziemann et al., 2009).

I have found that the venom of the Texas coral snake (*Micrurus tener tener*) depolarizes nociceptors through activation of ASIC channels, as described in Chapter 3. The purified active component of the venom, MitTx, elicits robust nocifensive behaviors on its own when injected into the mouse hindpaw (Bohlen et al., 2011). While MitTx may have effects in other tissues as well, it is likely responsible for the dramatic and lasting pain experienced by victims of coral snake envenomation (Morgan et al., 2007; Nishioka et al., 1993). ASICs that are activated by acidic pH desensitize completely over the course of a few seconds, but in contrast, MitTx-evoked responses are largely non-desensitizing and therefore carry far more impact than even severe acidification. MitTx preferentially activates ASIC1-containing channels, although it has profound sensitizing effects on ASIC2a homomers and can activate ASIC3 at high concentrations as well. Interestingly, the behavioral response to MitTx injection is completely absent (at least at the doses tested) in ASIC1 knockout mice, highlighting that activation of the ASIC1 subtype is capable of driving pain-related behaviors (Bohlen et al., 2011). In this case, the pain-producing toxin illustrates a receptor-targeting mechanism by which snakes produce pain as well as a little-considered role for ASIC1 in pain sensation.

Unlike the other toxins so far described, MitTx is formed by two protein subunits, MitTx-α and MitTx-β. Each subunit contains a characteristic pattern of cysteines that categorizes

them into well-characterized toxin families; MitTx-α is a Kunitz-type toxin and MitTx-β is a phospholipase-A2-like toxin. However, the MitTx subunits clearly deviate from the canonical protease-inhibiting and phospholipase functionalities of these toxin families, again illustrating how venoms duplicate and dramatically alter a core set of structural motifs. The toxins form a high-affinity complex with one another, and neither subunit demonstrates functional effects in the absence of the other (Bohlen et al., 2011). Why both toxin subunits are required for activation of ASICs remains unknown, but several hypotheses can be generated by considering other known toxin complexes.

Multi-component toxins

Venoms typically contain dozens to hundreds of molecules with varying structures and diverse functional effects. The resident toxins do not all operate independently however, as multiple toxins within a particular venom often target different steps of the same physiological signaling pathway in concert. For example, fish-hunting cone snails produce a so-called “motor cabal” of toxins, which includes voltage-gated sodium channel inhibitors that disrupt action potential propagation on the motor neuron, voltage-gated calcium channel inhibitors that disrupt vesicular release from the motor neuron, and acetylcholine receptor inhibitors that disrupt synaptic transmission (Terlau and Olivera, 2004). In addition to complementing the functional effects of other venom components, toxins can form direct multimeric complexes that demonstrate emergent properties. While multimeric toxins have been studied chiefly in snake venom, they have been identified in a range of venomous species, including cone snails, scorpions, and ants (Doley and Kini, 2009; Loughnan et al., 2006; Pluzhinikov et al., 1994; Zamudio et al., 1997).

What advantages do multimeric toxins provide over their monomeric counterparts? While venom proteins typically conform to a relatively small number of stable structural motifs, multimerization combinatorially expands the number of scaffolds that can be employed for target recognition, allowing improved tissue localization and/or receptor recognition. Indeed, toxin complexes often demonstrate novel activities that are completely absent from the singular subunits. For example, an acetylcholine receptor inhibitor from cobra venom, α-cobratoxin, utilizes cysteine residues that are dispensable for folding to form various disulfide-linked dimers. The α-cobratoxin homodimer demonstrates new functionality, potently inhibiting α3β2 acetylcholine receptors, a receptor subtype that is insensitive to monomeric α-cobratoxin in the same concentration range (Osipov et al., 2008). Although the dimeric species of α-cobratoxin are low in abundance and the mechanism by which dimerization changes subtype specificity remains undefined, α-cobratoxin dimers illustrate how functional toxins can become incorporated into multimeric complexes to expand a venom's repertoire of effects.

The heterodimeric MitTx complex is able to activate ASICs while the individual subunits have no apparent functional effects on their own. MitTx has an unusual molecular makeup (one PLA2-like subunit non-covalently linked to one Kunitz-type subunit), but the well-studied heterodimeric toxin β-bungarotoxin and its isoforms have a very similar composition and may be informative in considering the contribution of MitTx subunits. Mature β-bungarotoxin is formed by two disulfide-linked protein chains, one active PLA2 (chain-A) and one Kunitz-type toxin (chain-B) (Kondo et al., 1978). Chain-B binds and inhibits voltage-gated potassium channels (Dreyer and Penner, 1987), and has been proposed to act as a chaperone to localize the phospholipase activity of chain-A to presynaptic terminals, focally compromising membrane integrity and facilitating synaptic release. Such a chaperoning mechanism has been demonstrated for crotoxin (the first

multimeric toxin to be identified in venoms), whose two subunits are approximately ten-times more lethal when applied together than alone, despite the fact that they undergo a necessary dissociation step upon binding to synaptic membranes (Bon et al., 1979; Hendon and Tu, 1979). In the case of β-bungarotoxin, the contribution of each chain has not been unambiguously defined, and its mechanism of action might be more complicated (see (Rowan, 2001)), but these toxins illustrate how a chaperone-like subunit could enhance the activity of a multimeric toxin.

Taicatoxin, an inhibitor of voltage-gated calcium and potassium channels from Australian taipan (*Oxyuranus scutellatus scutellatus*) venom, is also formed by a non-covalent complex including PLA2 and Kunitz type subunits (Brown et al., 1987; Possani et al., 1992). However, taicatoxin is a hexameric complex with one PLA2 subunit, four Kunitz protein subunits, and one subunit belonging to the three-finger toxin family (Doorty et al., 1997; Possani et al., 1992). A high-resolution structure of this large complex and the contributions of the individual subunits have yet to be fully determined, but this complex toxin highlights the diversity of structures and functions that can arise from multimerization using common toxin structural motifs. Thus, similarities in subunit composition need not imply similarities in function or mechanism of action of low-homology toxins.

Another functional enhancement that may drive formation of higher-order toxin complexes is multivalency. This can be appreciated in C-type lectin-like proteins (CLPs) from snake venom, which form dimeric subunits that further aggregate into higher-order assemblies (Doley and Kini, 2009). In the case of particularly large and well-characterized CLP, convulxin, two disulfide-linked octamers assemble back-to-back, allowing the toxin to bind to multiple receptor molecules on each of two adjacent platelets, thereby forming a high-avidity multivalent complex that promotes platelet

agglutination (Horii et al., 2009). Additionally, several other multimeric toxins are likely to take advantage of a multivalent strategy, although a multivalent mode of action has not been demonstrated for them directly. Con-ikot-ikot is a toxin from *Conus striatus* venom that prevents desensitization of AMPA receptors. The toxin was found to have a unique 'dimer of dimers' composition, where two disulfide-linked homodimers interact with each other non-covalently to form a tetrameric complex (Walker et al., 2009). Considering the tetrameric nature of the glutamate receptor target, the close apposition of the gating modules found on each of the channel's four subunits (Sobolevsky et al., 2009), and the slow washout of toxin-evoked effects (Walker et al., 2009), con-ikot-ikot may act as a bivalent or tetravalent glutamate receptor ligand. Along a similar line, two acetylcholine receptor inhibitors from snake venoms, haditoxin and irditoxin, exist as disulfide-linked dimers and exhibit near-irreversible inhibition of their pentameric target receptors (Pawlak et al., 2009; Roy et al., 2010).

Multimeric toxins may also have improved pharmacological properties simply because they present more potential contact sites to strengthen interactions with their target. Along a similar vein, binding of two toxin subunits may result in conformational changes of each subunit's target-recognition surface. The second scenario seems to be the case for the conantokin family of NMDA receptor antagonists from *Conus* venoms, which can form dimers in the presence of divalent cations (Dai et al., 2004). Structures have been solved of monomeric and dimeric forms, revealing side-chain rotations opposite to the dimerization surface (Cnudde et al., 2010; Cnudde et al., 2007); additionally, synthetic stabilized dimers demonstrate different NMDA receptor subtype specificity than the monomeric form, suggesting that the conformational changes induced by dimerization are functionally significant (Dai et al., 2007).

Multimeric toxin subunits can act as chaperones, contribute to multivalent binding events, and adjust or expand the target-recognition/active site of partner subunits. A wide variety of multimeric forms have been identified to date, and unique complexes with unprecedented functional roles likely remain to be discovered. Still, the properties of well-studied complexes can be used to generate testable hypotheses about the function of individual subunits in other multimeric toxins.

Conclusion

Envenomation can sometimes induce euphoric catalysis or a relatively aloof hemorrhagic state, but more typically, venoms produce pronounced pain and inflammation (Chahl and Kirk, 1975). While in some cases, pain certainly occurs as a side-effect, the existence of toxins that target TRPV1, a receptor found predominantly in nociceptors, suggests that noxiousness is an end in itself for a subset of venom proteins (Siemens et al., 2006). In addition to the cases described above, there are many venoms that cause intense or characteristic pain for which the responsible toxins have not been identified. The Schmidt pain index, a metric describing the intensity of suffering that results from bites and stings from various organisms, highlights several species (e.g. the tarantula hawk and the bullet ant), which can evoke intense pain, but which lack a molecular description of how these severe effects are achieved (Schmidt, 1990). Pain is the principle symptom of envenomation from a number of fishes (weeverfish, lionfish, scorpionfish, and stingray) and a significant effect of centipede and Gila monster venoms (Mebs, 2002; Strimple et al., 1997; Undheim and King, 2011). However, the toxins and targets responsible for the sensations caused by these understudied venoms are still unknown. The diversity of painful sensations that accompany different types of envenomation (e.g. burning pain versus electrical pain) suggests that a diversity of strategies have evolved for manipulating the somatosensory system.

Venoms stand to inform our understanding of normal and pathological pain sensation, and reciprocally, function-based screening serves as a complementary approach to proteomic and transcriptomic efforts for understanding toxin diversity. The unusual compositions of the multivalent DkTx and the multimeric MitTx stand as testament to this claim, representing novel toxins that would likely have been overlooked by conventional transcriptomic and proteomic efforts. Understanding the function and targets of these (and other) toxins provides a light by which their molecular intricacy can be appreciated.

References

Alabi, A.A., Bahamonde, M.I., Jung, H.J., Kim, J.I., and Swartz, K.J. (2007). Portability of paddle motif function and pharmacology in voltage sensors. Nature *450*, 370-375.

Andreev, Y.A., Kozlov, S.A., Koshelev, S.G., Ivanova, E.A., Monastyrnaya, M.M., Kozlovskaya, E.P., and Grishin, E.V. (2008). Analgesic compound from sea anemone Heteractis crispa is the first polypeptide inhibitor of vanilloid receptor 1 (TRPV1). J Biol Chem *283*, 23914-23921.

Appendino, G., and Szallasi, A. (1997). Euphorbium: modern research on its active principle, resiniferatoxin, revives an ancient medicine. Life Sci *60*, 681-696.

Basbaum, A.I., Bautista, D.M., Scherrer, G., and Julius, D. (2009). Cellular and molecular mechanisms of pain. Cell *139*, 267-284.

Bautista, D.M., Movahed, P., Hinman, A., Axelsson, H.E., Sterner, O., Hogestatt, E.D., Julius, D., Jordt, S.E., and Zygmunt, P.M. (2005). Pungent products from garlic activate the sensory ion channel TRPA1. Proceedings of the National Academy of Sciences of the United States of America *102*, 12248-12252.

Beeton, C., Gutman, G.A., and Chandy, K.G. (2006). Targets and Therapeutic Properties of Venom Peptides. In Handbook of biologically active peptides, A.J. Kastin, ed. (Amsterdam ; Boston, Academic Press), pp. 403-412.

Bohlen, C.J., Chesler, A.T., Sharif-Naeini, R., Medzihradszky, K.F., Zhou, S., King, D., Sanchez, E.E., Burlingame, A.L., Basbaum, A.I., and Julius, D. (2011). A heteromeric Texas coral snake toxin targets acid-sensing ion channels to produce pain. Nature *479*, 410-414.

Bohlen, C.J., Priel, A., Zhou, S., King, D., Siemens, J., and Julius, D. (2010). A bivalent tarantula toxin activates the capsaicin receptor, TRPV1, by targeting the outer pore domain. Cell *141*, 834-845.

Bon, C., Changeux, J.P., Jeng, T.W., and Fraenkel-Conrat, H. (1979). Postsynaptic effects of crotoxin and of its isolated subunits. Eur J Biochem *99*, 471-481.

Brown, A.M., Yatani, A., Lacerda, A.E., Gurrola, G.B., and Possani, L.D. (1987). Neurotoxins that act selectively on voltage-dependent cardiac calcium channels. Circ Res *61*, I6-9.

Caleo, M., and Schiavo, G. (2009). Central effects of tetanus and botulinum neurotoxins. Toxicon *54*, 593-599.

Caterina, M.J., Leffler, A., Malmberg, A.B., Martin, W.J., Trafton, J., Petersen-Zeitz, K.R., Koltzenburg, M., Basbaum, A.I., and Julius, D. (2000). Impaired nociception and pain sensation in mice lacking the capsaicin receptor. Science *288*, 306-313.

Caterina, M.J., Schumacher, M.A., Tominaga, M., Rosen, T.A., Levine, J.D., and Julius, D. (1997). The capsaicin receptor: a heat-activated ion channel in the pain pathway. Nature *389*, 816-824.

Catterall, W.A., Cestele, S., Yarov-Yarovoy, V., Yu, F.H., Konoki, K., and Scheuer, T. (2007). Voltage-gated ion channels and gating modifier toxins. Toxicon *49*, 124-141.

Cavanaugh, D.J., Chesler, A.T., Jackson, A.C., Sigal, Y.M., Yamanaka, H., Grant, R., O'Donnell, D., Nicoll, R.A., Shah, N.M., Julius, D.*, et al.* (2011). Trpv1 reporter mice reveal highly restricted brain distribution and functional expression in arteriolar smooth muscle cells. J Neurosci *31*, 5067-5077.

Cestele, S., Qu, Y., Rogers, J.C., Rochat, H., Scheuer, T., and Catterall, W.A. (1998). Voltage sensor-trapping: enhanced activation of sodium channels by beta-scorpion toxin bound to the S3-S4 loop in domain II. Neuron *21*, 919-931.

Chahl, L.A., and Kirk, E.J. (1975). Toxins which produce pain. Pain *1*, 3-49.

Chang, C.C. (1999). Looking back on the discovery of alpha-bungarotoxin. J Biomed Sci *6*, 368-375.

Choi, S.-k. (2004). Synthetic multivalent molecules : concepts and biomedical applications (Hoboken, N.J., Wiley).

Christopoulos, A., Grant, M.K., Ayoubzadeh, N., Kim, O.N., Sauerberg, P., Jeppesen, L., and El-Fakahany, E.E. (2001). Synthesis and pharmacological evaluation of dimeric muscarinic acetylcholine receptor agonists. J Pharmacol Exp Ther *298*, 1260-1268.

Cnudde, S.E., Prorok, M., Castellino, F.J., and Geiger, J.H. (2010). Metal ion determinants of conantokin dimerization as revealed in the X-ray crystallographic structure of the Cd(2+)/Mg (2+)-con-T[K7gamma] complex. J Biol Inorg Chem *15*, 667-675.

Cnudde, S.E., Prorok, M., Dai, Q., Castellino, F.J., and Geiger, J.H. (2007). The crystal structures of the calcium-bound con-G and con-T[K7gamma] dimeric peptides demonstrate a metal-dependent helix-forming motif. J Am Chem Soc *129*, 1586-1593.

Conticello, S.G., Gilad, Y., Avidan, N., Ben-Asher, E., Levy, Z., and Fainzilber, M. (2001). Mechanisms for evolving hypervariability: the case of conopeptides. Mol Biol Evol *18*, 120-131.

Craik, D.J., and Adams, D.J. (2007). Chemical modification of conotoxins to improve stability and activity. ACS Chem Biol *2*, 457-468.

Cuypers, E., Yanagihara, A., Karlsson, E., and Tytgat, J. (2006). Jellyfish and other cnidarian envenomations cause pain by affecting TRPV1 channels. FEBS Lett *580*, 5728-5732.

Cuypers, E., Yanagihara, A., Rainier, J.D., and Tytgat, J. (2007). TRPV1 as a key determinant in ciguatera and neurotoxic shellfish poisoning. Biochem Biophys Res Commun *361*, 214-217.

Dai, Q., Prorok, M., and Castellino, F.J. (2004). A new mechanism for metal ion-assisted interchain helix assembly in a naturally occurring peptide mediated by optimally spaced gamma-carboxyglutamic acid residues. J Mol Biol *336*, 731-744.

Dai, Q., Sheng, Z., Geiger, J.H., Castellino, F.J., and Prorok, M. (2007). Helix-helix interactions between homo- and heterodimeric gamma-carboxyglutamate-containing conantokin peptides and their derivatives. J Biol Chem *282*, 12641-12649.

Daly, N.L., and Craik, D.J. (2011). Bioactive cystine knot proteins. Curr Opin Chem Biol *15*, 362-368.

Davis, J.B., Gray, J., Gunthorpe, M.J., Hatcher, J.P., Davey, P.T., Overend, P., Harries, M.H., Latcham, J., Clapham, C., Atkinson, K.*, et al.* (2000). Vanilloid receptor-1 is essential for inflammatory thermal hyperalgesia. Nature *405*, 183-187.

Deval, E., Gasull, X., Noel, J., Salinas, M., Baron, A., Diochot, S., and Lingueglia, E. (2010). Acid-sensing ion channels (ASICs): pharmacology and implication in pain. Pharmacol Ther *128*, 549-558.

Deval, E., Noel, J., Gasull, X., Delaunay, A., Alloui, A., Friend, V., Eschalier, A., Lazdunski, M., and Lingueglia, E. (2011). Acid-sensing ion channels in postoperative pain. J Neurosci *31*, 6059-6066.

Diochot, S., Baron, A., Rash, L.D., Deval, E., Escoubas, P., Scarzello, S., Salinas, M., and Lazdunski, M. (2004). A new sea anemone peptide, APETx2, inhibits ASIC3, a major acid-sensitive channel in sensory neurons. The EMBO journal *23*, 1516-1525.

Doley, R., and Kini, R.M. (2009). Protein complexes in snake venom. Cell Mol Life Sci *66*, 2851-2871.

Doorty, K.B., Bevan, S., Wadsworth, J.D., and Strong, P.N. (1997). A novel small conductance Ca2+-activated K+ channel blocker from Oxyuranus scutellatus taipan venom. Re-evaluation of taicatoxin as a selective Ca2+ channel probe. J Biol Chem *272*, 19925-19930.

Drew, L.J., Rohrer, D.K., Price, M.P., Blaver, K.E., Cockayne, D.A., Cesare, P., and Wood, J.N. (2004). Acid-sensing ion channels ASIC2 and ASIC3 do not contribute to mechanically activated currents in mammalian sensory neurones. J Physiol *556*, 691-710.

Dreyer, F., and Penner, R. (1987). The actions of presynaptic snake toxins on membrane currents of mouse motor nerve terminals. J Physiol *386*, 455-463.

Ducancel, F., Matre, V., Dupont, C., Lajeunesse, E., Wollberg, Z., Bdolah, A., Kochva, E., Boulain, J.C., and Menez, A. (1993). Cloning and sequence analysis of cDNAs encoding precursors of sarafotoxins. Evidence for an unusual "rosary-type" organization. J Biol Chem *268*, 3052-3055.

Dutton, J.L., and Craik, D.J. (2001). alpha-Conotoxins: nicotinic acetylcholine receptor antagonists as pharmacological tools and potential drug leads. Curr Med Chem *8*, 327-344.

Escoubas, P., De Weille, J.R., Lecoq, A., Diochot, S., Waldmann, R., Champigny, G., Moinier, D., Menez, A., and Lazdunski, M. (2000). Isolation of a tarantula toxin specific for a class of proton-gated Na+ channels. J Biol Chem *275*, 25116-25121.

Escoubas, P., Diochot, S., Celerier, M.L., Nakajima, T., and Lazdunski, M. (2002). Novel tarantula toxins for subtypes of voltage-dependent potassium channels in the Kv2 and Kv4 subfamilies. Mol Pharmacol *62*, 48-57.

French, R.J., Yoshikami, D., Sheets, M.F., and Olivera, B.M. (2010). The tetrodotoxin receptor of voltage-gated sodium channels--perspectives from interactions with micro-conotoxins. Mar Drugs *8*, 2153-2161.

Friedrich, T., Kroger, B., Bialojan, S., Lemaire, H.G., Hoffken, H.W., Reuschenbach, P., Otte, M., and Dodt, J. (1993). A Kazal-type inhibitor with thrombin specificity from Rhodnius prolixus. J Biol Chem *268*, 16216-16222.

Fry, B.G., Roelants, K., Champagne, D.E., Scheib, H., Tyndall, J.D., King, G.F., Nevalainen, T.J., Norman, J.A., Lewis, R.J., Norton, R.S.*, et al.* (2009). The toxicogenomic multiverse: convergent recruitment of proteins into animal venoms. Annu Rev Genomics Hum Genet *10*, 483-511.

Fry, B.G., Roelants, K., Winter, K., Hodgson, W.C., Griesman, L., Kwok, H.F., Scanlon, D., Karas, J., Shaw, C., Wong, L.*, et al.* (2010). Novel venom proteins produced by differential domain-expression strategies in beaded lizards and gila monsters (genus Heloderma). Mol Biol Evol *27*, 395-407.

Fry, B.G., Vidal, N., Norman, J.A., Vonk, F.J., Scheib, H., Ramjan, S.F., Kuruppu, S., Fung, K., Hedges, S.B., Richardson, M.K.*, et al.* (2006). Early evolution of the venom system in lizards and snakes. Nature *439*, 584-588.

Gargano, J.M., Ngo, T., Kim, J.Y., Acheson, D.W., and Lees, W.J. (2001). Multivalent inhibition of AB(5) toxins. J Am Chem Soc *123*, 12909-12910.

Harvey, A.L., and Karlsson, E. (1980). Dendrotoxin from the venom of the green mamba, Dendroaspis angusticeps. A neurotoxin that enhances acetylcholine release at neuromuscular junction. Naunyn Schmiedebergs Arch Pharmacol *312*, 1-6.

Hawgood, B.J. (1997). Mauricio Rocha e Silva MD: snake venom, bradykinin and the rise of autopharmacology. Toxicon *35*, 1569-1580.

Hendon, R.A., and Tu, A.T. (1979). The role of crotoxin subunits in tropical rattlesnake neurotoxic action. Biochim Biophys Acta *578*, 243-252.

Hesselager, M., Timmermann, D.B., and Ahring, P.K. (2004). pH Dependency and desensitization kinetics of heterologously expressed combinations of acid-sensing ion channel subunits. J Biol Chem *279*, 11006-11015.

Hoenderop, J.G., Voets, T., Hoefs, S., Weidema, F., Prenen, J., Nilius, B., and Bindels, R.J. (2003). Homo- and heterotetrameric architecture of the epithelial Ca2+ channels TRPV5 and TRPV6. The EMBO journal *22*, 776-785.

Horii, K., Brooks, M.T., and Herr, A.B. (2009). Convulxin forms a dimer in solution and can bind eight copies of glycoprotein VI: implications for platelet activation. Biochemistry *48*, 2907-2914.

Jasti, J., Furukawa, H., Gonzales, E.B., and Gouaux, E. (2007). Structure of acid-sensing ion channel 1 at 1.9 A resolution and low pH. Nature *449*, 316-323.

Joslyn, A.F., Luchowski, E., and Triggle, D.J. (1988). Dimeric 1,4-dihydropyridines as calcium channel antagonists. J Med Chem *31*, 1489-1492.

Kedei, N., Szabo, T., Lile, J.D., Treanor, J.J., Olah, Z., Iadarola, M.J., and Blumberg, P.M. (2001). Analysis of the native quaternary structure of vanilloid receptor 1. J Biol Chem *276*, 28613-28619.

Kitaguchi, T., and Swartz, K.J. (2005). An inhibitor of TRPV1 channels isolated from funnel Web spider venom. Biochemistry *44*, 15544-15549.

Kizuka, H., and Hanson, R.N. (1987). Beta-adrenoceptor antagonist activity of bivalent ligands. 1. Diamide analogues of practolol. J Med Chem *30*, 722-726.

Kondo, K., Narita, K., and Lee, C.Y. (1978). Amino acid sequences of the two polypeptide chains in beta1-bungarotoxin from the venom of Bungarus multicinctus. J Biochem *83*, 101-115.

Kordis, D., and Gubensek, F. (2000). Adaptive evolution of animal toxin multigene families. Gene *261*, 43-52.

Kramer, R.H., and Karpen, J.W. (1998). Spanning binding sites on allosteric proteins with polymer-linked ligand dimers. Nature *395*, 710-713.

Krause, S., Schmoldt, H.U., Wentzel, A., Ballmaier, M., Friedrich, K., and Kolmar, H. (2007). Grafting of thrombopoietin-mimetic peptides into cystine knot miniproteins yields high-affinity thrombopoietin antagonists and agonists. FEBS J *274*, 86-95.

Krishnamurthy, V.M., Semetey, V., Bracher, P.J., Shen, N., and Whitesides, G.M. (2007). Dependence of effective molarity on linker length for an intramolecular protein-ligand system. J Am Chem Soc *129*, 1312-1320.

Krishtal, O.A., and Pidoplichko, V.I. (1980). A receptor for protons in the nerve cell membrane. Neuroscience *5*, 2325-2327.

Leboulluec, K.L., Mattson, R.J., Mahle, C.D., Mcgovern, R.T., Nowak, H.P., and Gentile, A.J. (1995). Bivalent Indoles Exhibiting Serotonergic Binding-Affinity. Bioorganic & Medicinal Chemistry Letters *5*, 123-126.

Lee, S.Y., and MacKinnon, R. (2004). A membrane-access mechanism of ion channel inhibition by voltage sensor toxins from spider venom. Nature *430*, 232-235.

Lewis, R.J., and Garcia, M.L. (2003). Therapeutic potential of venom peptides. Nat Rev Drug Discov *2*, 790-802.

Liang, S. (2004). An overview of peptide toxins from the venom of the Chinese bird spider Selenocosmia huwena Wang [=Ornithoctonus huwena (Wang)]. Toxicon *43*, 575-585.

Lingueglia, E. (2007). Acid-sensing ion channels in sensory perception. J Biol Chem *282*, 17325-17329.

Long, S.B., Campbell, E.B., and Mackinnon, R. (2005). Crystal structure of a mammalian voltage-dependent Shaker family K+ channel. Science *309*, 897-903.

Loughnan, M., Nicke, A., Jones, A., Schroeder, C.I., Nevin, S.T., Adams, D.J., Alewood, P.F., and Lewis, R.J. (2006). Identification of a novel class of nicotinic receptor antagonists: dimeric conotoxins VxXIIA, VxXIIB, and VxXIIC from Conus vexillum. J Biol Chem *281*, 24745-24755.

Lwaleed, B.A., and Bass, P.S. (2006). Tissue factor pathway inhibitor: structure, biology and involvement in disease. J Pathol *208*, 327-339.

MacKinnon, R., Heginbotham, L., and Abramson, T. (1990). Mapping the receptor site for charybdotoxin, a pore-blocking potassium channel inhibitor. Neuron *5*, 767-771.

Mans, B.J., Andersen, J.F., Schwan, T.G., and Ribeiro, J.M. (2008). Characterization of anti-hemostatic factors in the argasid, Argas monolakensis: implications for the evolution of blood-feeding in the soft tick family. Insect Biochem Mol Biol *38*, 22-41.

Mazzuca, M., Heurteaux, C., Alloui, A., Diochot, S., Baron, A., Voilley, N., Blondeau, N., Escoubas, P., Gelot, A., Cupo, A*., et al.* (2007). A tarantula peptide against pain via ASIC1a channels and opioid mechanisms. Nature neuroscience *10*, 943-945.

McKemy, D.D., Neuhausser, W.M., and Julius, D. (2002). Identification of a cold receptor reveals a general role for TRP channels in thermosensation. Nature *416*, 52-58.

Mebs, D. (2002). Venomous and poisonous animals : a handbook for biologists, and toxicologists and toxinologists, Physicians and pharmacists (Boca Raton, Fla., CRC Press).

Milescu, M., Vobecky, J., Roh, S.H., Kim, S.H., Jung, H.J., Kim, J.I., and Swartz, K.J. (2007). Tarantula toxins interact with voltage sensors within lipid membranes. J Gen Physiol *130*, 497-511.

Morgan, D.L., Borys, D.J., Stanford, R., Kjar, D., and Tobleman, W. (2007). Texas coral snake (Micrurus tener) bites. South Med J *100*, 152-156.

Mouhat, S., Andreotti, N., Jouirou, B., and Sabatier, J.M. (2008). Animal toxins acting on voltage-gated potassium channels. Curr Pharm Des *14*, 2503-2518.

Negri, L., Lattanzi, R., Giannini, E., Colucci, M., Margheriti, F., Melchiorri, P., Vellani, V., Tian, H., De Felice, M., and Porreca, F. (2006). Impaired nociception and inflammatory pain sensation in mice lacking the prokineticin receptor PKR1: focus on interaction

between PKR1 and the capsaicin receptor TRPV1 in pain behavior. J Neurosci *26*, 6716-6727.

Negri, L., Lattanzi, R., Giannini, E., and Melchiorri, P. (2007). Bv8/Prokineticin proteins and their receptors. Life Sci *81*, 1103-1116.

Nishioka, S.A., Silveira, P.V., and Menzes, L.B. (1993). Coral snake bite and severe local pain. Ann Trop Med Parasitol *87*, 429-431.

Osipov, A.V., Kasheverov, I.E., Makarova, Y.V., Starkov, V.G., Vorontsova, O.V., Ziganshin, R., Andreeva, T.V., Serebryakova, M.V., Benoit, A., Hogg, R.C*., et al.* (2008). Naturally occurring disulfide-bound dimers of three-fingered toxins: a paradigm for biological activity diversification. J Biol Chem *283*, 14571-14580.

Pawlak, J., Mackessy, S.P., Sixberry, N.M., Stura, E.A., Le Du, M.H., Menez, R., Foo, C.S., Menez, A., Nirthanan, S., and Kini, R.M. (2009). Irditoxin, a novel covalently linked heterodimeric three-finger toxin with high taxon-specific neurotoxicity. FASEB J *23*, 534-545.

Pignataro, G., Simon, R.P., and Xiong, Z.G. (2007). Prolonged activation of ASIC1a and the time window for neuroprotection in cerebral ischaemia. Brain *130*, 151-158.

Pluzhinikov, K.A., Nol'de, D.E., Tertyshnikova, S.M., Sukhanov, S.V., Sobol, A.G., Torgov, M., Filippov, A.K., Arsen'ev, A.S., and Grishin, E.V. (1994). [Structure-activity study of the basic toxic component of venom from the ant Ectatomma tuberculatum]. Bioorg Khim *20*, 857-871.

Poirot, O., Berta, T., Decosterd, I., and Kellenberger, S. (2006). Distinct ASIC currents are expressed in rat putative nociceptors and are modulated by nerve injury. J Physiol *576*, 215-234.

Portoghese, P.S., Nagase, H., Lipkowski, A.W., Larson, D.L., and Takemori, A.E. (1988). Binaltorphimine-related bivalent ligands and their kappa opioid receptor antagonist selectivity. J Med Chem *31*, 836-841.

Possani, L.D., Martin, B.M., Yatani, A., Mochca-Morales, J., Zamudio, F.Z., Gurrola, G.B., and Brown, A.M. (1992). Isolation and physiological characterization of taicatoxin, a complex toxin with specific effects on calcium channels. Toxicon *30*, 1343-1364.

Rao, J., Lahiri, J., Isaacs, L., Weis, R.M., and Whitesides, G.M. (1998). A trivalent system from vancomycin.D-ala-D-Ala with higher affinity than avidin.biotin. Science *280*, 708-711.

Rodriguez-Ithurralde, D., Silveira, R., Barbeito, L., and Dajas, F. (1983). Fasciculin, a powerful anticholinesterase polypeptide from Dendroaspis angusticeps venom. Neurochem Int *5*, 267-274.

Rosini, M., Budriesi, R., Bixel, M.G., Bolognesi, M.L., Chiarini, A., Hucho, F., Krogsgaard-Larsen, P., Mellor, I.R., Minarini, A., Tumiatti, V*., et al.* (1999). Design, synthesis, and biological evaluation of symmetrically and unsymmetrically substituted methoctramine-related polyamines as muscular nicotinic receptor noncompetitive antagonists. J Med Chem *42*, 5212-5223.

Rowan, E.G. (2001). What does beta-bungarotoxin do at the neuromuscular junction? Toxicon *39*, 107-118.

Roy, A., Zhou, X., Chong, M.Z., D'Hoedt, D., Foo, C.S., Rajagopalan, N., Nirthanan, S., Bertrand, D., Sivaraman, J., and Kini, R.M. (2010). Structural and functional characterization of a novel homodimeric three-finger neurotoxin from the venom of Ophiophagus hannah (king cobra). J Biol Chem *285*, 8302-8315.

Sajevic, T., Leonardi, A., and Krizaj, I. (2011). Haemostatically active proteins in snake venoms. Toxicon *57*, 627-645.

Schmidt, J.O. (1990). Hymenoptera venoms: striving toward the ultimate defense against vertebrates. In Insect defenses: adaptive mechanisms and strategies of prey and predators, D.L. Evans, and J.O. Schmidt, eds. (Albany, State University of New York Press), pp. 387-419.

Schmidtko, A., Lotsch, J., Freynhagen, R., and Geisslinger, G. (2010). Ziconotide for treatment of severe chronic pain. Lancet *375*, 1569-1577.

Schweitz, H., Bidard, J.N., and Lazdunski, M. (1990). Purification and pharmacological characterization of peptide toxins from the black mamba (Dendroaspis polylepis) venom. Toxicon *28*, 847-856.

Siemens, J., Zhou, S., Piskorowski, R., Nikai, T., Lumpkin, E.A., Basbaum, A.I., King, D., and Julius, D. (2006). Spider toxins activate the capsaicin receptor to produce inflammatory pain. Nature *444*, 208-212.

Smith, J.A., Amagasu, S.M., Hembrador, J., Axt, S., Chang, R., Church, T., Gee, C., Jacobsen, J.R., Jenkins, T., Kaufman, E*., et al.* (2006). Evidence for a multivalent interaction of symmetrical, N-linked, lidocaine dimers with voltage-gated Na+ channels. Mol Pharmacol *69*, 921-931.

Sobolevsky, A.I., Rosconi, M.P., and Gouaux, E. (2009). X-ray structure, symmetry and mechanism of an AMPA-subtype glutamate receptor. Nature *462*, 745-756.

Strimple, P.D., Tomassoni, A.J., Otten, E.J., and Bahner, D. (1997). Report on envenomation by a Gila monster (Heloderma suspectum) with a discussion of venom apparatus, clinical findings, and treatment. Wilderness Environ Med *8*, 111-116.

Swartz, K.J. (2007). Tarantula toxins interacting with voltage sensors in potassium channels. Toxicon *49*, 213-230.

Swartz, K.J., and MacKinnon, R. (1997). Mapping the receptor site for hanatoxin, a gating modifier of voltage-dependent K+ channels. Neuron *18*, 675-682.

Terlau, H., and Olivera, B.M. (2004). Conus venoms: a rich source of novel ion channel-targeted peptides. Physiol Rev *84*, 41-68.

Tominaga, M., Caterina, M.J., Malmberg, A.B., Rosen, T.A., Gilbert, H., Skinner, K., Raumann, B.E., Basbaum, A.I., and Julius, D. (1998). The cloned capsaicin receptor integrates multiple pain-producing stimuli. Neuron *21*, 531-543.

Tominaga, M., and Tominaga, T. (2005). Structure and function of TRPV1. Pflugers Arch *451*, 143-150.

Tsetlin, V., Utkin, Y., and Kasheverov, I. (2009). Polypeptide and peptide toxins, magnifying lenses for binding sites in nicotinic acetylcholine receptors. Biochem Pharmacol *78*, 720-731.

Undheim, E.A., and King, G.F. (2011). On the venom system of centipedes (Chilopoda), a neglected group of venomous animals. Toxicon *57*, 512-524.

van de Locht, A., Stubbs, M.T., Bode, W., Friedrich, T., Bollschweiler, C., Hoffken, W., and Huber, R. (1996). The ornithodorin-thrombin crystal structure, a key to the TAP enigma? The EMBO journal *15*, 6011-6017.

Vassilevski, A.A., Fedorova, I.M., Maleeva, E.E., Korolkova, Y.V., Efimova, S.S., Samsonova, O.V., Schagina, L.V., Feofanov, A.V., Magazanik, L.G., and Grishin, E.V. (2010). Novel class of spider toxin: active principle from the yellow sac spider Cheiracanthium punctorium venom is a unique two-domain polypeptide. J Biol Chem *285*, 32293-32302.

Vellani, V., Colucci, M., Lattanzi, R., Giannini, E., Negri, L., Melchiorri, P., and McNaughton, P.A. (2006). Sensitization of transient receptor potential vanilloid 1 by the prokineticin receptor agonist Bv8. J Neurosci *26*, 5109-5116.

Voets, T., Prenen, J., Vriens, J., Watanabe, H., Janssens, A., Wissenbach, U., Bodding, M., Droogmans, G., and Nilius, B. (2002). Molecular determinants of permeation through the cation channel TRPV4. J Biol Chem *277*, 33704-33710.

Walker, C.S., Jensen, S., Ellison, M., Matta, J.A., Lee, W.Y., Imperial, J.S., Duclos, N., Brockie, P.J., Madsen, D.M., Isaac, J.T.*, et al.* (2009). A novel Conus snail polypeptide causes excitotoxicity by blocking desensitization of AMPA receptors. Curr Biol *19*, 900-908.

Welsh, J.H. (1967). Acetylcholine in snake venoms. In Animal toxins, F.E. Russell, and P.R. Saunders, eds. (New York, Pergamon Press), p. 263.

Yuan, C.H., He, Q.Y., Peng, K., Diao, J.B., Jiang, L.P., Tang, X., and Liang, S.P. (2008). Discovery of a distinct superfamily of Kunitz-type toxin (KTT) from tarantulas. PLoS One *3*, e3414.

Zamudio, F.Z., Conde, R., Arevalo, C., Becerril, B., Martin, B.M., Valdivia, H.H., and Possani, L.D. (1997). The mechanism of inhibition of ryanodine receptor channels by imperatoxin I, a heterodimeric protein from the scorpion Pandinus imperator. J Biol Chem *272*, 11886-11894.

Ziemann, A.E., Allen, J.E., Dahdaleh, N.S., Drebot, II, Coryell, M.W., Wunsch, A.M., Lynch, C.M., Faraci, F.M., Howard, M.A., 3rd, Welsh, M.J.*, et al.* (2009). The amygdala is a chemosensor that detects carbon dioxide and acidosis to elicit fear behavior. Cell *139*, 1012-1021.

CHAPTER 2

A Bivalent Tarantula Toxin Activates the Capsaicin Receptor, TRPV1, by Targeting the Outer Pore Domain

ABSTRACT

Toxins have evolved to target regions of membrane ion channels that underlie ligand binding, gating, or ion permeation, and have thus served as invaluable tools for probing channel structure and function. Here we describe a peptide toxin from the Earth Tiger tarantula that selectively and irreversibly activates the capsaicin- and heat-sensitive channel, TRPV1. This high avidity interaction derives from a unique tandem repeat structure of the toxin that endows it with an antibody-like bivalency, illustrating a new paradigm in toxin structure and evolution. The novel 'double-knot' toxin traps TRPV1 in the open state by interacting with residues in the presumptive pore-forming region of the channel, highlighting the importance of conformational changes in the outer pore region of TRP channels during activation.

INTRODUCTION

Venoms from spiders, snakes, fish, cone snails, and scorpions contain an evolutionarily honed pharmacopeia of natural toxins that target membrane receptors and ion channels to produce shock, paralysis, pain, or death. Toxins evolve to interact with functionally important protein domains, including agonist binding sites, ion permeation pores, and voltage-sensing domains, making them invaluable reagents with which to probe mechanisms underlying receptor and channel activation or modulation (Hille, 2001). In addition to well-known and deadly small molecule toxins, such as tetrodotoxin from puffer fish or saxitoxin from dinoflagellates, there exists a tremendous diversity of genetically encoded peptide toxins that have likewise proven invaluable for elucidating the structure, function, and physiological properties of membrane ion channels (Catterall et al., 2007; Escoubas and Rash, 2004; Miller, 1995; Swartz, 2007; Terlau and Olivera, 2004). Prototypical of this class is α-bungarotoxin, a 74 amino acid-long peptide from

elapid snakes that binds to the agonist pocket of nicotinic acetylcholine receptors with picomolar potency and an essentially irreversible rate of dissociation. As such, α-bungarotoxin has been an essential tool in the purification, localization, and functional analysis of both native and recombinant acetylcholine-gated channels (Tsetlin et al., 2009).

While genetically encoded peptide toxins exhibit substantial sequence and functional diversity, many share common structural elements - most notably the presence of several intramolecular disulfide bonds that limit conformational flexibility to enhance both specificity and avidity of toxin-target interactions. Included among such peptides are a large group of so-called inhibitor cysteine knot (ICK) toxins that are typically 25-50 residues in length and share a conserved gene structure, precursor organization, and three-dimensional fold. ICK peptides are commonly found in venoms from cone snails, spiders, and scorpions, where they are estimated to account for 10^5 - 10^6 unique toxin sequences (Craik et al., 2001; Zhu et al., 2003). Repeated use of the ICK motif through evolution presumably reflects the 'fitness' of this structural motif for generating large collections of stable and functionally diverse molecules that have the capacity to interact with a wide array of membrane protein partners. In essence, the venom sacs of these organisms can be viewed as functionally focused combinatorial peptide libraries. Not surprisingly, the vast majority of peptide toxins remain uncharacterized insofar as structure, physiologic effects, or molecular sites of action (Escoubas and Rash, 2004; Terlau and Olivera, 2004).

Among ICK toxins, charybdotoxin and hanatoxin (from scorpion and tarantula venom, respectively) are the best characterized. Both inhibit voltage-gated (K_v) potassium channels, but elegant mutagenesis and biophysical studies have shown that they do so in mechanistically distinct ways (Miller, 1995; Swartz, 2007). Charybdotoxin binds to the

so-called pore-loop domain of the channel located between the fifth and sixth transmembrane domains (S5 and S6), thereby blocking ion permeation directly (Goldstein et al., 1994; Gross et al., 1994; MacKinnon et al., 1990; Yu et al., 2005). In contrast, hanatoxin interacts primarily with residues in the C-terminal half of the third transmembrane region (S3b), which together with S4 and the intervening extracellular loop forms a flexible helix-turn-helix domain whose movements contribute to voltage-dependent gating (Alabi et al., 2007; Swartz and MacKinnon, 1997). Upon binding, hanatoxin inhibits movement of this voltage sensor region during membrane depolarization, thereby favoring the closed state (Lee et al., 2003; Phillips et al., 2005). The analysis of charybdotoxin- and hanatoxin-K_v channel interactions has been key to formulating and testing models of ion permeation and voltage sensor movement, respectively, as well as in delineating interactions of these functionally important protein domains with drugs and membrane lipids (Milescu et al., 2009; Schmidt and MacKinnon, 2008; Swartz, 2008).

The mammalian TRP channel family consists of >30 members, many of which are known to form tetrameric cation channels in vivo, or when heterologously expressed (Ramsey et al., 2006; Venkatachalam and Montell, 2007). Physiological roles for many TRP channels remain enigmatic, however several are known to contribute to sensory signaling, including thermosensation, nociception, and pain. Chief among these is TRPV1, which is activated by capsaicin (the main pungent ingredient in 'hot' chili peppers), extracellular protons and other inflammation agents, as well as noxious heat (>43ºC) (Julius and Basbaum, 2001). Despite their rather distinct physiological roles, TRP and voltage-gated ion channels likely resemble one another in so far as overall transmembrane topology and tetrameric subunit organization, consistent with the fact that TRP channels exhibit some (albeit modest) degree of voltage sensitivity (Brauchi et

al., 2004; Matta and Ahern, 2007; Voets et al., 2004). With this in mind, we recently asked whether spider or scorpion venoms also contain toxins that target TRP channels, particularly those expressed on primary afferent sensory nerve fibers of the pain pathway. As a result, we discovered a group of three novel ICK peptides (dubbed vanillotoxins, VaTx1, 2 and 3) from the 'Trinidad Chevron' tarantula (*Psalmopoeus cambridgei*) that activate TRPV1 to produce robust inflammatory pain (Siemens et al., 2006). Interestingly, vanillotoxins exhibit appreciable sequence similarity to hanatoxin, and some vanillotoxins (VaTx1 and VaTx2) also inhibit $K_v2.1$, furthering speculation that TRP and voltage-gated channels resemble one another in regard to structure and gating mechanisms.

Vanillotoxins are excellent pharmacological probes, but their relatively fast dissociation rates limits their usefulness as biochemical tools for studying TRP channel structure. Here we describe a novel toxin from the Earth Tiger tarantula that serves as a specific and irreversible TRPV1 agonist. The toxin contains two independently folded ICK domains, endowing it with an antibody-like bivalency that results in extremely high avidity for its multimeric channel target, making it a powerful new biochemical tool for probing TRP channel function. We found that this new toxin binds to and traps TRPV1 in the open state via association with the pore-forming region of the channel, rather than the voltage sensor equivalent region near the S3 and S4 helices. These and other observations support a critical role for the pore-forming domain in TRP channel gating and suggest that conformational changes in the outer pore may be more important than previously appreciated.

RESULTS

Multiple spider species target TRPV1 channels

The Chinese bird spider, *Ornithoctonus huwena* (a.k.a. Earth Tiger), is a large and aggressive Old World tarantula that inhabits deep underground burrows within tropical regions of Southern China and Vietnam (Figure 1A) (Liang, 2004). Bites are generally not lethal to humans, but can produce substantial pain and inflammation. Like the Trinidad Chevron, crude venom from this spider activates recombinant TRPV1, suggesting that it contains one or more peptide toxins that target nociceptors as part of its chemical defense strategy (Siemens et al., 2006). We purified the major active component to homogeneity using calcium imaging as a functional readout (Figures 1B and 8A).

Many peptide toxins, including VaTx1 and VaTx2, are known to target multiple channels subtypes. To assess specificity of the purified *O. huwena* toxin, we examined the effect of a relatively high dosage (2 μM) on a panel of TRP (TRPV2, TRPV3, TRPV4, TRPA1, and TRPM8), ligand-gated (5-HT_3R-A and $P2X_2$) and voltage-gated (K_v1.2, K_v2.1, and K_v4.3, Ca_V1.2, Ca_V3.3, and Na_V1.7) channels (Figure 8B), many of which are expressed in sensory neurons. No discernable effect was observed when DkTx was applied to oocytes or HEK293 cells expressing any of these channels. In keeping with this apparent selectivity for TRPV1, calcium imaging experiments with cultured trigeminal neurons showed toxin-evoked calcium influx in a subset of neurons corresponding to the capsaicin-sensitive cohort. Moreover, this response that was absent in cultures derived from TRPV1-deficient mice (Figure 2A).

O. huwena toxin is a novel bivalent ICK peptide

The absorbance and migration profile of *O. huwena* toxin on reversed-phase matrix suggested that the active component is hydrophobic and peptidic in nature. Given its

rather large size (monoisotopic mass of 8521.9 Da) and relative paucity in venom, we could only obtain a partial sequence of the toxin by *de novo* peptide sequencing. To circumvent this problem, we prepared total RNA from venom glands of *O. huwena* spiders and used this material to clone cDNAs encoding the mature toxin. Indeed, the predicted sequence thusly obtained matched the observed mass of the full-length toxin and proteolytically derived fragments. Moreover, the native toxin contained a C-terminal amidated arginine, consistent with the fact that cDNA sequence predicts transfer of an amide group from a glycine residue in the n+1 position of the precursor peptide.

Although the new *O. huwena* toxin contains a pattern of cysteine residues that conforms to the ICK motif seen in the vanillotoxins, the new toxin bears little sequence similarity with the vanillotoxins, suggesting that *P. cambridgei* and *O. huwena* spiders have independently developed TRPV1 agonists through a process of convergent evolution. Most strikingly, the new *O. huwena* toxin is approximately twice the size of the vanillotoxins and consists of two head-to-tail ICK unit repeats separated by a short linker (Figure 1C). ICK units adopt a characteristically compact and rigid structure and thus we propose that the novel *O. huwena* toxin forms two independently folded domains connected by a kinked tether (Figure 1D). As this new *O. huwena* peptide is the first known example of a toxin containing tandemly repeated ICK motifs, we have dubbed it the “double-knot” toxin (DkTx).

DkTx is a virtually irreversible TRPV1 activator

The apparent structure of DkTx suggests that it behaves as a bivalent ligand, in which case it should demonstrate an exceptionally high avidity for its multimeric target, reminiscent of an antibody-antigen complex. To test this prediction, we carried out whole cell patch clamp recordings from capsaicin-sensitive trigeminal neurons to assess the

persistence of DkTx-evoked currents. Application of purified DkTx (1 μM) produced characteristic outwardly rectifying, ruthenium red blockable currents resembling those elicited by capsaicin (Figure 2B). However, we observed a striking difference between these two agonists in regard to the kinetics of the response. Whereas capsaicin-evoked currents returned to baseline within 10 seconds of washout, those elicited by DkTx persisted for minutes with minimal decline in magnitude (Figure 2B).

To characterize this phenomenon in greater detail, we compared off rates of various agonists by recording from TRPV1-expressing HEK293 cells. As expected, responses to capsaicin and extracellular protons (pH 5.5) declined rapidly with washout, exhibiting τ_{off} = 0.17 and 0.005 minutes, respectively. In contrast, currents evoked by purified vanillotoxins showed substantially slower decay rates, with τ_{off} ranging from 1.6 to 2.5 minutes (Figure 2C), as expected for relatively large and molecularly complex peptide agonists. Remarkably, currents elicited by DkTx were even more persistent, verging on irreversible, thereby precluding meaningful measurements of τ_{off} (Figure 2C). This phenomenon was independent of concentration since currents persisted for >15 minutes when elicited by 0.2 μM or 2 μM toxin (Figure 2C, 9A). In either case, >50% of maximal toxin-evoked response remained after an extended washout period. In light of these observations, we conclude that DkTx exhibits a high avidity for TRPV1, presumably reflecting association of this bivalent ligand with the homotetrameric channel so as to form an extremely stable complex exhibiting very slow rates of toxin dissociation.

Bivalence accounts for irreversible toxin action

To test the prediction that the tandem-repeat nature of DkTx accounts for its high avidity for TRPV1, we generated a modified toxin that could be proteolytically separated to yield the component ICK lobes for direct functional comparison. To achieve this, we

introduced a Genenase I cleavage site (-HYR-) into the linker region of the mature DkTx sequence (Figure 3A) and expressed both wild type (DkTx) and modified (DkTx-HYR) peptides recombinantly using a bacterial expression system. Heterologous expression of ICK toxins is notoriously difficult to achieve owing to the low probability of proper disulfide bond formation (Bulaj and Olivera, 2008). Nonetheless, a substantial amount (40 mg/liter culture) of total unfolded toxin peptide was produced, of which a workable fraction (1%) could be refolded to yield chromatographically well-behaved peptide (Figure 9A). Native DkTx, recombinant DkTx, and recombinant DkTx-HYR all activated TRPV1 with similar potency (EC_{50} = 0.23, 0.14, and 0.24 μM, respectively, Figure 3B, 3D), eliciting essentially irreversible, outwardly rectifying, ruthenium red blockable currents (Figure 3C).

Incubation of purified DkTx-HYR with Genenase I resulted in quantitative cleavage into the N- and C-terminal ICK peptides (K1 and K2, respectively), which were subsequently separated and purified by reversed-phase chromatography, as confirmed by mass spectrometry (Figure 9B). With these reagents in hand, we could assess relative potencies and kinetics of TRPV1 activation. Clearly, separation of DkTx-HYR into K1 and K2 single knot peptides was associated with a substantial drop in potency when compared to the intact toxin, as evidenced by a 5- and 50-fold increase in EC_{50} values for K2 and K1, respectively (Figure 3D). This was accompanied by a marked increase in cooperativity (indicated by a shift in hill coefficient from ~1 to 4), suggesting that more single knot toxins must bind per TRPV1 complex to promote channel activation. Moreover, we also observed a striking difference in the time course of toxin action, such that responses to K1 or K2 declined rapidly upon washout and showed no sign of the persistent currents elicited by the parental DkTx-HYR (Figure 3E). Co-administration of K1 and K2 produced the same response observed with K2 alone (the more potent of the

two peptides) (not shown), indicating that these ICK lobes must be physically tethered to achieve the potency and irreversibility of native or recombinant double-knot toxin.

Are sequence differences in the similar but non-identical K1 and K2 essential for irreversible TRPV1 activation? To address this issue, we generated a modified toxin in which the K2 sequence was replaced by K1, thereby producing a toxin with two identical ICK lobes. The K1-K1 double knot had higher potency than K1 alone (EC_{50} = 0.44 μM) and resembled wild type DkTx in its ability to elicit irreversible channel activation (Figure 10B). This ability to generate a high avidity toxin by simply duplicating one knot suggests that each lobe of K1-K1 (and by analogy, K1 and K2 of native DkTx) interacts with equivalent sites on separate channel subunits to produce a stable, high avidity complex.

DkTx binds to and locks TRPV1 in the open state

Given the bivalent nature of DkTx, we asked whether the toxin must bind simultaneously to multiple channels to effect persistent activation. To address this question, we analyzed single channel responses in excised outside-out membrane patches taken from TRPV1-expressing HEK293 cells. Like other vanillotoxins (Siemens et al., 2006), DkTx activated the channel in the outside-out, but not inside-out configuration, consistent an extracellular site of action (Figure 12A). Using a saturating dose of capsaicin (1 μM), we first identified patches containing a single functional TRPV1 channel (Figure 11A). Subsequent exposure to recombinant DkTx produced single channel events whose unitary conductance was within 15% of that evoked by capsaicin (103 and 118 pS, respectively), but whose mean open times were dramatically longer (Figure 11A, 12B). These results demonstrate that irreversible gating can be achieved through interaction of DkTx with a single TRPV1 channel.

Consistent with whole cell recordings, single channel records showed that persistent activation by DkTx is time dependent (Figure 11A). Interestingly, onset of the persistent phase could be substantially accelerated when toxin was applied in the presence of capsaicin. Thus, even brief co-application of capsaicin and DkTx converted flickering capsaicin-evoked responses to non-flickering openings that persisted long after washout of both agonists (Figure 11B). Consistent with this, we observed similar behavior at the macroscopic (whole cell) level, where co-application of toxin and capsaicin enhanced both the rate and efficiency with which irreversible currents developed (Figure 12C). Taken together, these findings suggest that DkTx binds to TRPV1 in an open state-dependent manner, trapping it there to produce irreversible currents.

Toxin activation is specified by residues within the pore-forming region of TRPV1

Based on the known mechanism of hanatoxin action and presumed similarities between TRP and voltage-gated channels, we initially assumed that vanillotoxins would mediate their effects through interaction with the topologically equivalent domain (S3b-S4) of TRPV1. However, alanine scanning of this region (residues 517 through 550) failed to identify residues that contribute significantly to VaTx3- or DkTx-evoked channel activation (Figure 14A). We therefore adopted a different strategy for identifying the site(s) of TRPV1-toxin interaction.

Sensory receptors show substantial functional diversification as organisms evolve to inhabit different ecological niches. This most often manifests as differential sensitivity to physiological stimuli, which can be exploited to delineate receptor domains that contribute to ligand binding or activation. Indeed, this strategy has been especially fruitful for pinpointing residues that are required for activation or inhibition of TRP channels by chemical ligands (Chou et al., 2004; Chuang et al., 2004; Gavva et al., 2004; Jordt and

Julius, 2002; Phillips et al., 2004). We therefore asked whether ICK toxins activate TRPV1 orthologues from non-mammalian species. We found that *X. laevis* frog TRPV1 (xTRPV1) is insensitive to VaTx3 or DkTx, although it responds to other stimuli, such as capsaicin or extracellular protons. By analyzing a series of rat-frog TRPV1 chimeras and point mutants, we traced this differential response profile to a single amino acid located at the extracellular boundary of the S6 domain (Figure 4A). Thus, rat TRPV1 harboring the frog residue at this site (A657P) retained sensitivity to capsaicin and low pH, but was unresponsive to VaTx3 or DkTx (Figure 4B). Detailed dose-response analysis revealed a 100-fold drop in DkTx potency at rTRPV1 (A657P) mutant compared to the wild type channel. Although toxin-evoked responses were observed at high DkTx concentrations, currents returned to baseline shortly after toxin washout (Figure 13A). Thus, changes at this position diminish both toxin potency and persistence, suggesting that A657 is located within or near a site of toxin-channel interaction. For all other 18 amino acid substitutions, only A657W showed a substantial loss of toxin sensitivity compared to capsaicin (Figure 13B). Mutants bearing charged or polar side chains did not respond to either agonist, suggesting that uncharged or hydrophobic side chains at this position are required for normal channel function, and that the toxin does not tolerate the bulkiest residues, proline and tryptophan.

To determine whether the A657 residue is both necessary and sufficient to account for the species-specific toxin sensitivity, we asked whether the reciprocal mutant (P663A) conferred toxin responsiveness to frog TRPV1. The xTRPV1 (P663A) mutant is poorly expressed compared to the wild type channel, but nevertheless showed robust responses to DkTx at concentrations (20 μM) that had no effect on the wild type frog channel (Figure 4C). Thus, all other amino acid differences between the rat and frog channels (Figure 13C) must have only minor effects on toxin sensitivity. Taken together,

these results suggest that toxin-TRPV1 association is specified by residues within the pore-forming domain of the channel, near the S6 region.

The TRPV1 (A657P) mutation disrupts DkTx binding

Our electrophysiological results are consistent with a model in which peptide toxins promote TRPV1 gating through a direct interaction with the pore-forming region of the channel complex. To assess binding directly, we immobilized histidine-tagged recombinant DkTx on nickel resin and asked whether this toxin affinity column could retain purified TRPV1 protein. Detergent solubilized and purified FLAG-tagged TRPV1 was incubated with DkTx-coupled resin, which was then washed extensively (30 min) before elution of the retained proteins. Indeed, DkTx-coupled (but not control untreated) resin depleted TRPV1 quantitatively from the detergent extract and elution released the channel in complex with DkTx (Figure 5A). Toxin-channel association could also be observed using the converse protocol in which TRPV1 was immobilized on a FLAG immunoaffinity column to which soluble DkTx was applied (not shown). Importantly, no interaction was observed with either protocol when TRPV2 was used in place of TRPV1, attesting to the specificity of toxin binding (Figure 5A).

To further demonstrate the specificity of toxin-channel binding, we performed a similar experiment using crude detergent solubilized membrane extracts from TRPV1-expressing HEK293 cells, rather than purified channel protein. Although TRPV1 represents only a small fraction of total membrane protein (even after induced over-expression), it was greatly enriched in the material eluted from the toxin-coupled resin (Figure 5B). In fact, the purity of this sample rivaled that generally obtained by FLAG purification, supporting a direct and specific biochemical interaction between DkTx and TRPV1. Consistent with its decreased toxin sensitivity, we found that the TRPV1

(A657P) mutant protein was retained on the DkTx affinity column, but only when toxin density exceeded that required for efficient purification of the wild type channel (Figure 5C). These biochemical results support our conclusions from physiological experiments that toxin interacts directly with residues in the pore-forming region of TRPV1.

Multiple sites within the TRPV1 outer pore domain are critical for toxin activation

To further delineate a footprint of toxin-channel interaction, we asked whether mutations in other residues within the S5-S6 domain would abrogate toxin-evoked TRPV1 activation. Indeed, alanine scanning of this region (residues 592-665) revealed three new sites (I599, F649, and F659) where alanine substitutions produced marked diminution of toxin responses, while retaining capsaicin sensitivity (Figure 6A, 6B, and 14B). Together with A657, these residues delineate a potential toxin interaction site bracketed by the extracellular boundaries of S5 and S6, corresponding to the outer pore domain (Figure 6D). At high toxin concentrations ($\geq$ 20 μM), residual responses can be observed with each of these single point mutations (Figure 13C and not shown), whereas a quadruple mutant (I599A, F649A, A657P, F659A) completely eliminates toxin sensitivity (Figure 6C). This result suggests that these sites impact toxin binding in non-identical ways, and that the outer pore domain plays a dominant and necessary role in mediating toxin sensitivity.

ICK toxins interact differentially with TRPV1 and K_v2.1

In contrast to our findings with TRPV1-activating toxins, hanatoxin has been shown to inhibit K_v channels by associating with the S3b-S4 voltage-sensing paddle domain, thereby retarding its movement during depolarization. We therefore asked whether VaTx1, which both activates TRPV1 and inhibits K_v2.1, also interacts with the S3b-S4 region of the latter. To answer this question, we examined three K_v2.1 voltage sensor

domain mutants (I273Y, F274R, and E277K) that have been previously shown to disrupt hanatoxin-mediated inhibition of this channel (Li-Smerin and Swartz, 2000). Two of these mutations (F274R, and E277K) eliminated VaTx1-mediated inhibition (even at toxin concentrations exceeding the IC_{50} value for wild type $K_v2.1$), whereas the third (I273Y) had a modest effect (Figure 7B). These results strongly suggest that VaTx1, like hanatoxin, targets the voltage sensor of $K_v2.1$ to mediate channel inhibition. VaTx1 activation of TRPV1, on the other hand, was abolished by the TRPV1 (A657P) mutation in the pore domain (Figure 7A). Thus, vanillotoxins likely interact with different regions of TRP and K_v channels in their capacity to serve as agonists or antagonists, respectively.

DISCUSSION

Bivalency as a novel toxin feature

To date, over a thousand ICK peptides have been characterized, demonstrating substantial variation in length, amino acid sequence, the number and configuration of disulfide bonds, and post-translational modification (Gelly et al., 2004; Terlau and Olivera, 2004). However, DkTx is the first member of this extended peptide family known to contain tandemly repeated ICK units. Our results show that each unit can exist as structurally and functionally independent entities which, when combined, synergize to produce a ligand of exceedingly high avidity. The irreversible action of DkTx should translate into excruciating and prolonged pain, perhaps in keeping with the reputation of the *O. huwena* spider as an aggressive and fearsome creature (Liang, 2004). Indeed, persistent activation of TRPV1 will be accompanied by intense pain and robust neurogenic inflammation that will cease only upon desensitization and/or neurotoxic injury to the primary afferent fiber. Venoms contain hundreds of ICK toxins that evolve through a process of gene duplication and divergence (Diao et al., 2003; Duda and

Palumbi, 1999). Homology between the two DkTx knots indicates that this peptide has likewise been produced by gene duplication, but in this case within a single coding region. With the advent of new high throughput methods for sequencing complex mixtures of ICK peptides (Ueberheide et al., 2009), it will be interesting to see whether this double knot motif represents a general evolutionary strategy for producing toxins that target homomeric and heteromeric receptors with high avidity. In any case, much as polymer-linked small molecules have been used to probe channel structure (Kramer and Karpen, 1998), DkTx inspires a biosynthetic strategy for the rational design of multivalent peptide ligands (agonists or antagonists) using the ICK fold as a template. Indeed, our engineered K1-K1 peptide demonstrates the feasibility of this approach. Thus, just as hanatoxin and charybdotoxin have served as essential tools for defining the basic functional components of voltage-gated channels, DkTx and genetically engineered derivatives provide analogous new biochemical tools for dissecting the unique properties of TRP channels and facilitating structural studies.

ICK toxins target distinct domains of TRP and voltage-gated ion channels

Peptide toxins, particularly those within the ICK family, modulate voltage-gated channels through two main mechanisms. One, exemplified by hanatoxin or β-scorpion toxin, involves association of the toxin with the S3b-S4 domain of K_v or Na_v channels, respectively, trapping the voltage sensor so as to favor the closed or open state (Catterall et al., 2007; Cestele et al., 1998; Li-Smerin and Swartz, 1998; Sokolov et al., 2008; Swartz, 2007). The second, exemplified by charybdotoxin, involves a more passive mechanism in which the toxin binds to the S5-S6 region of closed or open K_v channels to occlude passage of ions through the pore (Goldstein et al., 1994; Gross et al., 1994; MacKinnon et al., 1990; Yu et al., 2005). Vanillotoxins, including DkTx, now introduce a third mechanism in which gating equilibrium is modulated by interaction with

the pore domain (rather than the S3b-S4 region) to promote channel opening (rather than occlusion) (Figure 7C). This is reminiscent of hydrophobic small molecule modulators such as dihydropyridines or batrachotoxin, which alter voltage-gated calcium or sodium channel activity through interactions with intramembrane sites close to or within the S6 helix (Catterall et al., 2007; Wang and Wang, 2003). While vanillotoxin activation of TRPV1 likewise involves interaction with residues in the S5-S6 region, these are predicted to reside on the extracellular face of the plasma membrane, rather than deep within the lipid bilayer.

The vanillotoxin, VaTx1, serves as both a K_v2.1 inhibitor and a TRPV1 activator. VaTx1 resembles hanatoxin in so far as predicted fold and primary sequence, and thus it makes sense that mutations within the S3b-S4 region of K_v2.1 abrogate both hanatoxin- and VaTx1-mediated inhibition, consistent with a common mechanism of toxin action. In contrast, we were surprised to find that vanillotoxins (VaTx1 and DkTx) interact with a completely different domain of TRPV1, namely the outer pore region, which has little, if any, influence on hanatoxin-K_v interaction (Alabi et al., 2007; Li-Smerin and Swartz, 2000). Our evidence disfavoring a role for the S3-S4 domain in TRPV1-vanillotoxin interaction rests on 'negative' results, namely an inability to identify mutations within this region that disrupt toxin-evoked channel activation, despite extensive scanning. Thus, it remains formally possible that the S3-S4 region of TRPV1 plays some role in vanillotoxin binding. However, our ready identification of functionally important sites within S5-S6, together with the chimeric channel experiments, strongly suggests that the outer pore domain constitutes a major and essential locus underlying toxin sensitivity. Thus, vanillotoxins recognize distinct, non-overlapping sites on different channels to produce activation or inhibition. Presumably, this differential interaction of ICK toxins with TRP and voltage-gated channels highlights the relative importance of these domains to

channel gating. Moreover, the ability some toxins (such as VaTx1) to modulate both types of ion channels may conspire to enhance neuronal depolarization.

The TRPV1 outer pore domain as a key locus of channel activation

Our electrophysiological and biochemical studies indicate that residues at the extracellular face of the TRPV1 S6 domain engage in DkTx binding (Figure 7C). Because DkTx binds preferentially to TRPV1 in the open state, it follows that the pore domain of the channel likely undergoes substantial conformational rearrangement during gating, consistent with recent mutagenesis studies indicating that the outer pore region is critical for gating of TRPV channels (Grandl et al., 2008; Myers et al., 2008; Yeh et al., 2005). This stands in contrast to K_v channels, where the outer pore domain has been suggested to remain relatively stationary during the gating process (Long et al., 2005b; Tombola et al., 2006). Thus, while TRP and voltage-gated channels likely share gross architectural features, they must also possess unique structural elements that enable them to fulfill different physiological roles, such as detection of membrane voltage versus thermal or chemical stimuli. Future structural studies will be necessary to understand the full extent of similarities and differences in the gating process for these distinct ion channel families.

EXPERIMENTAL PROCEDURES

Native Toxin Purification and Peptide Sequencing

Crude *O. huwena* venom was obtained from Spider Pharm Inc. Lyophilized venom was dissolved in water containing 0.1% trifluoroacetic acid (TFA). The suspension was filtered through an 0.2 μm filter (Amicon) and fractionated by HPLC (Prostar 210, Varian) on a semi-preparative reversed-phase C18 column (Vydac, 10 mm x 250 mm) employing a 28 min linear gradient from 18% to 43% acetonitrile with 0.1% TFA (flow

rate 3 ml/min). Fractions were lyophilized and dissolved in water, and aliquots were stored at -80°C. Protein concentration was determined by predicted extinction coefficient at 280 nm (http://us.expasy.org /tools/protparam.html), and the predicted extinction coefficient was confirmed experimentally by amino acid analysis of recombinant DkTx. VaTx1, VaTx2, and VaTx3 were purified as described (Siemens et al., 2006). Native DkTx mass was measured on a Bruker Apex III ESI-Q-FTICR (9.4T magnet) mass spectrometer, and the peptide was sequenced on an Applied Biosystems 492 Procise Sequencer.

DkTx Cloning

To clone the gene encoding mature DkTx, RNA was extracted from two *O. huwena* venom glands (tissue provided by Spider Pharm Inc.) using TRIZOL (Invitrogen) and reverse transcribed using SuperScript II MMLV-RT (Invitrogen). A degenerate primer derived from DkTx N-terminal peptide sequence was used to perform 3' RACE (SMART-RACE kit, Clontech). A conserved "prepro" sequence found in some *O. huwena* toxin cDNAs (GGATTAGTTCTGCTTTTCGTTGTTTGCTATGC) (Diao et al., 2003) and the reverse-complement of the determined 3'UTR sequence (TTACACAGTGAATATAGTGTAAAC CAAAGG) were used as PCR primers to amplify the full coding sequence for the mature toxin. The full-length DkTx cDNA encoded a propeptide region, which is cleaved post-translationally, the mature toxin, and four extra C-terminal amino acids (Gly-Arg-Asn-Glu), which are removed during amidation of the C-terminus. The cDNA-derived peptide sequence predicted the observed molecular weight and digestion pattern of purified DkTx.

Recombinant Toxin Expression and Purification

Each toxin construct was expressed in *E. coli* (Origami B strain, Novagen) using a pET19b derived vector (Hillier et al., 1999) to generate a fusion protein with a cleavable hexahistidine tag at the N-terminus. For protein expression, cells were grown at 37°C in LB broth supplemented with 0.1 mg/liter carbenicillin to OD_{600} ~ 0.6 – 0.7 before induction with 0.3 mM isopropyl β-d-thiogalactoside. After 4 h of induction, cells were harvested by centrifugation (15 min, 5,000 × *g*, 4°C) and stored at -20°C. Thawed cells from 1 liter were resuspended in 20 ml lysis buffer [(mM): 150 NaCl, 2 $MgCl_2$, 40 Tris, pH 8.0] and lysed with 3 passages at 10,000–15,000 ψ in an EmulsiFlex-C5 high-pressure homogenizer (Avestin). Misfolded DkTx, expressed in inclusion bodies, was recovered by centrifugation (10 min, 26,000 × *g*, 4°C) and washed three times with lysis buffer containing 0.1% Triton X-100, then one final time with lysis buffer without Triton X-100. Washed inclusion bodies from 1L culture were dissolved for 2 hrs in 5 ml of freshly prepared buffer containing 8 M Urea, 10 mM DTT, 10 mM Tris, pH 8.0, centrifuged, and dialyzed against refolding buffer (2.5 mM reduced glutathione, 0.25 mM oxidized glutathione, 20 mM Tris, pH 8.5) for 2 days at room temperature (RT). Refolded peptides were passed through a 0.2 μm syringe filter before being separated by HPLC on a semi-preparative reversed-phase C18 column, employing a 12 min linear gradient from 22% to 44% acetonitrile with 0.1% TFA (flow rate 3 ml/min). Lyophilized fractions were dissolved in water and stored in aliquots at -80 °C.

His-tagged toxin was tested for activity and used for binding assays, but for all other experiments, the hexahistidine tag was removed by incubation with TEV protease (1:25 molar ratio) in 20 mM Tris, pH 8.0, for 2-4 h at 30°C. The cleaved product contained a vector-derived sequence Gly-Ser at the N-terminus and lacked the C-terminal amidation observed in the native DkTx peptide. Cleaved protein was purified by HPLC and stored as before. For cleavage into K1 and K2, DkTx-HYR was diluted to 15 μM and incubated

with Genenase I (New England Biolabs) at a 1:1 molar ratio for 24 h at RT in buffer containing 200 mM NaCl, 20 mM Tris, pH 8.0. K1 and K2 were separated by HPLC with a semi-preparative reversed-phase C18 column, employing a 30 min linear gradient from 0 to 50 % acetonitrile with 0.1% TFA (flow rate 3 ml/min). Molecular weight and purity was confirmed for all purified peptides by MALDI-TOF mass spectrometry and SDS-PAGE. All protein concentrations were determined by predicted extinction coefficient at 280 nm.

Molecular Biology

Full-length TRPV1 (rat), FLAG-TRPV1 (rat), FLAG-TRPV2 (rat), and FLAG-TRPV1 (A657P) were stably expressed in Flp-in T-REX 293 cells according to the manufacturer's protocol (Invitrogen). For transient expression, channels were cloned into pMO (rat TRPV1) or pFROG3 (frog TRPV1, rat TRPV2, human TRPV3, rat TRPV4, and rat TRPA1) and transfected into HEK293t cells with Lipofectamine 2000 (Invitrogen). Rat K_v channel clones were kindly provided in the pRBG4 vector by James Trimmer (University of California, Davis, Davis, CA) (Shi et al., 1994), Cav channel clones were kindly provided by Daniel Minor (University of California, San Francisco, CA), and Nav channels were kindly provided by Stephen Waxman (Yale School of Medicine, New Haven, CT). To clone *Xenopus laevis* TRPV1, total RNA was isolated from freshly dissected adult *Xenopus laevis* trigeminal and dorsal root ganglia and reverse-transcribed into first-strand cDNA (SuperScript II, Invitrogen). A fragment of the gene was amplified by PCR, using primers that anneal to evolutionarily conserved regions of TRPV1, as determined by alignment of rat, human, chick, and *Xenopus tropicalis* genome sequences. The complete *Xenopus laevis* TRPV1 coding sequence was subsequently determined using 5' and 3' RACE (SMART-RACE kit, Clontech). Full-

length TRPV1 was amplified using primers GATTCAACAAAATGAAGAAAAT (fwd) and GACAGATTCACTCAGCCTTG (rev).

Mutations and chimeras were generated using standard overlap extension PCR, and residue numbers were counted from the first methionine. Fragments of residues that were replaced in rat TRPV1 with *Xenopus laevis* TRPV1 sequence were as follows (rat/xenopus): E458-V486/D469-I495 for the first extracellular loop between S1 and S2, V518-M552/S527-V561 for the second loop between S3 and S4, S592-A665/A601-T671 for the S5-S6 loop (including the pore helix), S592-F655/A601–Y661, and A657-I661/P663-F667. All constructs were confirmed by DNA sequencing (Elim Bioscience). RNA was synthesized using the T7 mMessage mMachine kit (Ambion, Austin, TX) and dissolved in water for storage at –80°C.

Neuronal Cell Culture, Calcium Imaging and Electrophysiology

Trigeminal ganglia (TG) were dissected from newborn (P0-P3) mice (wild-type or TRPV1-deficient) and dissociated with 0.125% collagenase P (Boehringer) solution in CMF Hank's solution at 37 °C for 30 min, washed, and re-incubated in 0.25% trypsin at 37 °C for 10 min. Ganglia were triturated gently with a fire-polished Pasteur pipette in culture medium (MEM Eagle's/Earle's BSS with 10% horse serum, vitamins, penicillin–streptomycin, L-glutamine). Cells were centrifuged for 10 min at 100 x g, and resuspended in culture medium.

Calcium imaging was performed in 10 μl adhesive silicone isolators (Invitrogen) attached to Poly-D-Lysine (PDL) (0.1 mg/ml, Sigma) coated microscope slides (Fisher). Cells were loaded with Fura-2-AM (10 μM, Invitrogen) dissolved in Ringer solution [(mM): 140 NaCl, 2.8 KCl, 2 $CaCl_2$, 2 $MgCl_2$, 10 HEPES and 10 D-glucose, adjusted to pH-7.4 with NaOH, 290-300 mOsmol kg^{-1}] plus pluronic acid (0.02%, Invitrogen), for 1 h at RT. Cells

were washed three times with Ringer solution. Drugs dissolved in Ringer solution were rapidly added and mixed with a pipette. Fluorescent images were acquired with Metafluor Software (Molecular Devices) and analyzed in Igor Pro (Wavemetrics). All experiments were performed at RT.

For electrophysiology, cells were plated onto coverslips (12 mm, Fisher) coated with PDL (1 mg/ml; Sigma) and laminin (5 μg/ml; Invitrogen). Recordings were carried out 4-6 h after dissociation of the TG. Membrane currents were recorded using ramps (-80 to +40 mV) under the whole-cell configuration of the patch-clamp technique using the Axopatch 200B amplifier (Axon Instruments, Foster City, CA). Membrane currents were digitized online using a Digidata 1322A interface board and pCLAMP 10.2 software (Axon Instruments). Sampling frequency was set to 20 kHz, and the low-pass filter was set to 1 kHz. Patch electrodes were fabricated from borosilicate glass with a resistance of 2–4 MΩ. The extracellular solution contained (mM): 150 NaCl, 2.8 KCl, 1 $MgSO_4$, 1 $CaCl_2$, 10 HEPES, 0.01 tetrodotoxin (TTX) adjusted to pH 7.4 with NaOH, 300-310 mOsmol kg^{-1}. The pipette solution contained (mM): 130 K-gluconate, 15 KCl, 4 NaCl, 0.5 $CaCl_2$, 1 EGTA, 10 HEPES, 3 MgATP, and adjusted to pH 7.2 with KOH, 285 mOsmol kg^{-1}. For application of drugs, solutions were applied from the micro-perfusion system SmartSquirt (Automate Scientific). Data were analyzed using pCLAMP 10.2 software (Axon Instruments).

HEK293 Cell Culture, Calcium Imaging and Electrophysiology

Human embryo kidney 293 (HEK293) cells were grown in DMEM (Sigma) supplemented with 10% FBS, 100 unit/ml penicillin, 0.1 mg/ml streptomycin at 37°C and 5% CO_2. Cells were passed twice a week until pass #20. Calcium imaging was performed as described above for neuronal cells.

For electrophysiology, cells were plated onto coverslips (12 mm, Fisher) coated with PDL (1 mg /ml; Sigma) for excised patch recordings or Matrigel (0.5 μg/ml; Invitrogen) for whole-cell recordings. Whole-cell recordings and multi-channel patch recordings (outside-out or inside-out) were carried out as describe above for neuronal cells. The extracellular solution contained (mM): 150 NaCl, 2.8 KCl, 1 $MgSO_4$, 10 HEPES, adjusted to pH 7.4 with NaOH, 290-305 mOsmol kg^{-1}. For low pH (5.5) MES was used instead of HEPES. The pipette solution contained (mM): 130 $CsMeSO_3$, 15 CsCl, 4 NaCl, 5 BAPTA, 10 HEPES, and adjusted to pH 7.4 with CsOH, 300 mOsmol kg^{-1}. For application of drugs, solutions were applied from the micro-perfusion system SmartSquirt (Automate Scientific). Data were analyzed using pCLAMP 10.2 software (Axon Instruments) and Sigmaplot (Systat Software Inc).

Single-channel currents were recorded in the outside-out patch configuration of the patch-clamp technique. The external solution and pipette solution contained (mM): 150 Na-gluconate, 15 NaCl, 5 EGTA, and 10 HEPES, adjusted to pH 7.4 with NaOH, 300 mOsmol kg^{-1}. $Gluconate^-$ was used as the major anion in the pipette solution since it was very difficult to obtain an outside-out patch when only Cl^- was used. In whole-cell experiments, the effects of DkTx were the same when either $MeSO_3^-$, Cl^- or $gluconate^-$ was the major intracellular anion. Single-channel currents were low-pass filtered at 1 kHz, digitized at 100 kHz. Occasional large brief noise spikes were visually identified and removed from the current traces. For application of drugs, solutions were applied from the micro-perfusion system SmartSquirt (Automate Scientific). Data were analyzed using pCLAMP 10.2 software (Axon Instruments).

Recordings of voltage-gated potassium channels to test DkTx specificity were performed as above except the intracellular solution contained (mM): 130 K-gluconate, 15 KCl, 4

NaCl, 0.5 $CaCl_2$, 1 EGTA, 10 HEPES, 3 MgATP, and adjusted to pH 7.2 with KOH, 285 mOsmol kg^{-1}. A 250 ms voltage step to +20 mV from a holding potential of -80 mV was applied with enough time between steps to allow for >85% recovery from the inactivated state when applicable.

Oocyte Preparation and Electrophysiology

Stage V–VI *Xenopus laevis* oocytes were prepared as previously described (Myers et al., 2008). Oocytes were injected up to 24 h after isolation with 3–50 ng cRNA per oocyte, and assayed 3–7 days later. Two electrode voltage-clamp recordings were carried out at RT using GeneClamp500 connected to a Digidata1322A and pCLAMP 9 (Axon Instruments). Electrodes (Sutter Instruments) were filled with 3 M KCl and had resistance of 0.3–1 MΩ. Oocytes were continuously perfused with solution containing (mM): 115NaCl, 2.5 KCl, 1.5 $MgCl_2$, and 10 HEPES, adjusted to pH 7.4 with NaOH. For low pH (5.5) MES was used instead of HEPES. Recordings sampling, and filtering were as described for the HEK293 cells. $Ca_v1.2$ expressing cells were given a 200 ms voltage step to -20 mV from a resting potential of -60 mV, $Ca_v3.3$ expressing cells wer given a 700 ms voltage step to -20 mV from a resting potential of -80 mV, and $Na_v1.7$ expressing cells were given a 25 ms voltage step to -10 mV from a resting potential of -80mV. Ca_v channels were recorded in BaCl2 solution to eliminate calcium-dependent inactivation, and all other channels were given sufficient time between voltage pulses to reach >85% of maximal recovery from the inactivated state. $Na_v1.7$ recordings were leak-subtracted using a p/-8 protocol applied after each step to reduce capacitance transients. In all recordings, drugs were applied using gravity-based perfusion, except for toxin which was applied manually. Data were analyzed using pCLAMP 9.

Binding Assay

FLAG-tagged rat TRPV1, TRPV2, and TRPV1(A657P) expressing cells were grown to 90% confluence and induced with 2 μg/ml doxycycline for 20 h at 37°C. Cells were rinsed twice, scraped into phosphate-buffered saline (PBS) solution, pelleted at 500 x g for 3 min at RT, and frozen in liquid nitrogen.

For protein preparation, cell pellets from one 15 cm dish were thawed and resuspended in 1 ml of 0.32 M sucrose, 1 mM EDTA, and 20 mM Tris, pH 7.5 containing protease inhibitor cocktail (Roche). Cells were broken by sonication then centrifuged at 2,000 × g for 10 min to remove cell debris; the supernatant was decanted and centrifuged at 65,000 × g for 60 min to pellet membranes, which were then solubilized in TBS (200 mM NaCl, 20 mM Tris, pH 7.4) containing 10 mM *n*-dodecyl-β-d-maltoside (DDM, Anatrace) and protease inhibitors for 2 hrs at 4 °C. Detergent-soluble extract was clarified by centrifuging at 14,000 x g for 10 min at 4°C and applied directly to toxin-coupled resin (see below), or incubated with equilibrated M2-FLAG resin (Sigma) for 2 hrs at 4 °C. FLAG-resin was washed extensively with TBS containing 2 mM DDM, and then eluted in TBS containing 0.5 mM DDM and 150 μg/ml synthesized FLAG peptide.

To produce toxin-coupled resin, His-tagged DkTx was diluted into PBS (200 mM NaCl 50 mM sodium phosphate, pH 7.6) and incubated with Ni-NTA agarose resin (Qiagen) 30 min at RT. Typically, 2.5 nmols of His-DkTx were incubated with 12 μl resin, but for the experiment described in Figure 6C, 0.7, 1.2, and 1.7 nmols of toxin were used. Purified TRPV1, TRPV2, TRPV1(A657P), or crude membrane extract were diluted into PBS containing 0.5 mM DDM 40 mM imidazole and incubated with toxin-coupled resin for 2 h at 4 °C. Resin was then washed 3 x 10 min with PBS containing 0.5 mM DDM 40 mM imidazole at RT before elution with Laemmli SDS gel-loading buffer. Samples were separated by SDS-PAGE on 4-12% Bis-Tris gels (Invitrogen) then either silver-stained (SilverXpress Kit, Invitrogen) or transferred onto Immobilon-P membranes (Millipore).

Blocking and antibody incubations were done in PBS that contained 3% BSA and 0.2% Tween-20 (Sigma). Membranes were cut in half and stained with anti-6xHis (1:2000 dilution, Santa Cruz Biotechnology) or HRP-conjugated anti-FLAG (1:4000, Sigma) antibodies for 1 h at RT. Membranes stained with anti-6xHis antibodies were incubated for an additional 20 min with HRP-conjugated goat anti-mouse antibody (1:5000, Jackson Immunoresearch). Blots were visualized by chemiluminescence (ECL PLUS, Amersham).

A

B

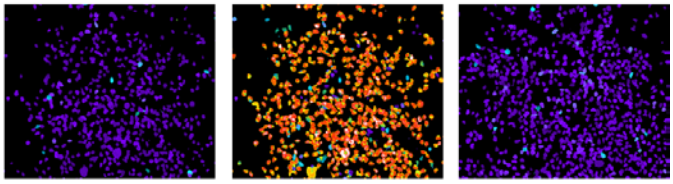

Background DkTx DkTx + RR

C

```
DkTx (K1)    DCAKEGEVCSWGKKCCDLDNFYCPMEFIPHCKKYKPYVPVTT-
DkTx (K2)   -NCAKEGEVCGWGSKCCHGLD..CPLAFIPYCEKYR
VaTx1       SECRWFMGGCDSTLDCCKHLS..CKMGLY.YCAWDGTF
VaTx2       GACRWFLGGCKSTSDCCEHLS..CKMGLD.YCAWDGTF
VaTx3        ECRWYLGGCKEDSECCEHLQ..CHSYWE.WCLWDGSF
HaTx         ECRYLFGGCKTTSDCCKHLG..CKFRDK.YCAWDFTFS
```

D

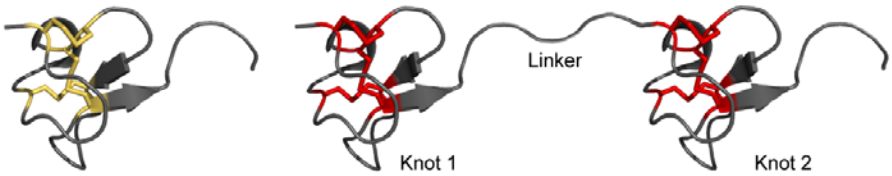

Figure 1 The Chinese bird spider produces a novel bivalent TRPV1 toxin

(**A**) The Chinese bird spider (*Ornithoctonus huwena*) is a large terrestrial tarantula with a leg span of up to 12 cm. It is found primarily in the Guangxi province of China (photo courtesy of Chuck Kristensen, SpiderPharm, Inc.). (**B**) Purified DkTx toxin evokes robust calcium increases in HEK293 cells expressing the rat TRPV1 channel. Co-application of ruthenium red (RR; 10 μM), a non-selective TRP channel pore blocker, inhibits toxin-evoked responses. Purple denotes low resting cytoplasmic calcium and orange indicates calcium increase. (**C**) DkTx is a new member of the ICK peptide family. Other than the highly conserved arrangement of cysteine residues (highlighted in yellow), DkTx shows no obvious sequence similarity with other ICK peptides, including the vanillotoxins (VaTx1-3) and hanatoxin (HaTx). (**D**) DkTx consists of two ICK lobes (Knot 1 and Knot 2) separated by a short linker region. The NMR solution structure of HaTx (Takahashi et al., 2000) served as a template for a hypothetical model of DkTx, showing the conserved disulfides in yellow for HaTx and red for DkTx (generated using PyMOL, http://www.pymol.org). These tandemly repeated lobes show significant sequence identity (see panel C), suggesting that they arose by gene duplication.

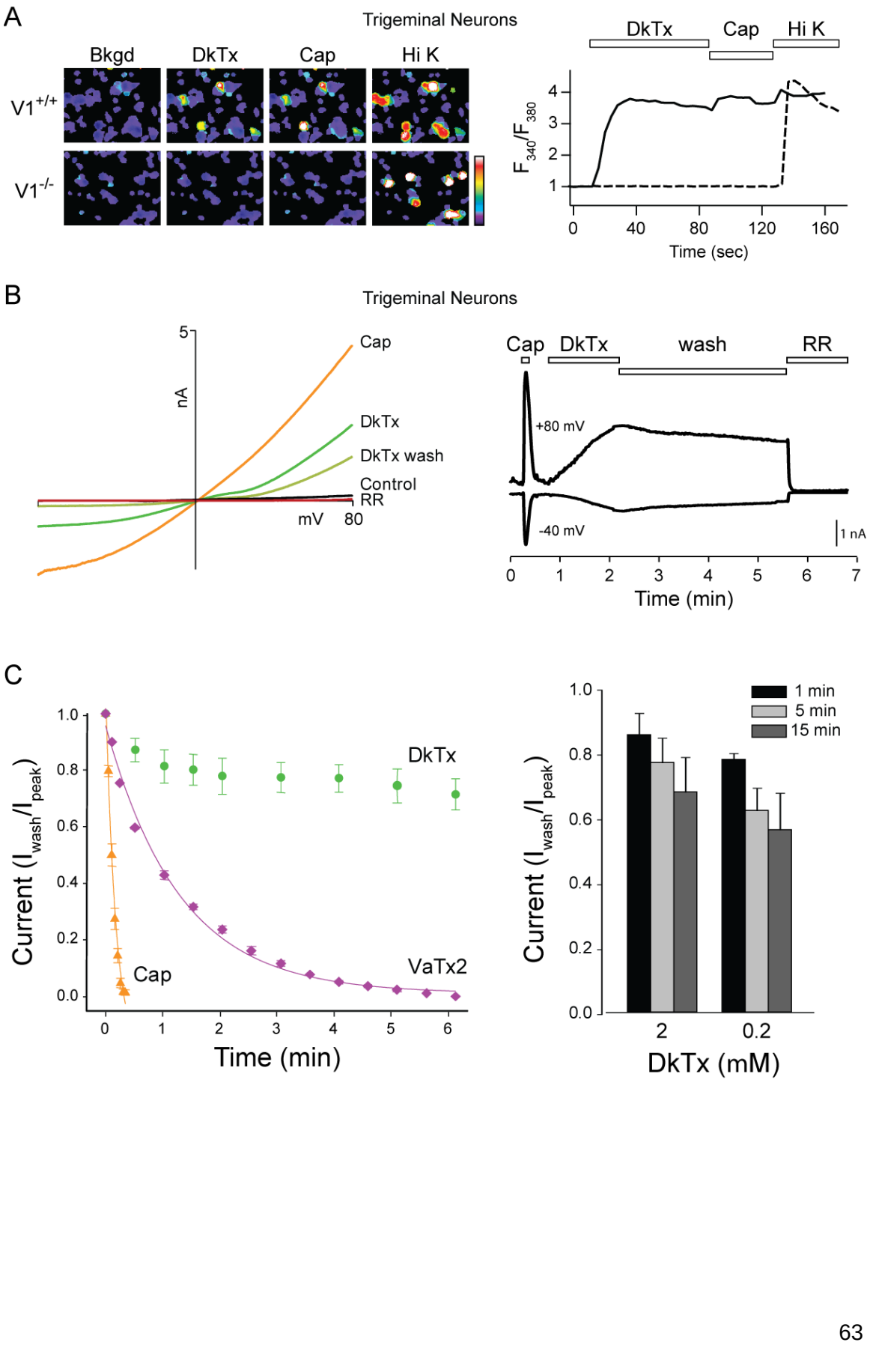
A
Trigeminal Neurons
Bkgd
DkTx
Cap
Hi K
V1+/+
V1-/-
DkTx
Cap
Hi K
F340/F380
Time (sec)
B
Trigeminal Neurons
5
nA
Cap
DkTx
DkTx wash
Control
RR
mV 80
Cap DkTx wash RR
+80 mV
-40 mV
1 nA
Time (min)
C
Current (Iwash/Ipeak)
DkTx
VaTx2
Cap
Time (min)
1 min
5 min
15 min
2
0.2
DkTx (mM)

Figure 2 DkTx is a selective and irreversible TRPV1 activator

(**A**) Trigeminal sensory neurons from wild type ($V1^{+/+}$) or TRPV1-deficient ($V1^{-/-}$) mice were examined for responses to capsaicin (1 μM; Cap) and DkTx (5 μM) using ratiometric calcium imaging. Depolarization with high extracellular potassium (75 mM; Hi K) identified all neurons in the field. (Left) Pseudocolor images of Fura-2-loaded cells (color bar indicates relative change in fluorescence ratio, with purple and white denoting lowest and highest cytoplasmic calcium). (Right) Average ratiometric calcium responses as a function of time. Solid and dashed lines represent responses from wild type and TRPV1-deficient trigeminal neurons, respectively. Note lack of DkTx-evoked response by TRPV1-deficient neurons (n ≥ 50 cells per trace). (**B**) Both capsaicin (Cap; 1 μM) and DkTx (2 μM) elicited outwardly rectifying, ruthenium red (RR; 4 μM) blockable currents in cultured mouse trigeminal neurons (recorded in whole-cell patch clamp configuration). Current-voltage relationships and representative current trace are shown at left and right, respectively. Note persistence of DkTx-evoked response even after 3-4 min washout period. (**C**) (Left) Relative washout rates were determined for electrophysiological responses to saturating doses of capsaicin (1 μM; orange), VaTx2 (2 μM; purple), or DkTx (2 μM; green). Individual points represent fractional current remaining as measured by whole-cell patch-clamp recording from TRPV1-expressing HEK293 cells (V_h = +80 mV). When washout was complete, a time constant of decay could be determined by exponential fit of the data (τ_{off} = 0.17 min and 1.3 min for capsaicin and VaTx2, respectively) (n = 4-7 cells per point). (Right) Plot of fractional DkTx-evoked current remaining after a 1, 5, or 15 min washout period as determined for two different toxin concentrations (n = 5-9 cells per bar). Average values represent mean ± s.e.m.

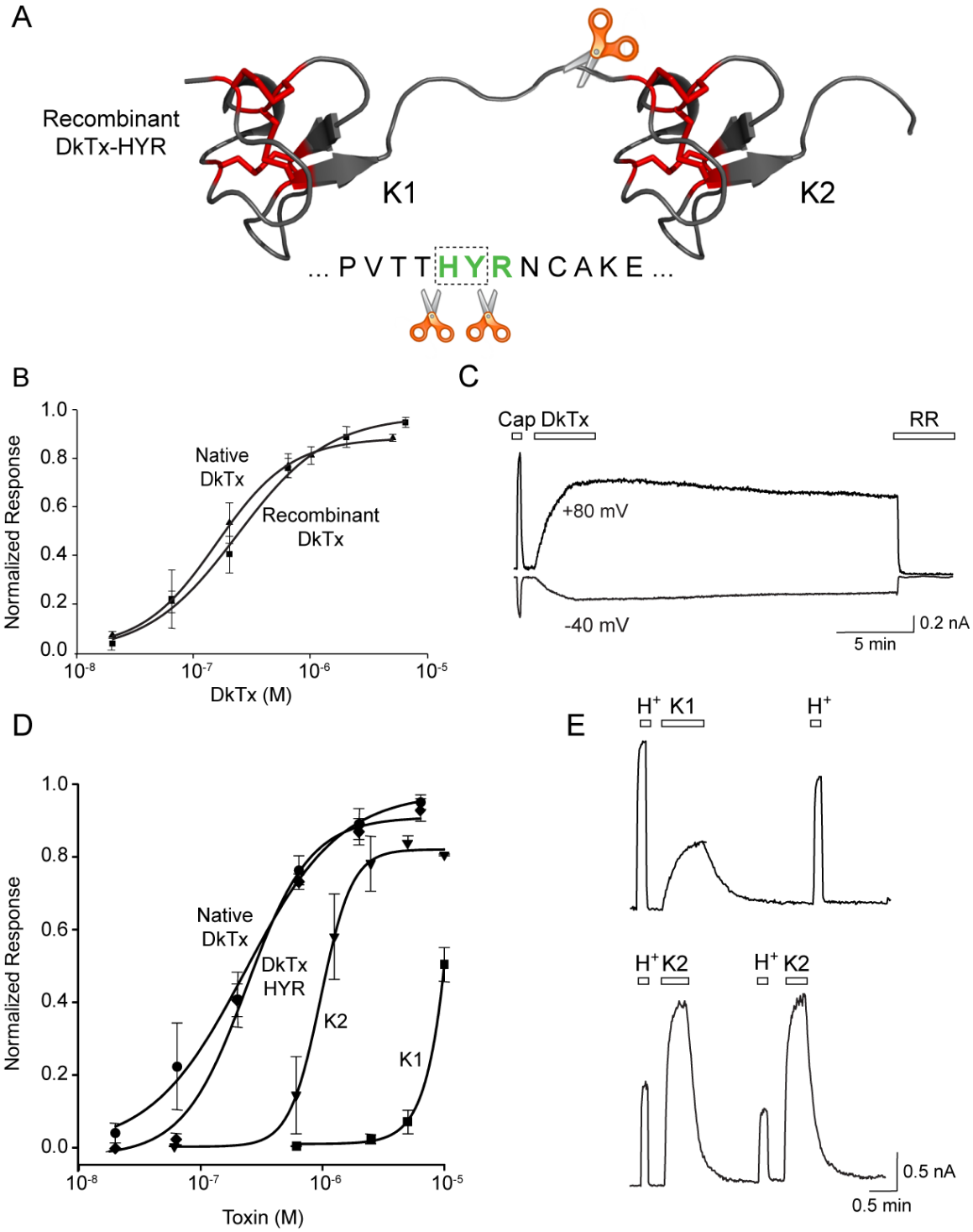
A
Recombinant
DkTx-HYR
K1
K2
... P V T T H Y R N C A K E ...
B
Normalized Response
Native
DkTx
Recombinant
DkTx
DkTx (M)
C
Cap DkTx
RR
+80 mV
-40 mV
0.2 nA
5 min
D
Normalized Response
Native
DkTx
DkTx
HYR
K2
K1
Toxin (M)
E
H+ K1
H+
H+ K2
H+ K2
0.5 nA
0.5 min

Figure 3 Bivalency is required for persistent toxin action

(**A**) Schematic depicts location of engineered protease (Genenase I) cleavage site in recombinant DkTx. (**B**) Native and recombinant DkTx are equipotent as determined by calcium imaging using TRPV1-expressing HEK293 cells. Values are normalized to maximal capsaicin (10 μM)-evoked responses (n = 3-4 wells per point). (**C**) Whole cell patch-clamp recording from TRPV1-expressing HEK293 cells shows that recombinant DkTx (2 μM) produces persistent, ruthenium red (RR) blockable membrane currents comparable in magnitude to those elicited by capsaicin (1 μM). (**D**) Dose-response analysis (carried out as in 'B') shows that native and recombinant DkTx containing the Genenase I cleavage site (HYR) are equipotent. Knot 1 and Knot 2 peptides (K1 and K2), derived from Genenase I cleavage of HYR, are active but significantly less potent (EC_{50} = 8.9 and 0.97 μM respectively). Values are normalized to maximal capsaicin (10 μM)-evoked responses (n = 3-4 wells per point). (**E**) Representative whole cell patch-clamp recordings (+80 mV) from TRPV1-expressing HEK293 cells showing responses to extracellular protons (H^+; pH 5.5), K1 (20 μM; top trace) or K2 (20 μM; bottom trace) peptides. Note rapidly reversible (i.e. non-persistent) nature of K1- or K2-evoked responses following washout. Average values represent mean ± s.e.m.

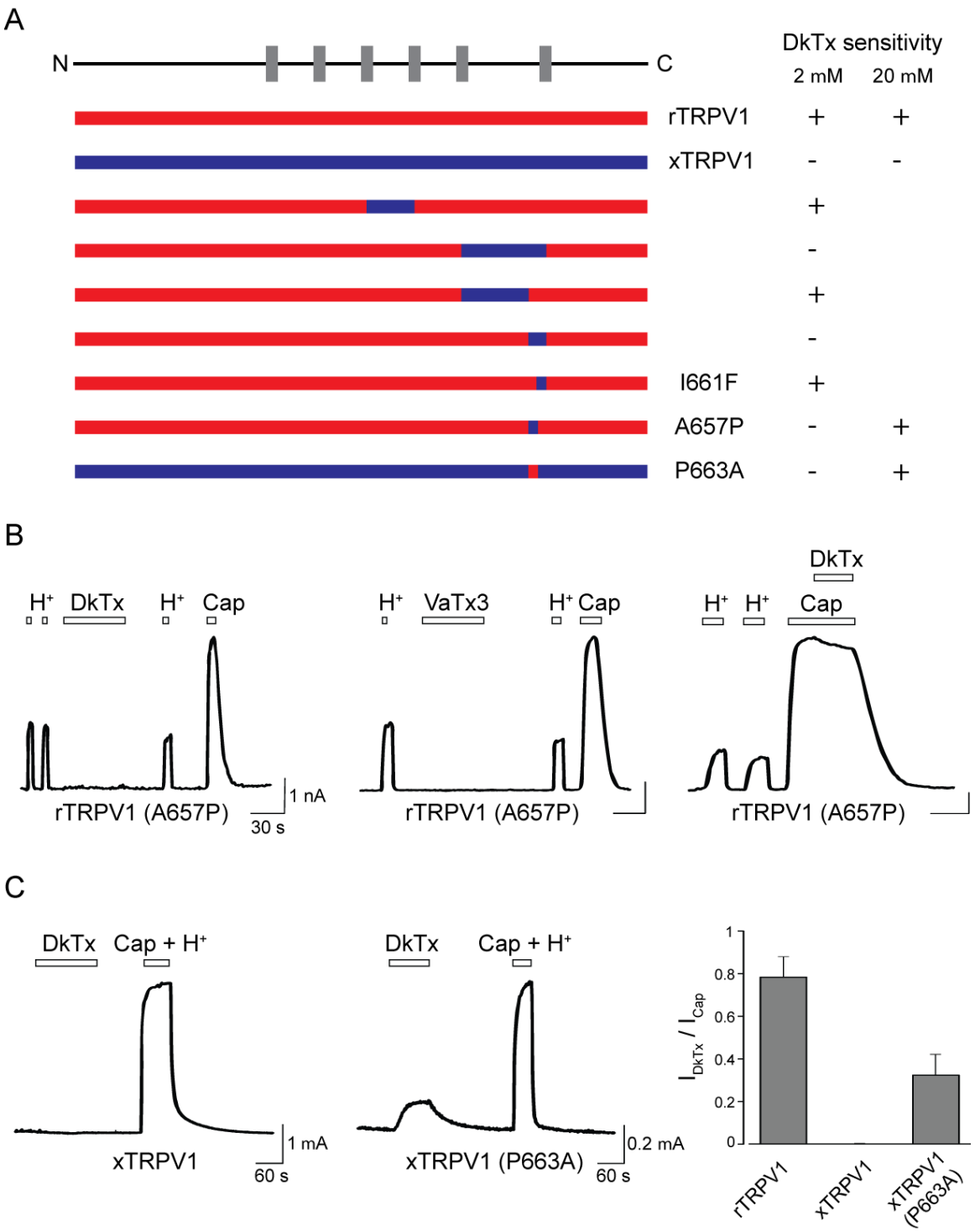
A
N
C
DkTx sensitivity
2 mM
20 mM
rTRPV1
+
+
xTRPV1
-
-
+
-
+
-
I661F
+
A657P
-
+
P663A
-
+
B
H+
DkTx
H+
Cap
1 nA
30 s
rTRPV1 (A657P)
H+
VaTx3
H+
Cap
rTRPV1 (A657P)
DkTx
H+
H+
Cap
rTRPV1 (A657P)
C
DkTx
Cap + H+
1 mA
60 s
xTRPV1
DkTx
Cap + H+
0.2 mA
60 s
xTRPV1 (P663A)
I DkTx / I Cap
1
0.8
0.6
0.4
0.2
0
rTRPV1
xTRPV1
xTRPV1 (P663A)

Figure 4 The TRPV1 pore domain specifies toxin sensitivity

(**A**) Chimeric channels were generated between rat and *Xenopus* TRPV1 orthologues (red and blue bars, respectively) based on the location of putative transmembrane domains (grey bars) All chimeras shown were activated by capsaicin. Selective sensitivity of rat TRPV1 to DkTx mapped to residue A657, which when replaced by the equivalent residue from the frog channel (P663) led to dramatically reduced toxin sensitivity. (**B**) Representative whole cell patch clamp recording (+80 mV) from HEK293 cells expressing the rat TRPV1 (A657P) mutant showed selective loss of DkTx (2 μM; left) or VaTx3 (2 μM; center) sensitivity. In contrast, sensitivity to capsaicin (Cap; 1 μM) and extracellular protons (H^+; pH 5.5) was retained. Co-application of capsaicin and DkTx (right) failed to produce persistent channel activation. (**C**) Representative two-electrode voltage clamp recordings (+80 mV) from *Xenopus* oocytes expressing wild type frog TRPV1 channel (left) shows specific insensitivity to DkTx (20 μM) versus capsaicin and protons (50 μM at pH 5.5). The frog TRPV1 P663A mutant (center) showed acquisition of toxin sensitivity. Note reversibility of toxin-evoked current. Graph at right shows average toxin responses for wild type rat, wild type frog, and mutant frog (P663A) channels normalized to capsaicin-evoked responses (n = 3-5 cells per bar; average values represent mean ± s.e.m.).

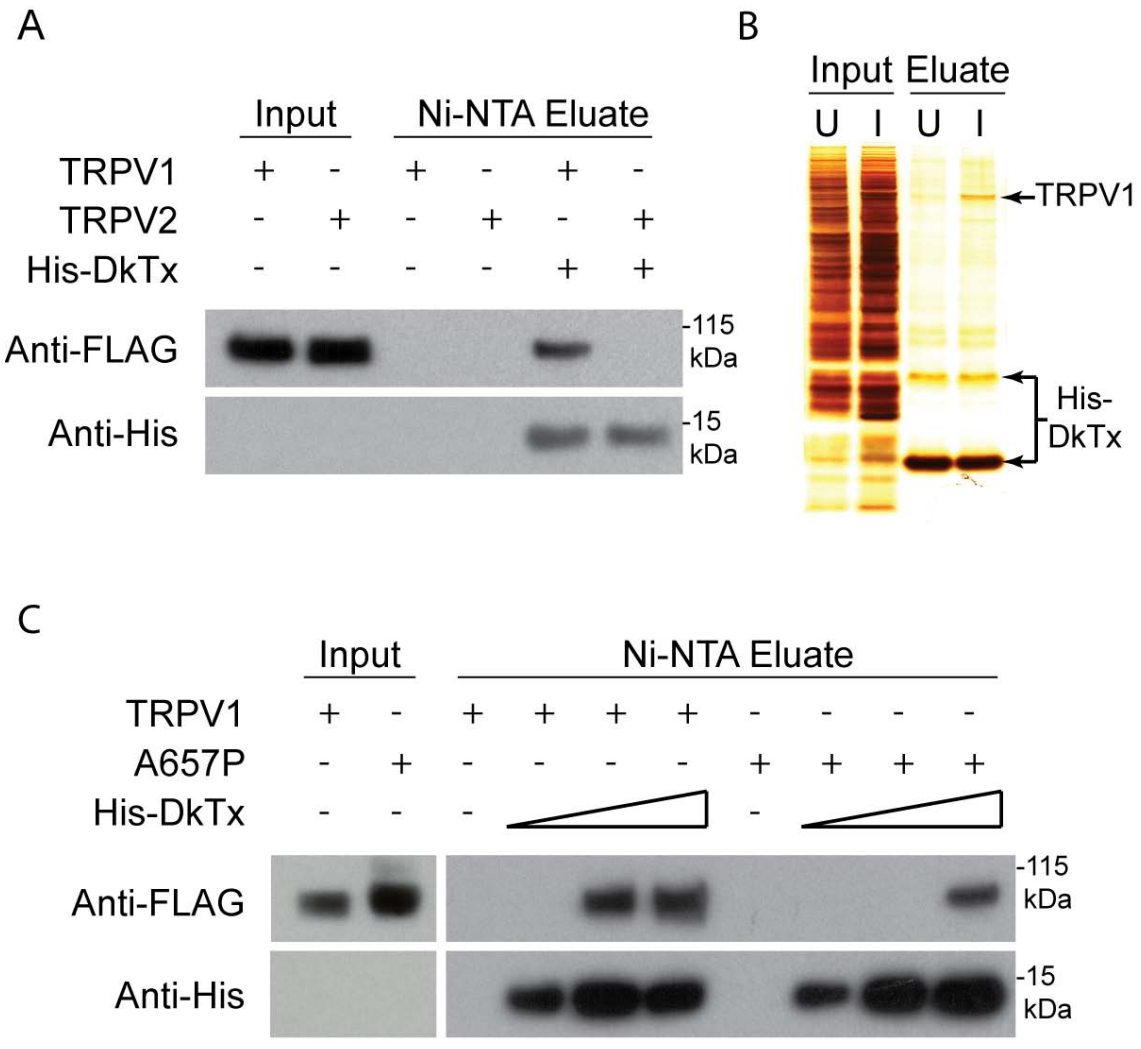
A
Input
Ni-NTA Eluate
TRPV1
TRPV2
His-DkTx
Anti-FLAG
Anti-His
-115 kDa
-15 kDa
B
Input Eluate
U I U I
TRPV1
His-DkTx
C
Input
Ni-NTA Eluate
TRPV1
A657P
His-DkTx
Anti-FLAG
Anti-His
-115 kDa
-15 kDa

Figure 5 DkTx binds directly to TRPV1 via association with the pore domain

(**A**) DkTx affinity resin retains detergent solubilized TRPV1, but not TRPV2 protein. Recombinant His-tagged DkTx was immobilized on nickel affinity (Ni-NTA) resin, to which affinity purified FLAG-tagged TRPV1 or TRPV2 protein (Input) was subsequently applied. After extensive washing, toxin-channel complexes were eluted and analyzed by Western blotting using anti-FLAG or anti-His antisera to detect channel or toxin protein, respectively. Complexes were observed with TRPV1, but not TRPV2 input, and were not detected with Ni-NTA beads lacking toxin. (**B**) Crude membrane extracts (Input) from uninduced (U) or induced (I) TRPV1-HEK293 cells were applied to DkTx-coupled resin. Bound material (Eluate) was recovered and analyzed by silver staining, showing substantial enrichment of TRPV1-toxin complexes over other membrane proteins. (**C**) TRPV1 A657P mutant binds less avidly to DkTx affinity resin. Purified wild type (TRPV1) and mutant (A657P) protein were analyzed for toxin binding as described in (A) using resins with increasing DkTx substitution (wedges depict 3-fold concentration range). Mutant (A657P) channel protein was retained only at the highest toxin density.

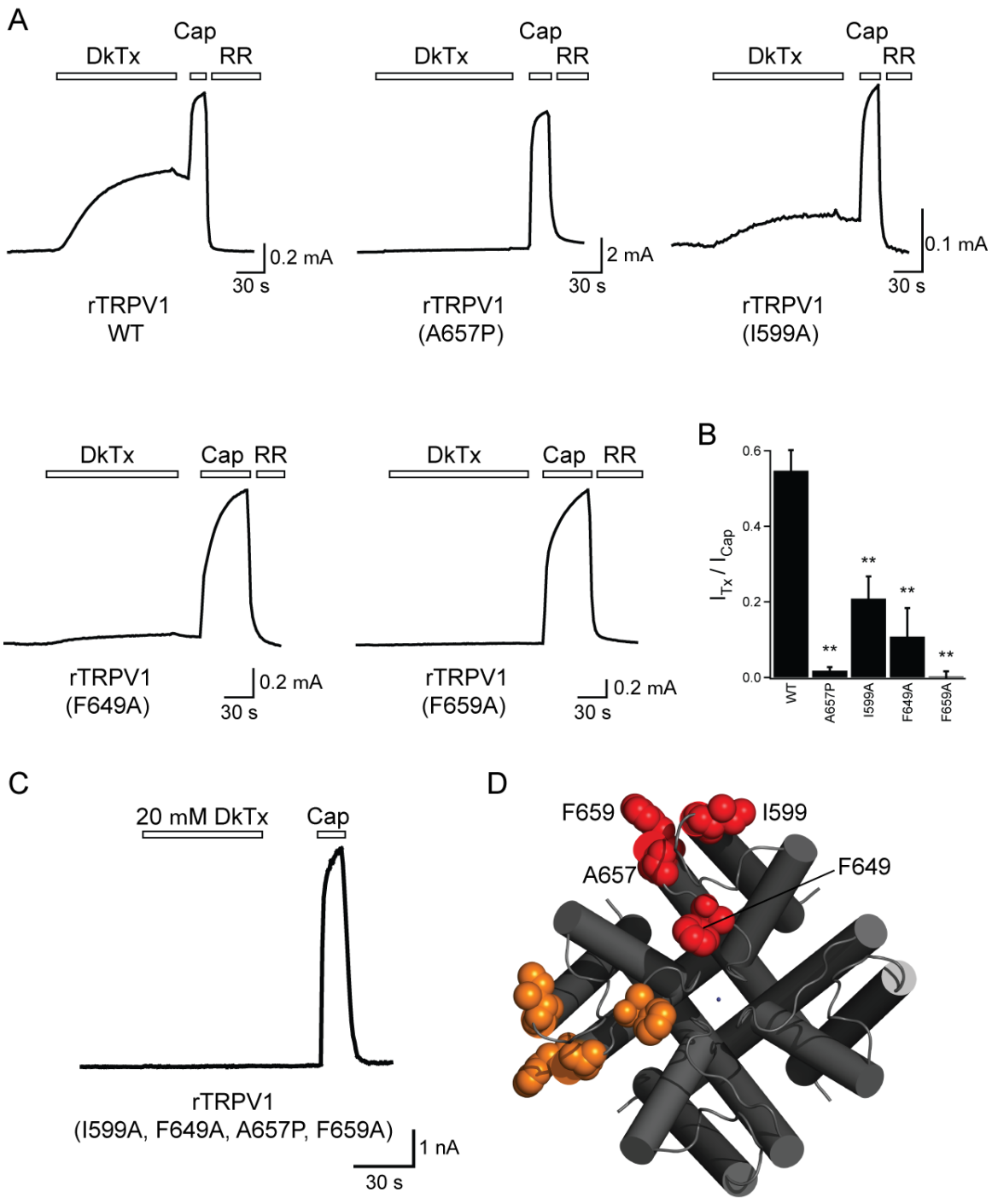
A
Cap
DkTx
RR
0.2 mA
30 s
rTRPV1
WT
2 mA
rTRPV1
(A657P)
0.1 mA
rTRPV1
(I599A)
rTRPV1
(F649A)
rTRPV1
(F659A)
B
I_{Tx} / I_{Cap}
0.6
0.4
0.2
0.0
**
WT
A657P
I599A
F649A
F659A
C
20 mM DkTx
rTRPV1
(I599A, F649A, A657P, F659A)
1 nA
D
F659
I599
A657
F649

Figure 6 Mutagenesis outlines a DkTx footprint on the extracellular face of TRPV1

(**A**) Representative voltage-clamp recordings (V_h = +80 mV) from oocytes expressing wild type or mutant rat TRPV1 channels in response to double knot toxin (DkTx; 1.5 μM), then capsaicin (Cap; 3 μM), followed by block with ruthenium red (RR; 80 mM). (**B**) Quantitative comparison of toxin-evoked responses normalized to a maximal capsaicin-evoked response. Note substantial and significant (n = 5 – 8 cells per mutant; average values represent mean ± s.e.m.; $p < 0.01$, one-way ANOVA) decrement in toxin sensitivity for all mutants shown versus wild type TRPV1. (**C**) Whole cell patch-clamp recording from a transfected HEK293 cell expressing a TRPV1 channel containing all four outer pore mutations shows complete loss of toxin sensitivity even when challenged with DkTx at a concentration (20 μM) exceeding the EC_{50} by 100-fold. (D) Putative locations of residues required for DkTx sensitivity are mapped onto a model pore domain based on the structure of the bacterial potassium channel, KcsA (Doyle et al., 1998). Amino acid side chains of TRPV1 residues I599, F649, A657, and F659 are shown in color, depicting a potential footprint of toxin binding. Red and orange groups correspond to bivalent DkTx attachment sites on adjacent channel subunits. Such an interaction may also be mediated through interaction with non-adjacent (orthogonal) subunits.

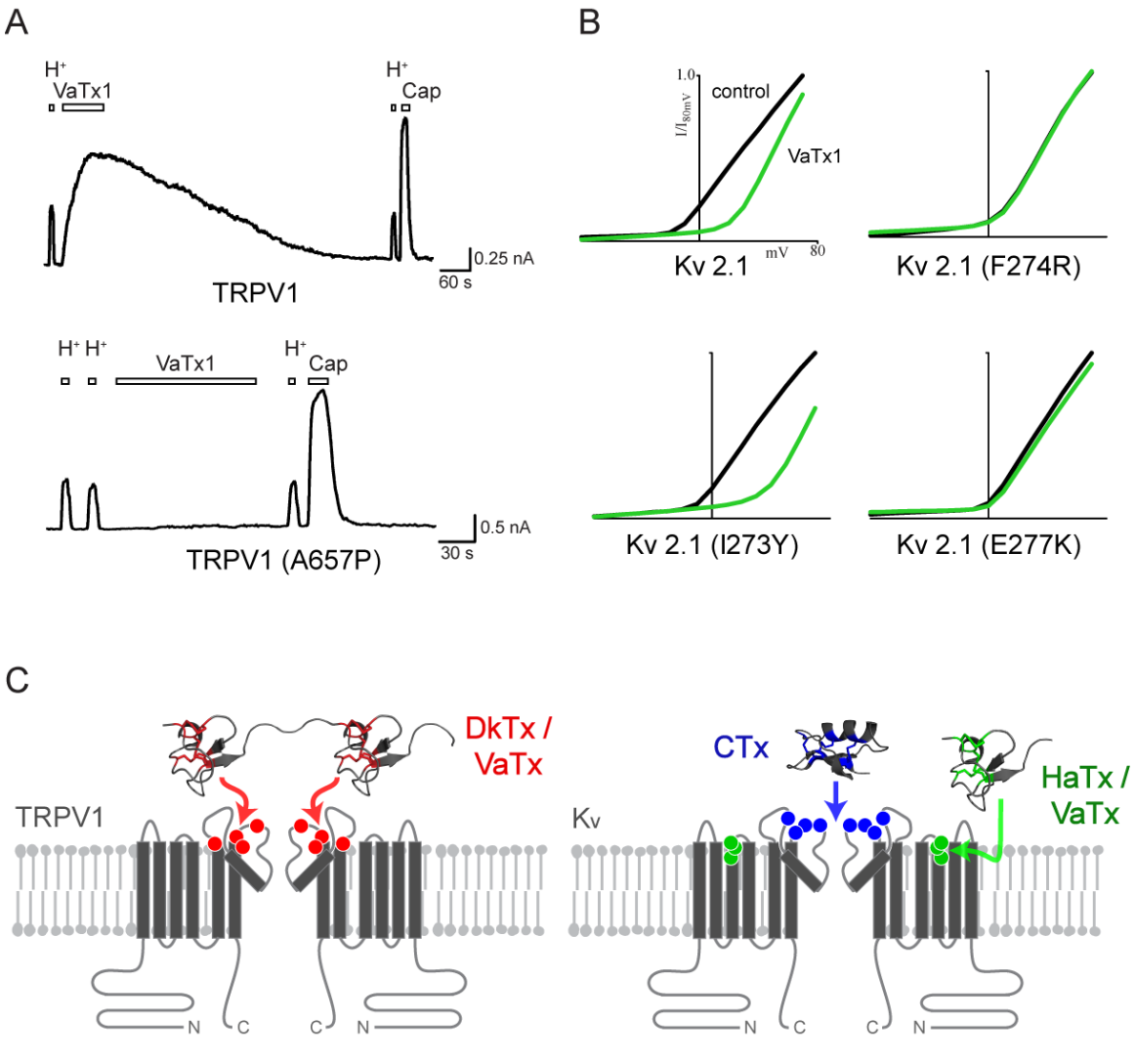
A
H+
VaTx1
H+
Cap
0.25 nA
60 s
TRPV1
H+ H+
VaTx1
H+
Cap
0.5 nA
30 s
TRPV1 (A657P)
B
1.0
control
VaTx1
mV
80
Kv 2.1
Kv 2.1 (F274R)
Kv 2.1 (I273Y)
Kv 2.1 (E277K)
C
TRPV1
DkTx /
VaTx
N
C
C
N
Kv
CTx
HaTx /
VaTx
N
C
C
N

Figure 7 VaTx1 targets distinct regions of TRPV1 and K_v2.1

(**A**) Representative whole cell patch clamp recording (+80 mV) from HEK293 cells expressing rat TRPV1 (top) or the TRPV1 (A657P) mutant (bottom) show VaTx1 (100 μM) activation of the wild type, but not the mutant channel. Capsaicin (Cap; 1 μM) and extracellular protons (H^+; pH 5.5) are shown for reference. (**B**) Two-electrode voltage clamp recordings from *Xenopus* oocytes expressing rat K_v2.1 voltage-gated potassium channels in the absence (black) and presence (green) of the vanillotoxin VaTx1 (20 μM). Two mutations (F274R and E277K) that are known to abrogate the inhibitory effect of hanatoxin on this channel also eliminated VaTx1-evoked inhibition, whereas a third (I273Y) had no substantial effect on VaTx1 action (n = 3 - 5 cells per trace). (**C**) Model of the transmembrane topology of TRPV1 (gray bars represent transmembrane helices) highlighting residues (red dots) that are crucial for double-knot toxin (DkTx) activation. In the simplest scenario, the two knots of DkTx bind to two equivalent sites on multiple subunits of the same channel. Kv channels likely possess the same overall transmembrane topology as TRPV1, but interact with ICK toxins in different ways. For example, charybdotoxin (CTx) binds within the ion permeation path to block ion flux, and voltage-modulator toxins, such as hanatoxin (HaTx), target the voltage sensor to modify gating properties (blue and green dots represent mutations that attenuate CTx and HaTx inhibition, respectively). Our findings suggest that single-knot vanillotoxins (VaTx) also target the S3-S4 helices of K_v channels, but activate TRPV1 through the pore region.

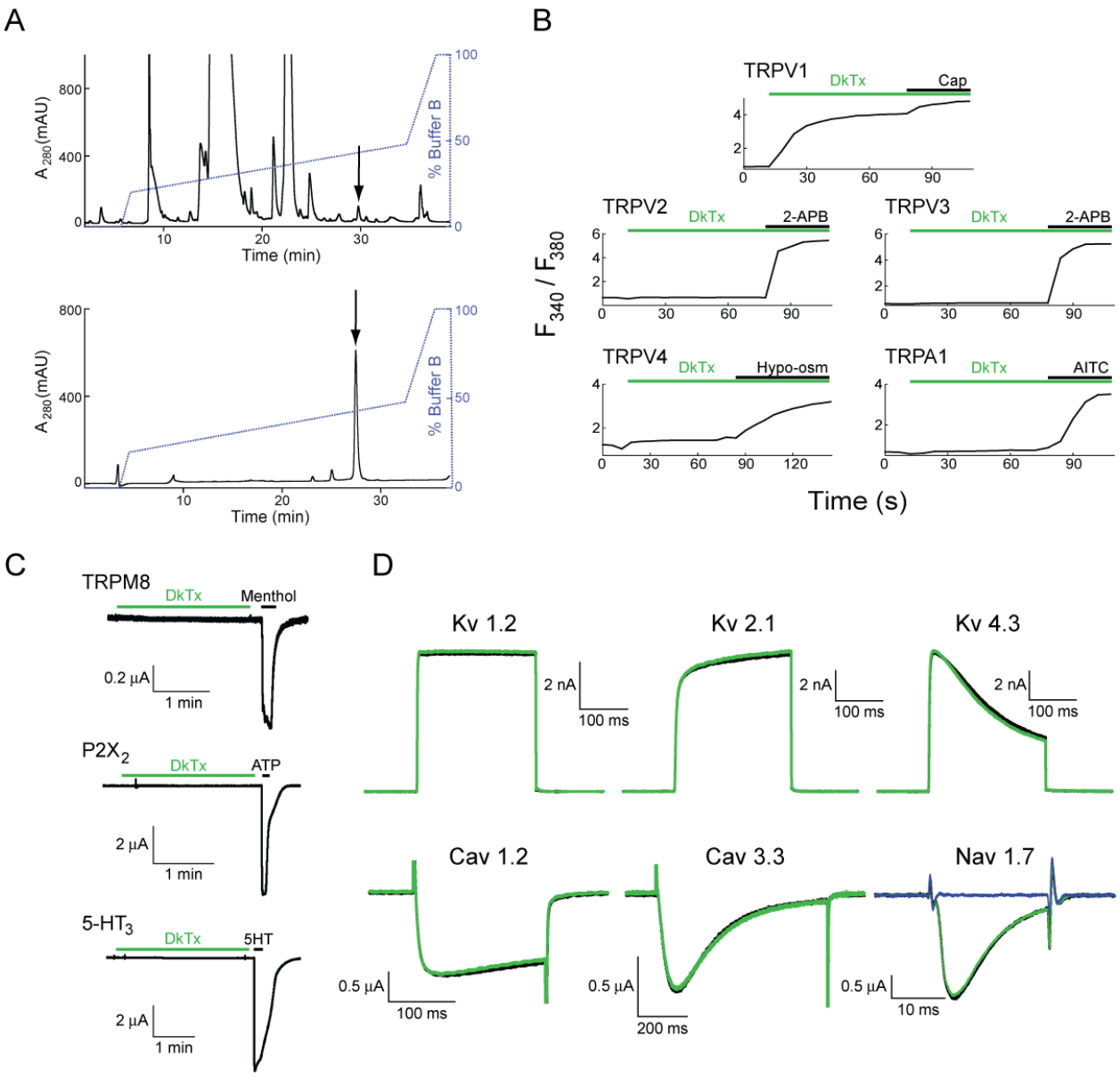
A
B
C
D
A280 (mAU)
% Buffer B
Time (min)
TRPV1
DkTx
Cap
TRPV2
2-APB
TRPV3
TRPV4
Hypo-osm
TRPA1
AITC
F340 / F380
Time (s)
TRPM8
Menthol
0.2 µA
1 min
P2X2
ATP
2 µA
5-HT3
5HT
Kv 1.2
Kv 2.1
Kv 4.3
2 nA
100 ms
Cav 1.2
Cav 3.3
Nav 1.7
0.5 µA
200 ms
10 ms

Figure 8 Purification and specificity of DkTx

(**A**) Reversed-phase C18 chromatogram of crude venom (top) or purified DkTx (bottom) from *O. huwena* spider. Arrows indicate position and retention time of DkTx (see Experimental Procedures for purification details). (**B**) Specificity of DkTx was examined using live cell ratiometric calcium imaging to test activation of various sensory TRP channels when expressed in transfected HEK293 cells. Application of purified DkTx (2 μM) was followed by a control agonist to confirm expression of functional channels; n≥ 75 cells per trace. (**C**) DkTx was tested for activity against several ligand-gated channels expressed in oocytes using two-electrode voltage-clamp methods (Vh=+80mV). Each channel tested (TRPM8, $P2X_2$, and 5-HT_3R-A) showed no response to extended application of DkTx (2μM), and responded normally to agonists applied immediately afterwards (200 μM menthol, 1mM ATP, and 10 μM serotonin respectively). (**D**) DkTx also did not affect the properties of voltage-gated potassium channels (K_v1.2, K_v2.1, and K_v4.3) expressed in HEK293 cells or voltage-gated calcium (Ca_v1.2 and Ca_v3.3) and sodium (Na_v1.7) channels expressed in oocytes, which all show equivalent responses both before (black) and after (green) application of 2μM DkTx for >1 minute. Na_v1.7 channels were blocked with 5 μM tetrodotoxin (blue).

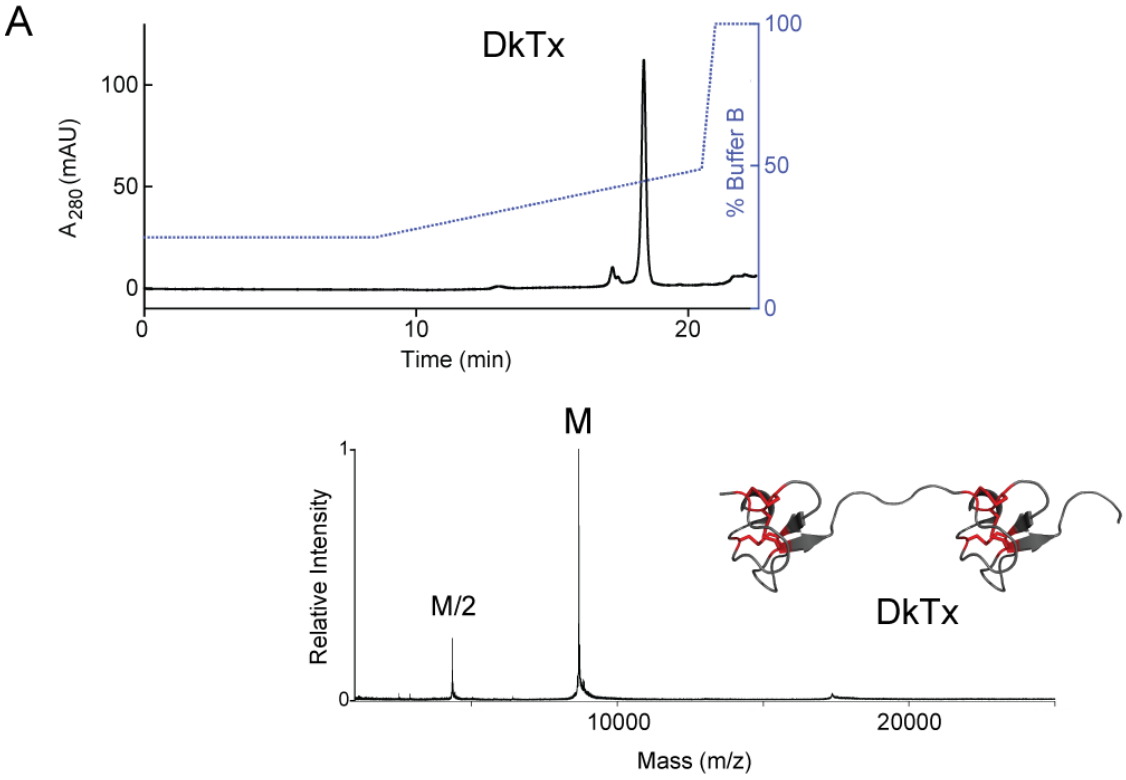
A
DkTx
100
50
0
A_{280} (mAU)
% Buffer B
100
50
0
0
10
20
Time (min)
M
1
0
Relative Intensity
M/2
DkTx
10000
20000
Mass (m/z)

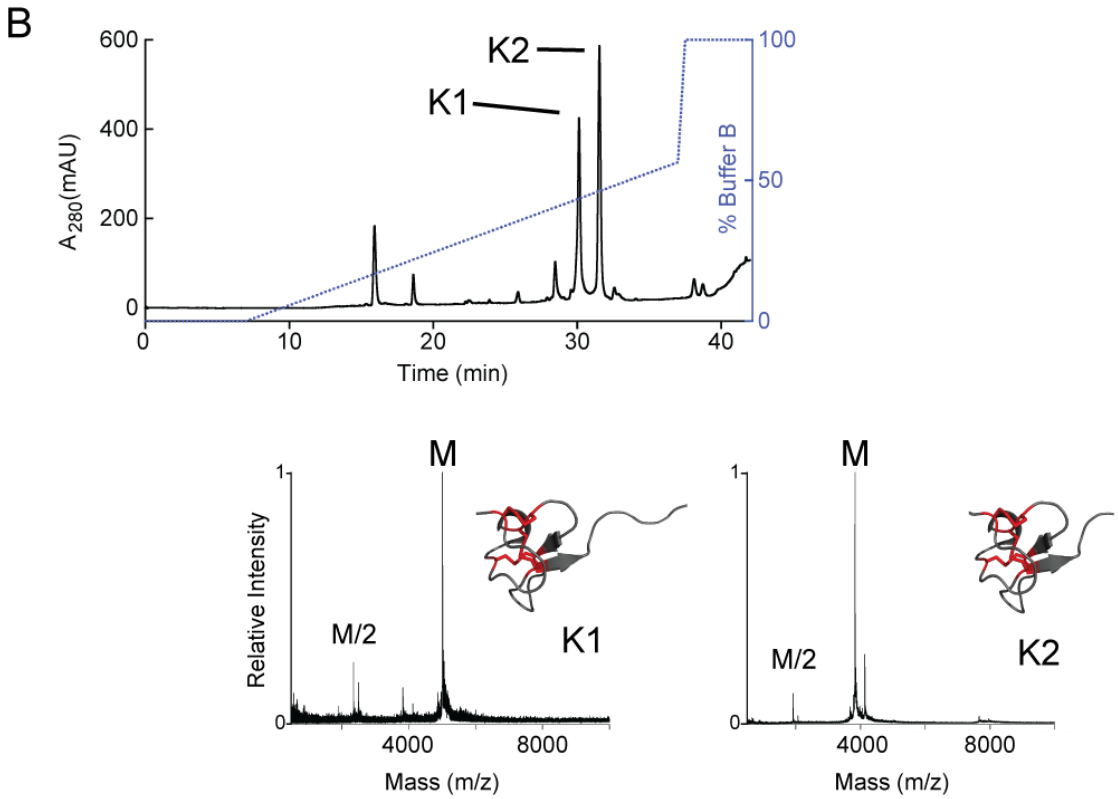
B
600
400
200
0
A_{280}(mAU)
K2
K1
100
50
0
% Buffer B
0
10
20
30
40
Time (min)
M
1
0
Relative Intensity
M/2
K1
4000
8000
Mass (m/z)
M
1
0
M/2
K2
4000
8000
Mass (m/z)

Figure 9 Biochemical analysis of recombinant toxins

(**A**) (Top) Reversed-phase C18 chromatogram of recombinant DkTx demonstrating its purity and similar retention time to the native toxin (see Figure 8). (Bottom) MALDI-TOF mass spectrometry profile of recombinant DkTx. The main species (M) and its doubly charged counterpart (M/2) exhibit a unit mass consistent with the molecular weight predicted from the toxin's deduced amino acid sequence (8684 versus 8685 Da). (**B**) Same analysis as in (A) for K1 and K2 products derived from Genenase I cleavage of recombinant HYR toxin. Observed and predicted masses were 5021 versus 5022 Da for K1 and 3837 versus 3837 Da for K2.

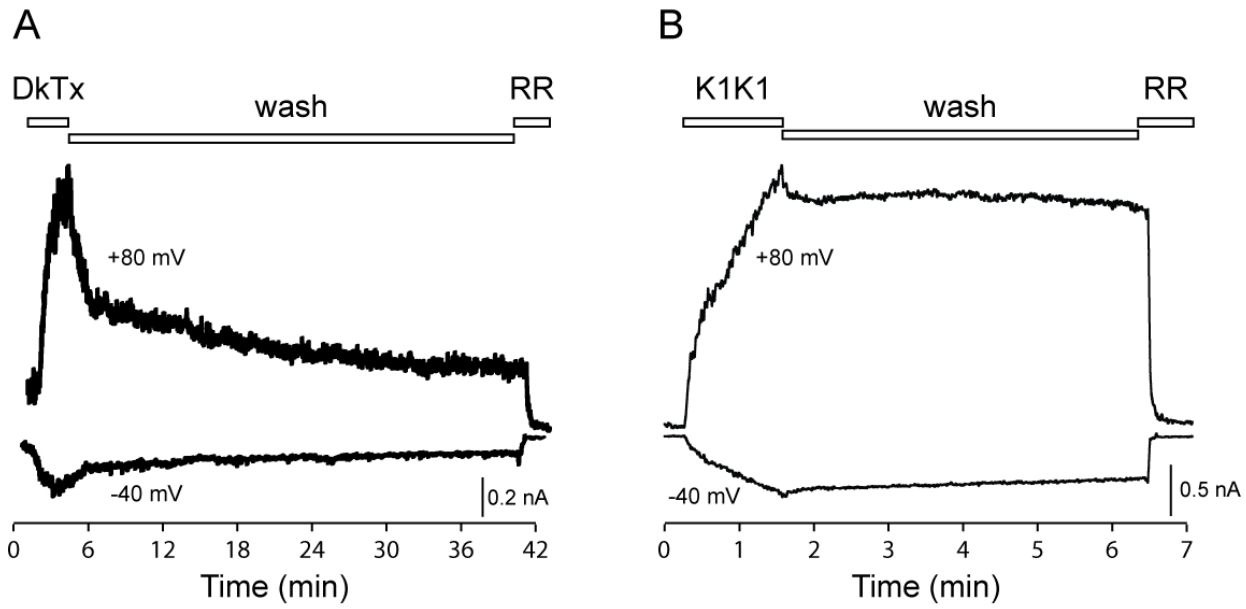

Figure 10 Double knot toxins elicit persistent TRPV1 activation

(**A**) Whole cell patch clamp recording from TRPV1-expressing HEK293 cells shows that exposure to native purified DkTx, even at low concentration (200 nM), produces an essentially irreversible, ruthenium red (RR; 4 μM) blockable current. Note persistence of toxin response even after 30 min washout (wash) period. (**B**) Same experiment as in (A) performed with synthetic K1K1 double know toxin (10 μM).

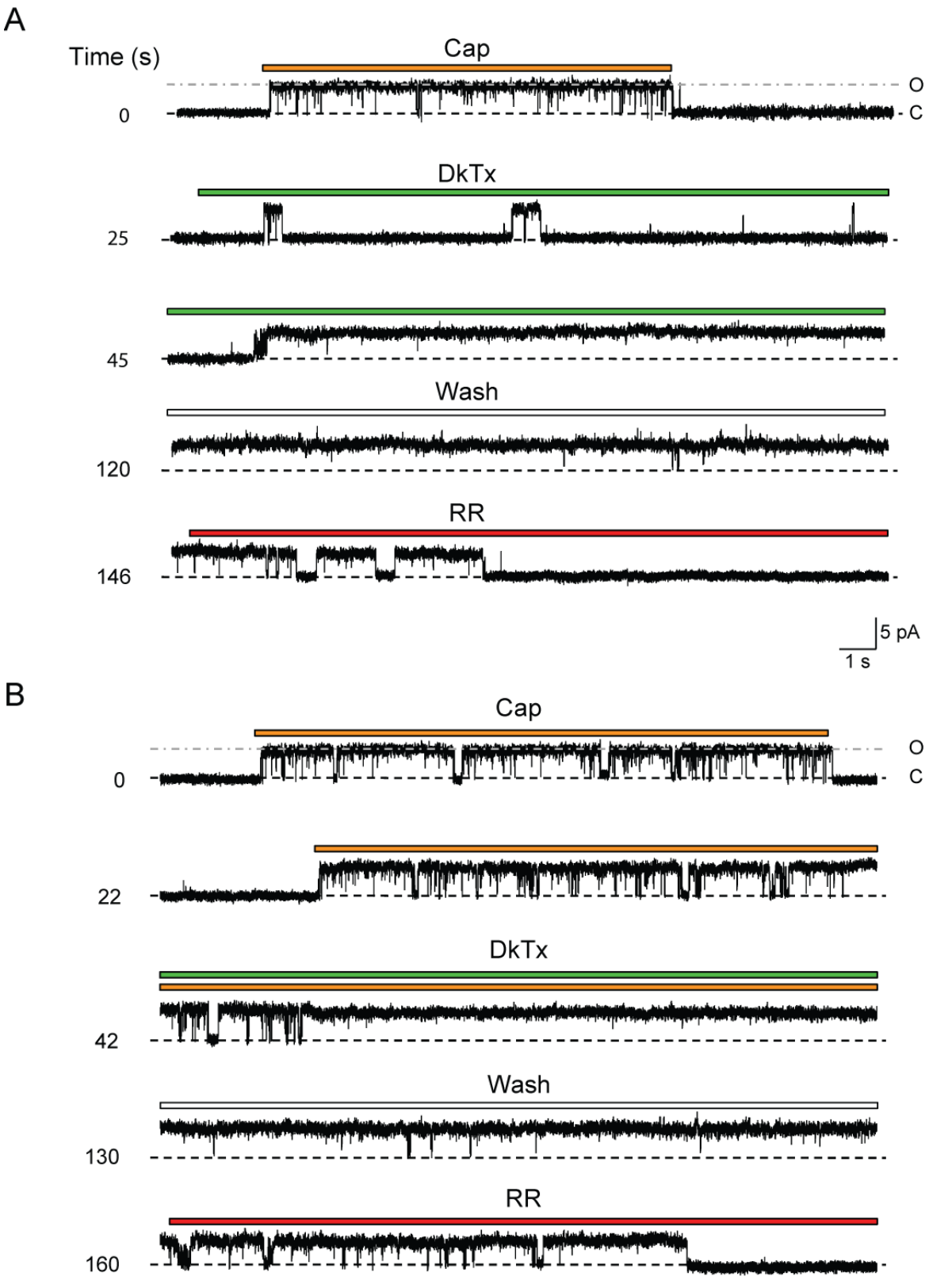
A
Time (s)
Cap
O
C
0
DkTx
25
45
Wash
120
RR
146
5 pA
1 s
B
Cap
O
C
0
22
DkTx
42
Wash
130
RR
160

Figure 11 DkTx traps single TRPV1 channels in the open state

(**A**) DkTx activates a single channel in an outside-out membrane patch excised from TRPV1-expressing HEK293 cells. A saturating concentration of capsaicin (Cap; 1 μM; orange bar) was initially applied to identify patches containing a single TRPV1 channel (V_h = +50 mV). Following capsaicin washout, DkTx (2 μM; green bar) was applied for 1 min, during which transient single channel events were initially observed, followed by conversion to a stable open state, which persisted even after 2 min of toxin washout (Wash; open bar). Subsequent application of the pore blocker, ruthenium red (RR; 5 μM; red bar) blocked the toxin-evoked current, first partially and then completely. Each trace shows a 20 s segment of a continuous record, with segment times denoted at left. Top and bottom dashed lines indicate open and closed states, respectively. (**B**) Application of DkTx to a capsaicin-activated channel promotes rapid conversion to the persistent open state. This experiment wad carried out as described in (A), except that capsaicin was both pre- and co-applied with a brief (30 sec) pulse of DkTx. Under these conditions, conversion to the persistent open state occurred within 5 sec, versus 25 sec when toxin was applied alone.

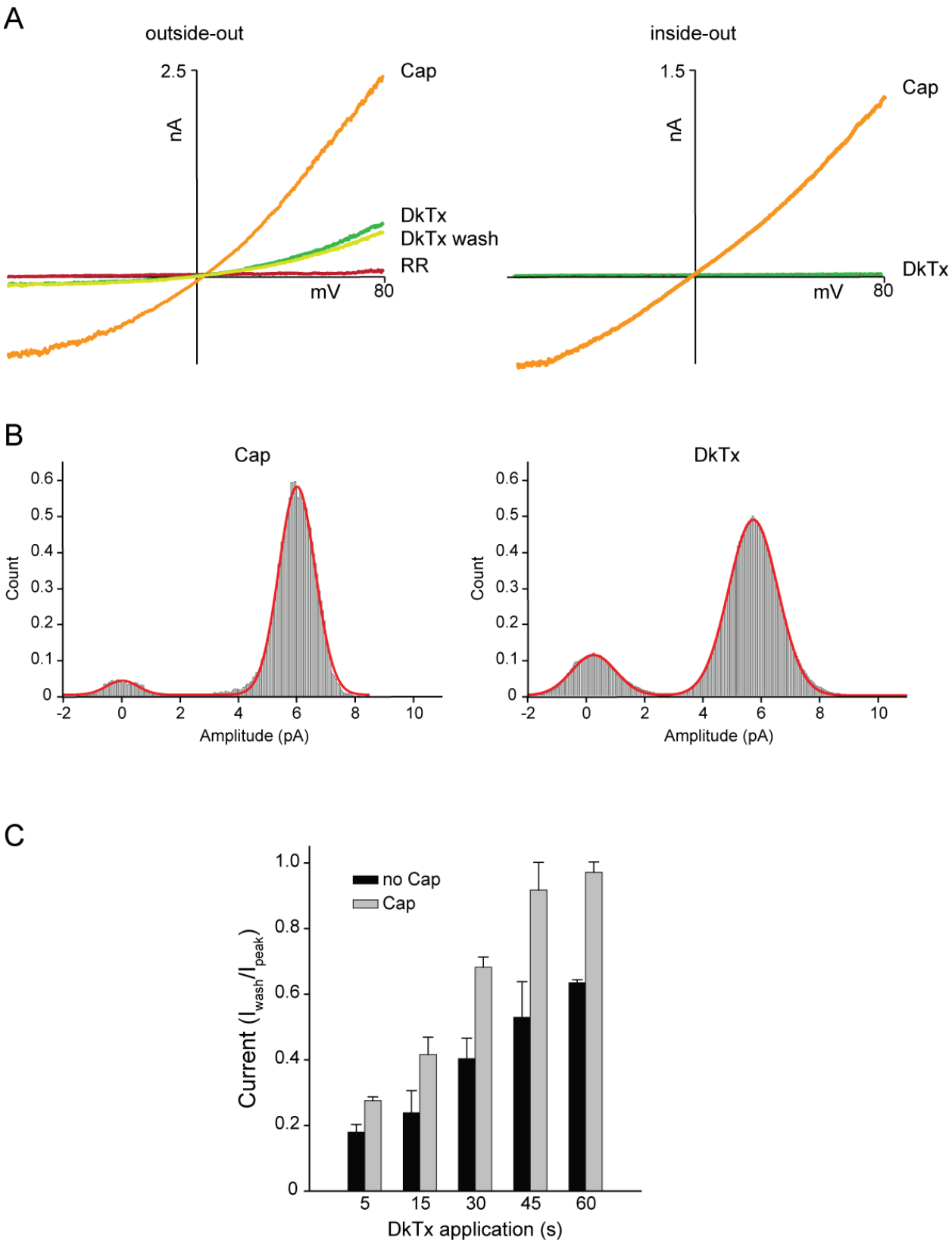
A
outside-out
2.5
nA
Cap
DkTx
DkTx wash
RR
mV
80
inside-out
1.5
nA
Cap
DkTx
mV
80
B
Cap
DkTx
Count
0.6
0.5
0.4
0.3
0.2
0.1
0
-2
0
2
4
6
8
10
Amplitude (pA)
C
no Cap
Cap
Current (I_wash/I_peak)
1.0
0.8
0.6
0.4
0.2
0
5
15
30
45
60
DkTx application (s)

Figure 12 Biophysical properties of DkTx-evoked responses

(**A**) Recordings from excised membrane patches showing that responses to DkTx (2 μM; dark green) could be elicited in the outside-out configuration only, and that this response persisted after a 5 min washout period (light green). Responses to capsaicin (1 μM; orange) served as positive control. (**B**) All point amplitude histograms of capsaicin (Cap) or DkTx-evoked single channel currents fitted with the sum of two Gaussian functions to determine closed and open amplitudes. Histograms were generated from recordings shown in Figure 4A. Unitary conductances (+50 mV) for capsaicin and DkTx were 118 and 103 pS, respectively. (**C**) Average DkTx (2 μM)-evoked persistent response (i.e. following 2 min washout) in the absence or presence of capsaicin (1 μM) measured over time and normalized to responses evoked by capsaicin alone (n = 3 – 8 cells per condition; for 30, 45, and 60 s time points, $p < 0.01$, unpaired Student's t-test). Average values represent mean ± s.e.m.

A

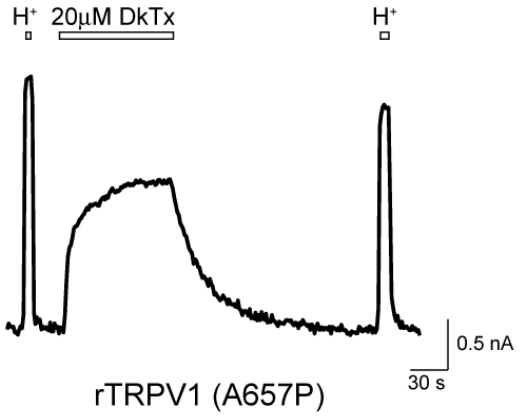

B

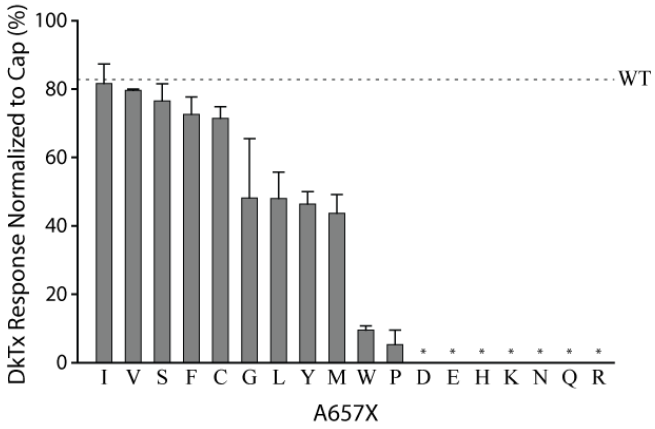

C

```
                    S1
WDRFVKRIFYFNFFVYCLYMIIFTAAAYYRPVEGLPPYKLKNTVGDYFRVTGEILSVSGG
WDHFVKRIFYFNFFAYIIYVIIFTIAAYYRPVDGSPPFPVQ--YGSYLRTSGELITVIGG
** ********** *  * **** ******* * **       * * *  **   * **
   S2                                  S3
VYFFFRGIQYFLQRRPSLKSLFVDSYSEILFFVQSLFMLVSVVLYFSQRKEYVASMVFSL
IYFFFRAIQYFTQRRPSLKALLADSYCEFLFFSQSVFLLLSTVLYFCGRNEYVAFLVICL
 ***** **** ******* *  *** * *** ** * * * ****  * ****  *  *
     S4                                      S5
AMGWTNMLYYTRGFQQMGIYAVMIEKMILRDLCRFMFVYLVFLFGFSTAVVTLIEDGKNN
AMSWANVLYYTRGFQLMGIYSVMIEKLILSDMVRFLFVYLLFLFGFAAALVTLIEDGEGR
** * * ******** **** ***** ** * *** **** *****  * *******
                          PH
SLPMESTPHKCRGSACKPG-NSYNSLYSTCLELFKFTIGMGDLEFTENYDFKAVFIILLL
----TDVNNTCGRRCCKPEPASYNNLYYTCQELFKFAIGMGDLEFTDNYKYKPVFIFLLI
          *    ***   *** ** ** ***** ********* **  * *** **
       S6
AYVILTYILLLNMLIALMGETVNKIA
TYVILTYILLLNMLIALMGETVSKVA
 ********************* * *
```

Figure 13 Mutational analysis of toxin action

(**A**) Whole cell patch clamp recording from HEK293 cells expressing the TRPV1 (A657P) mutant channel shows reversible (i.e. non-persistent) response to high dose (20 μM) DkTx. Responses to extracellular protons (H^+; pH 5.5) serve as positive control. (**B**) Average response of rTRPV1 A657X mutants to DkTx (0.5 μM) as measured by ratiometric live cell calcium imaging of transfected HEK293 cells. Dashed line indicated relative response obtained with wild type channel. All responses are normalized to that evoked by a saturating dose (10 μM) of capsaicin. Asterisks denote mutants showing no response to capsaicin; n = 3 - 4 trials per mutation. (**C**) Alignment between the transmembrane portions of rat and *Xenopus laevis* TRPV1 shows some identity (asterisks) but also substantial differences. Transmembrane helices S1-S6 predicted for rat TRPV1 (HHMTOP, http://www.enzim.hu/hmmtop/) are highlighted in yellow, with the presumptive pore helix (PH) shown in green. Residues that greatly impact toxin activation when mutated are in red.(Siemens et al., 2006)

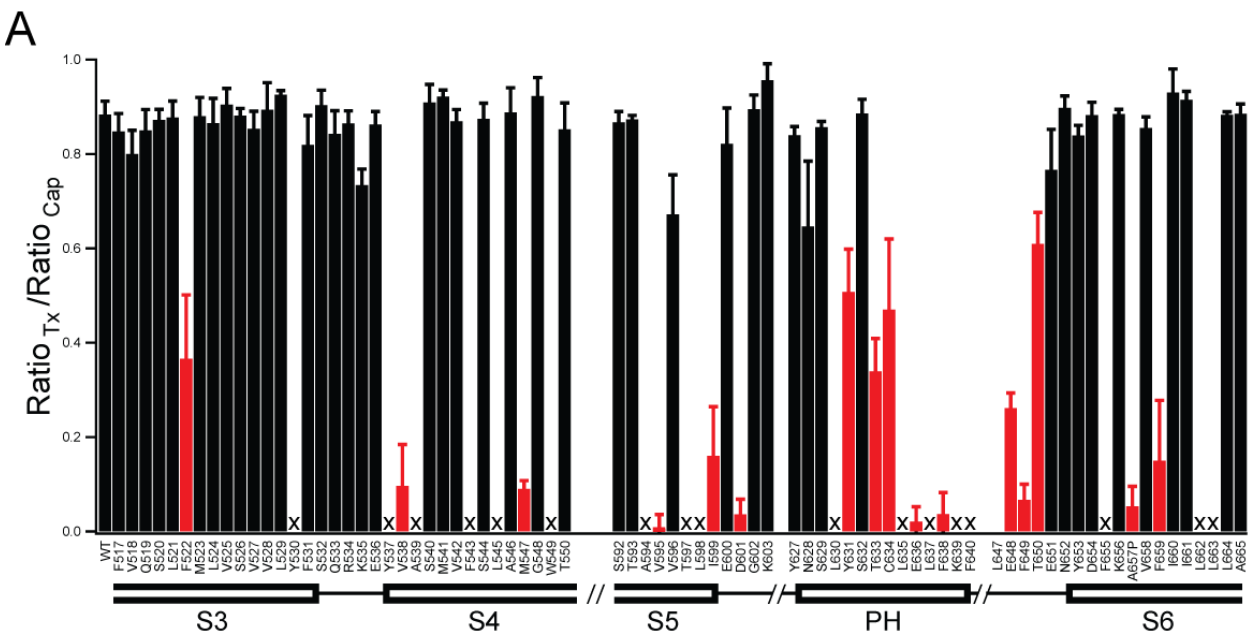
A
Ratio Tx /Ratio Cap
1.0
0.8
0.6
0.4
0.2
0.0
S3
S4
S5
PH
S6

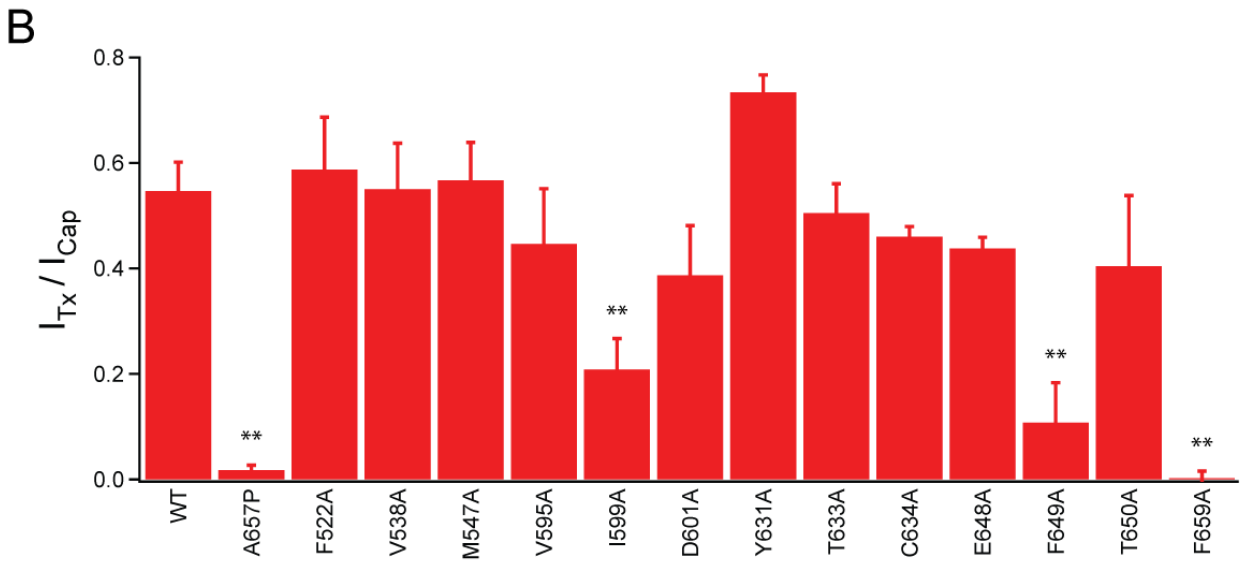
B
I Tx / I Cap
0.8
0.6
0.4
0.2
0.0
**
WT
A657P
F522A
V538A
M547A
V595A
I599A
D601A
Y631A
T633A
C634A
E648A
F649A
T650A
F659A

Figure 14 Alanine scanning of TRPV1 transmembrane region

(**A**) Alanine scanning mutagenesis was carried out on residues spanning the transmembrane (S3 through S6) and pore helix (PH) regions of rat TRPV1, as indicated. Sensitivity of each mutation to DkTx (2μM) versus capsaicin (10 μM) was assessed by ratiometric calcium imaging in transfected HEK293 cells (n = 75 cells per mutant in 3 independent trials; average values represent mean ± s.e.m.). 'X' marks mutations lacking response to either agonist. Each residue was mutated to alanine, except native alanines, which were changed to leucine. Because general decreases in channel expression and/or trafficking can produce false positive in this assay, all 'hits' (red bars) were taken forward for quantitative electrophysiological analysis. (**B**) Mutations taken forward from the initial calcium imaging screen were examined by two-electrode voltage-clamp analysis in oocytes (V_h = +80 mV). Of these, several mutants were confirmed as selectively diminishing toxin-evoked (1.5 μM) responses when normalized to those elicited by capsaicin (3 μM) (n = 4 - 8 cells per mutant; average values represent mean ± s.e.m.; ** $p < 0.01$, one-way ANOVA).

ACKNOWLEDGEMENTS

We thank Ben Myers for cloning the frog TRPV1 cDNA and making it available for this study, and to Roger Nicoll, Alex Chesler, Julio Cordero, Erhu Cao, and other members of our lab for helpful criticism and reading of the manuscript. We also thank the UCSF Mass Spectrometry Resource for instrumentation and technical assistance, supported by the NIH NRCC. This work was supported by a NIH/NINDS Ruth Kirschstein predoctoral fellowship (C.B.), postdoctoral fellowships from the Damon Runyon Cancer Research Foundation (A.P.) and the International Human Frontier Science Program Organization (J.S.), and grants from the NIH/NINDS (D.J.).

REFERENCES

Abe, T. (1978). [beta-bungarotoxin (author's transl)]. Tanpakushitsu Kakusan Koso *23*, 170-181.

Alabi, A.A., Bahamonde, M.I., Jung, H.J., Kim, J.I., and Swartz, K.J. (2007). Portability of paddle motif function and pharmacology in voltage sensors. Nature *450*, 370-375.

Andreev, Y.A., Kozlov, S.A., Koshelev, S.G., Ivanova, E.A., Monastyrnaya, M.M., Kozlovskaya, E.P., and Grishin, E.V. (2008). Analgesic compound from sea anemone Heteractis crispa is the first polypeptide inhibitor of vanilloid receptor 1 (TRPV1). J Biol Chem *283*, 23914-23921.

Appendino, G., and Szallasi, A. (1997). Euphorbium: modern research on its active principle, resiniferatoxin, revives an ancient medicine. Life Sci *60*, 681-696.

Askwith, C.C., Cheng, C., Ikuma, M., Benson, C., Price, M.P., and Welsh, M.J. (2000). Neuropeptide FF and FMRFamide potentiate acid-evoked currents from sensory neurons and proton-gated DEG/ENaC channels. Neuron *26*, 133-141.

Basbaum, A.I., Bautista, D.M., Scherrer, G., and Julius, D. (2009). Cellular and molecular mechanisms of pain. Cell *139*, 267-284.

Bautista, D.M., Movahed, P., Hinman, A., Axelsson, H.E., Sterner, O., Hogestatt, E.D., Julius, D., Jordt, S.E., and Zygmunt, P.M. (2005). Pungent products from garlic activate the sensory ion channel TRPA1. Proceedings of the National Academy of Sciences of the United States of America *102*, 12248-12252.

Beeton, C., Gutman, G.A., and Chandy, K.G. (2006). Targets and Therapeutic Properties of Venom Peptides. In Handbook of biologically active peptides, A.J. Kastin, ed. (Amsterdam ; Boston, Academic Press), pp. 403-412.

Berg, O.G., Gelb, M.H., Tsai, M.D., and Jain, M.K. (2001). Interfacial enzymology: the secreted phospholipase A(2)-paradigm. Chem Rev *101*, 2613-2654.

Bohlen, C.J., Chesler, A.T., Sharif-Naeini, R., Medzihradszky, K.F., Zhou, S., King, D., Sanchez, E.E., Burlingame, A.L., Basbaum, A.I., and Julius, D. (2011). A heteromeric Texas coral snake toxin targets acid-sensing ion channels to produce pain. Nature *479*, 410-414.

Bohlen, C.J., Priel, A., Zhou, S., King, D., Siemens, J., and Julius, D. (2010). A bivalent tarantula toxin activates the capsaicin receptor, TRPV1, by targeting the outer pore domain. Cell *141*, 834-845.

Bon, C., Changeux, J.P., Jeng, T.W., and Fraenkel-Conrat, H. (1979). Postsynaptic effects of crotoxin and of its isolated subunits. Eur J Biochem *99*, 471-481.

Brauchi, S., Orio, P., and Latorre, R. (2004). Clues to understanding cold sensation: thermodynamics and electrophysiological analysis of the cold receptor TRPM8. Proceedings of the National Academy of Sciences of the United States of America *101*, 15494-15499.

Brown, A.M., Yatani, A., Lacerda, A.E., Gurrola, G.B., and Possani, L.D. (1987). Neurotoxins that act selectively on voltage-dependent cardiac calcium channels. Circ Res *61*, I6-9.

Bulaj, G., and Olivera, B.M. (2008). Folding of conotoxins: formation of the native disulfide bridges during chemical synthesis and biosynthesis of Conus peptides. Antioxidants & redox signaling *10*, 141-155.

Caleo, M., and Schiavo, G. (2009). Central effects of tetanus and botulinum neurotoxins. Toxicon *54*, 593-599.

Caterina, M.J., Leffler, A., Malmberg, A.B., Martin, W.J., Trafton, J., Petersen-Zeitz, K.R., Koltzenburg, M., Basbaum, A.I., and Julius, D. (2000). Impaired nociception and pain sensation in mice lacking the capsaicin receptor. Science *288*, 306-313.

Caterina, M.J., Schumacher, M.A., Tominaga, M., Rosen, T.A., Levine, J.D., and Julius, D. (1997). The capsaicin receptor: a heat-activated ion channel in the pain pathway. Nature *389*, 816-824.

Catterall, W.A., Cestele, S., Yarov-Yarovoy, V., Yu, F.H., Konoki, K., and Scheuer, T. (2007). Voltage-gated ion channels and gating modifier toxins. Toxicon *49*, 124-141.

Cavanaugh, D.J., Chesler, A.T., Jackson, A.C., Sigal, Y.M., Yamanaka, H., Grant, R., O'Donnell, D., Nicoll, R.A., Shah, N.M., Julius, D.*, et al.* (2011). Trpv1 reporter mice reveal highly restricted brain distribution and functional expression in arteriolar smooth muscle cells. J Neurosci *31*, 5067-5077.

Cavanaugh, D.J., Lee, H., Lo, L., Shields, S.D., Zylka, M.J., Basbaum, A.I., and Anderson, D.J. (2009). Distinct subsets of unmyelinated primary sensory fibers mediate behavioral responses to noxious thermal and mechanical stimuli. Proceedings of the National Academy of Sciences of the United States of America *106*, 9075-9080.

Cestele, S., Qu, Y., Rogers, J.C., Rochat, H., Scheuer, T., and Catterall, W.A. (1998). Voltage sensor-trapping: enhanced activation of sodium channels by beta-scorpion toxin bound to the S3-S4 loop in domain II. Neuron *21*, 919-931.

Chahl, L.A., and Kirk, E.J. (1975). Toxins which produce pain. Pain *1*, 3-49.

Chang, C.C. (1999). Looking back on the discovery of alpha-bungarotoxin. J Biomed Sci *6*, 368-375.

Chen, X., Kalbacher, H., and Grunder, S. (2006). Interaction of acid-sensing ion channel (ASIC) 1 with the tarantula toxin psalmotoxin 1 is state dependent. J Gen Physiol *127*, 267-276.

Choi, S.-k. (2004). Synthetic multivalent molecules : concepts and biomedical applications (Hoboken, N.J., Wiley).

Chou, M.Z., Mtui, T., Gao, Y.D., Kohler, M., and Middleton, R.E. (2004). Resiniferatoxin binds to the capsaicin receptor (TRPV1) near the extracellular side of the S4 transmembrane domain. Biochemistry *43*, 2501-2511.

Christopoulos, A., Grant, M.K., Ayoubzadeh, N., Kim, O.N., Sauerberg, P., Jeppesen, L., and El-Fakahany, E.E. (2001). Synthesis and pharmacological evaluation of dimeric muscarinic acetylcholine receptor agonists. J Pharmacol Exp Ther *298*, 1260-1268.

Chuang, H.H., Neuhausser, W.M., and Julius, D. (2004). The super-cooling agent icilin reveals a mechanism of coincidence detection by a temperature-sensitive TRP channel. Neuron *43*, 859-869.

Cnudde, S.E., Prorok, M., Castellino, F.J., and Geiger, J.H. (2010). Metal ion determinants of conantokin dimerization as revealed in the X-ray crystallographic structure of the Cd(2+)/Mg (2+)-con-T[K7gamma] complex. J Biol Inorg Chem *15*, 667-675.

Cnudde, S.E., Prorok, M., Dai, Q., Castellino, F.J., and Geiger, J.H. (2007). The crystal structures of the calcium-bound con-G and con-T[K7gamma] dimeric peptides demonstrate a metal-dependent helix-forming motif. J Am Chem Soc *129*, 1586-1593.

Conticello, S.G., Gilad, Y., Avidan, N., Ben-Asher, E., Levy, Z., and Fainzilber, M. (2001). Mechanisms for evolving hypervariability: the case of conopeptides. Mol Biol Evol *18*, 120-131.

Craik, D.J., and Adams, D.J. (2007). Chemical modification of conotoxins to improve stability and activity. ACS Chem Biol *2*, 457-468.

Craik, D.J., Daly, N.L., and Waine, C. (2001). The cystine knot motif in toxins and implications for drug design. Toxicon *39*, 43-60.

Cuypers, E., Yanagihara, A., Karlsson, E., and Tytgat, J. (2006). Jellyfish and other cnidarian envenomations cause pain by affecting TRPV1 channels. FEBS Lett *580*, 5728-5732.

Cuypers, E., Yanagihara, A., Rainier, J.D., and Tytgat, J. (2007). TRPV1 as a key determinant in ciguatera and neurotoxic shellfish poisoning. Biochem Biophys Res Commun *361*, 214-217.

Dai, Q., Prorok, M., and Castellino, F.J. (2004). A new mechanism for metal ion-assisted interchain helix assembly in a naturally occurring peptide mediated by optimally spaced gamma-carboxyglutamic acid residues. J Mol Biol *336*, 731-744.

Dai, Q., Sheng, Z., Geiger, J.H., Castellino, F.J., and Prorok, M. (2007). Helix-helix interactions between homo- and heterodimeric gamma-carboxyglutamate-containing conantokin peptides and their derivatives. J Biol Chem *282*, 12641-12649.

Daly, N.L., and Craik, D.J. (2011). Bioactive cystine knot proteins. Curr Opin Chem Biol *15*, 362-368.

Davis, J.B., Gray, J., Gunthorpe, M.J., Hatcher, J.P., Davey, P.T., Overend, P., Harries, M.H., Latcham, J., Clapham, C., Atkinson, K.*, et al.* (2000). Vanilloid receptor-1 is essential for inflammatory thermal hyperalgesia. Nature *405*, 183-187.

Deval, E., Gasull, X., Noel, J., Salinas, M., Baron, A., Diochot, S., and Lingueglia, E. (2010). Acid-sensing ion channels (ASICs): pharmacology and implication in pain. Pharmacol Ther *128*, 549-558.

Deval, E., Noel, J., Gasull, X., Delaunay, A., Alloui, A., Friend, V., Eschalier, A., Lazdunski, M., and Lingueglia, E. (2011). Acid-sensing ion channels in postoperative pain. J Neurosci *31*, 6059-6066.

Diao, J., Lin, Y., Tang, J., and Liang, S. (2003). cDNA sequence analysis of seven peptide toxins from the spider Selenocosmia huwena. Toxicon *42*, 715-723.

Diochot, S., Baron, A., Rash, L.D., Deval, E., Escoubas, P., Scarzello, S., Salinas, M., and Lazdunski, M. (2004). A new sea anemone peptide, APETx2, inhibits ASIC3, a major acid-sensitive channel in sensory neurons. The EMBO journal *23*, 1516-1525.

Doley, R., and Kini, R.M. (2009). Protein complexes in snake venom. Cell Mol Life Sci *66*, 2851-2871.

Doorty, K.B., Bevan, S., Wadsworth, J.D., and Strong, P.N. (1997). A novel small conductance Ca2+-activated K+ channel blocker from Oxyuranus scutellatus taipan venom. Re-evaluation of taicatoxin as a selective Ca2+ channel probe. J Biol Chem *272*, 19925-19930.

Doyle, D.A., Morais Cabral, J., Pfuetzner, R.A., Kuo, A., Gulbis, J.M., Cohen, S.L., Chait, B.T., and MacKinnon, R. (1998). The structure of the potassium channel: molecular basis of K+ conduction and selectivity. Science *280*, 69-77.

Drew, L.J., Rohrer, D.K., Price, M.P., Blaver, K.E., Cockayne, D.A., Cesare, P., and Wood, J.N. (2004). Acid-sensing ion channels ASIC2 and ASIC3 do not contribute to

mechanically activated currents in mammalian sensory neurones. J Physiol *556*, 691-710.

Dreyer, F., and Penner, R. (1987). The actions of presynaptic snake toxins on membrane currents of mouse motor nerve terminals. J Physiol *386*, 455-463.

Ducancel, F., Matre, V., Dupont, C., Lajeunesse, E., Wollberg, Z., Bdolah, A., Kochva, E., Boulain, J.C., and Menez, A. (1993). Cloning and sequence analysis of cDNAs encoding precursors of sarafotoxins. Evidence for an unusual "rosary-type" organization. J Biol Chem *268*, 3052-3055.

Duda, T.F., Jr., and Palumbi, S.R. (1999). Molecular genetics of ecological diversification: duplication and rapid evolution of toxin genes of the venomous gastropod Conus. Proceedings of the National Academy of Sciences of the United States of America *96*, 6820-6823.

Dutton, J.L., and Craik, D.J. (2001). alpha-Conotoxins: nicotinic acetylcholine receptor antagonists as pharmacological tools and potential drug leads. Curr Med Chem *8*, 327-344.

Escoubas, P., De Weille, J.R., Lecoq, A., Diochot, S., Waldmann, R., Champigny, G., Moinier, D., Menez, A., and Lazdunski, M. (2000). Isolation of a tarantula toxin specific for a class of proton-gated Na+ channels. J Biol Chem *275*, 25116-25121.

Escoubas, P., Diochot, S., Celerier, M.L., Nakajima, T., and Lazdunski, M. (2002). Novel tarantula toxins for subtypes of voltage-dependent potassium channels in the Kv2 and Kv4 subfamilies. Mol Pharmacol *62*, 48-57.

Escoubas, P., and Rash, L. (2004). Tarantulas: eight-legged pharmacists and combinatorial chemists. Toxicon *43*, 555-574.

French, R.J., Yoshikami, D., Sheets, M.F., and Olivera, B.M. (2010). The tetrodotoxin receptor of voltage-gated sodium channels--perspectives from interactions with micro-conotoxins. Mar Drugs *8*, 2153-2161.

Friedrich, T., Kroger, B., Bialojan, S., Lemaire, H.G., Hoffken, H.W., Reuschenbach, P., Otte, M., and Dodt, J. (1993). A Kazal-type inhibitor with thrombin specificity from Rhodnius prolixus. J Biol Chem *268*, 16216-16222.

Fry, B.G., Roelants, K., Champagne, D.E., Scheib, H., Tyndall, J.D., King, G.F., Nevalainen, T.J., Norman, J.A., Lewis, R.J., Norton, R.S.*, et al.* (2009). The toxicogenomic multiverse: convergent recruitment of proteins into animal venoms. Annu Rev Genomics Hum Genet *10*, 483-511.

Fry, B.G., Roelants, K., Winter, K., Hodgson, W.C., Griesman, L., Kwok, H.F., Scanlon, D., Karas, J., Shaw, C., Wong, L.*, et al.* (2010). Novel venom proteins produced by differential domain-expression strategies in beaded lizards and gila monsters (genus Heloderma). Mol Biol Evol *27*, 395-407.

Fry, B.G., Vidal, N., Norman, J.A., Vonk, F.J., Scheib, H., Ramjan, S.F., Kuruppu, S., Fung, K., Hedges, S.B., Richardson, M.K.*, et al.* (2006). Early evolution of the venom system in lizards and snakes. Nature *439*, 584-588.

Gargano, J.M., Ngo, T., Kim, J.Y., Acheson, D.W., and Lees, W.J. (2001). Multivalent inhibition of AB(5) toxins. J Am Chem Soc *123*, 12909-12910.

Gavva, N.R., Klionsky, L., Qu, Y., Shi, L., Tamir, R., Edenson, S., Zhang, T.J., Viswanadhan, V.N., Toth, A., Pearce, L.V.*, et al.* (2004). Molecular determinants of vanilloid sensitivity in TRPV1. J Biol Chem *279*, 20283-20295.

Gelly, J.C., Gracy, J., Kaas, Q., Le-Nguyen, D., Heitz, A., and Chiche, L. (2004). The KNOTTIN website and database: a new information system dedicated to the knottin scaffold. Nucleic acids research *32*, D156-159.

Goldstein, S.A., Pheasant, D.J., and Miller, C. (1994). The charybdotoxin receptor of a Shaker K+ channel: peptide and channel residues mediating molecular recognition. Neuron *12*, 1377-1388.

Grandl, J., Hu, H., Bandell, M., Bursulaya, B., Schmidt, M., Petrus, M., and Patapoutian, A. (2008). Pore region of TRPV3 ion channel is specifically required for heat activation. Nature neuroscience *11*, 1007-1013.

Gross, A., Abramson, T., and MacKinnon, R. (1994). Transfer of the scorpion toxin receptor to an insensitive potassium channel. Neuron *13*, 961-966.

Hawgood, B.J. (1997). Mauricio Rocha e Silva MD: snake venom, bradykinin and the rise of autopharmacology. Toxicon *35*, 1569-1580.

Hendon, R.A., and Tu, A.T. (1979). The role of crotoxin subunits in tropical rattlesnake neurotoxic action. Biochim Biophys Acta *578*, 243-252.

Hesselager, M., Timmermann, D.B., and Ahring, P.K. (2004). pH Dependency and desensitization kinetics of heterologously expressed combinations of acid-sensing ion channel subunits. J Biol Chem *279*, 11006-11015.

Hille, B. (2001). Ion channels of excitable membranes, Third edn (Sunderland, MA, Sinauer Associates, Inc.).

Hillier, B.J., Christopherson, K.S., Prehoda, K.E., Bredt, D.S., and Lim, W.A. (1999). Unexpected modes of PDZ domain scaffolding revealed by structure of nNOS-syntrophin complex. Science *284*, 812-815.

Hoenderop, J.G., Voets, T., Hoefs, S., Weidema, F., Prenen, J., Nilius, B., and Bindels, R.J. (2003). Homo- and heterotetrameric architecture of the epithelial Ca2+ channels TRPV5 and TRPV6. The EMBO journal *22*, 776-785.

Horii, K., Brooks, M.T., and Herr, A.B. (2009). Convulxin forms a dimer in solution and can bind eight copies of glycoprotein VI: implications for platelet activation. Biochemistry *48*, 2907-2914.

Jasti, J., Furukawa, H., Gonzales, E.B., and Gouaux, E. (2007). Structure of acid-sensing ion channel 1 at 1.9 A resolution and low pH. Nature *449*, 316-323.

Jordt, S.E., and Julius, D. (2002). Molecular basis for species-specific sensitivity to "hot" chili peppers. Cell *108*, 421-430.

Joslyn, A.F., Luchowski, E., and Triggle, D.J. (1988). Dimeric 1,4-dihydropyridines as calcium channel antagonists. J Med Chem *31*, 1489-1492.

Julius, D., and Basbaum, A.I. (2001). Molecular mechanisms of nociception. Nature *413*, 203-210.

Kedei, N., Szabo, T., Lile, J.D., Treanor, J.J., Olah, Z., Iadarola, M.J., and Blumberg, P.M. (2001). Analysis of the native quaternary structure of vanilloid receptor 1. J Biol Chem *276*, 28613-28619.

Kitaguchi, T., and Swartz, K.J. (2005). An inhibitor of TRPV1 channels isolated from funnel Web spider venom. Biochemistry *44*, 15544-15549.

Kizuka, H., and Hanson, R.N. (1987). Beta-adrenoceptor antagonist activity of bivalent ligands. 1. Diamide analogues of practolol. J Med Chem *30*, 722-726.

Kondo, K., Narita, K., and Lee, C.Y. (1978). Amino acid sequences of the two polypeptide chains in beta1-bungarotoxin from the venom of Bungarus multicinctus. J Biochem *83*, 101-115.

Kordis, D., and Gubensek, F. (2000). Adaptive evolution of animal toxin multigene families. Gene *261*, 43-52.

Kramer, R.H., and Karpen, J.W. (1998). Spanning binding sites on allosteric proteins with polymer-linked ligand dimers. Nature *395*, 710-713.

Krause, S., Schmoldt, H.U., Wentzel, A., Ballmaier, M., Friedrich, K., and Kolmar, H. (2007). Grafting of thrombopoietin-mimetic peptides into cystine knot miniproteins yields high-affinity thrombopoietin antagonists and agonists. FEBS J *274*, 86-95.

Krishnamurthy, V.M., Semetey, V., Bracher, P.J., Shen, N., and Whitesides, G.M. (2007). Dependence of effective molarity on linker length for an intramolecular protein-ligand system. J Am Chem Soc *129*, 1312-1320.

Krishtal, O.A., and Pidoplichko, V.I. (1980). A receptor for protons in the nerve cell membrane. Neuroscience *5*, 2325-2327.

Leboulluec, K.L., Mattson, R.J., Mahle, C.D., Mcgovern, R.T., Nowak, H.P., and Gentile, A.J. (1995). Bivalent Indoles Exhibiting Serotonergic Binding-Affinity. Bioorganic & Medicinal Chemistry Letters *5*, 123-126.

Lee, H.C., Wang, J.M., and Swartz, K.J. (2003). Interaction between extracellular Hanatoxin and the resting conformation of the voltage-sensor paddle in Kv channels. Neuron *40*, 527-536.

Lee, S.Y., and MacKinnon, R. (2004). A membrane-access mechanism of ion channel inhibition by voltage sensor toxins from spider venom. Nature *430*, 232-235.

Leffler, A., Monter, B., and Koltzenburg, M. (2006). The role of the capsaicin receptor TRPV1 and acid-sensing ion channels (ASICS) in proton sensitivity of subpopulations of primary nociceptive neurons in rats and mice. Neuroscience *139*, 699-709.

Lewis, R.J., and Garcia, M.L. (2003). Therapeutic potential of venom peptides. Nat Rev Drug Discov *2*, 790-802.

Li-Smerin, Y., and Swartz, K.J. (1998). Gating modifier toxins reveal a conserved structural motif in voltage-gated Ca2+ and K+ channels. Proceedings of the National Academy of Sciences of the United States of America *95*, 8585-8589.

Li-Smerin, Y., and Swartz, K.J. (2000). Localization and molecular determinants of the Hanatoxin receptors on the voltage-sensing domains of a K(+) channel. J Gen Physiol *115*, 673-684.

Liang, S. (2004). An overview of peptide toxins from the venom of the Chinese bird spider Selenocosmia huwena Wang [=Ornithoctonus huwena (Wang)]. Toxicon *43*, 575-585.

Lingueglia, E. (2007). Acid-sensing ion channels in sensory perception. J Biol Chem *282*, 17325-17329.

Long, S.B., Campbell, E.B., and Mackinnon, R. (2005a). Crystal structure of a mammalian voltage-dependent Shaker family K+ channel. Science *309*, 897-903.

Long, S.B., Campbell, E.B., and Mackinnon, R. (2005b). Voltage sensor of Kv1.2: structural basis of electromechanical coupling. Science *309*, 903-908.

Loughnan, M., Nicke, A., Jones, A., Schroeder, C.I., Nevin, S.T., Adams, D.J., Alewood, P.F., and Lewis, R.J. (2006). Identification of a novel class of nicotinic receptor antagonists: dimeric conotoxins VxXIIA, VxXIIB, and VxXIIC from Conus vexillum. J Biol Chem *281*, 24745-24755.

Lwaleed, B.A., and Bass, P.S. (2006). Tissue factor pathway inhibitor: structure, biology and involvement in disease. J Pathol *208*, 327-339.

MacKinnon, R., Heginbotham, L., and Abramson, T. (1990). Mapping the receptor site for charybdotoxin, a pore-blocking potassium channel inhibitor. Neuron *5*, 767-771.

Mans, B.J., Andersen, J.F., Schwan, T.G., and Ribeiro, J.M. (2008). Characterization of anti-hemostatic factors in the argasid, Argas monolakensis: implications for the evolution of blood-feeding in the soft tick family. Insect Biochem Mol Biol *38*, 22-41.

Matta, J.A., and Ahern, G.P. (2007). Voltage is a partial activator of rat thermosensitive TRP channels. J Physiol *585*, 469-482.

Mazzuca, M., Heurteaux, C., Alloui, A., Diochot, S., Baron, A., Voilley, N., Blondeau, N., Escoubas, P., Gelot, A., Cupo, A.*, et al.* (2007). A tarantula peptide against pain via ASIC1a channels and opioid mechanisms. Nature neuroscience *10*, 943-945.

McKemy, D.D., Neuhausser, W.M., and Julius, D. (2002). Identification of a cold receptor reveals a general role for TRP channels in thermosensation. Nature *416*, 52-58.

Mebs, D. (2002). Venomous and poisonous animals : a handbook for biologists, and toxicologists and toxinologists, Physicians and pharmacists (Boca Raton, Fla., CRC Press).

Milescu, M., Bosmans, F., Lee, S., Alabi, A.A., Kim, J.I., and Swartz, K.J. (2009). Interactions between lipids and voltage sensor paddles detected with tarantula toxins. Nature structural & molecular biology.

Milescu, M., Vobecky, J., Roh, S.H., Kim, S.H., Jung, H.J., Kim, J.I., and Swartz, K.J. (2007). Tarantula toxins interact with voltage sensors within lipid membranes. J Gen Physiol *130*, 497-511.

Miller, C. (1995). The charybdotoxin family of K+ channel-blocking peptides. Neuron *15*, 5-10.

Morgan, D.L., Borys, D.J., Stanford, R., Kjar, D., and Tobleman, W. (2007). Texas coral snake (Micrurus tener) bites. South Med J *100*, 152-156.

Mouhat, S., Andreotti, N., Jouirou, B., and Sabatier, J.M. (2008). Animal toxins acting on voltage-gated potassium channels. Curr Pharm Des *14*, 2503-2518.

Myers, B.R., Bohlen, C.J., and Julius, D. (2008). A yeast genetic screen reveals a critical role for the pore helix domain in TRP channel gating. Neuron *58*, 362-373.

Negri, L., Lattanzi, R., Giannini, E., Colucci, M., Margheriti, F., Melchiorri, P., Vellani, V., Tian, H., De Felice, M., and Porreca, F. (2006). Impaired nociception and inflammatory pain sensation in mice lacking the prokineticin receptor PKR1: focus on interaction between PKR1 and the capsaicin receptor TRPV1 in pain behavior. J Neurosci *26*, 6716-6727.

Negri, L., Lattanzi, R., Giannini, E., and Melchiorri, P. (2007). Bv8/Prokineticin proteins and their receptors. Life Sci *81*, 1103-1116.

Nishioka, S.A., Silveira, P.V., and Menzes, L.B. (1993). Coral snake bite and severe local pain. Ann Trop Med Parasitol *87*, 429-431.

Osipov, A.V., Kasheverov, I.E., Makarova, Y.V., Starkov, V.G., Vorontsova, O.V., Ziganshin, R., Andreeva, T.V., Serebryakova, M.V., Benoit, A., Hogg, R.C.*, et al.* (2008).

Naturally occurring disulfide-bound dimers of three-fingered toxins: a paradigm for biological activity diversification. J Biol Chem *283*, 14571-14580.

Pawlak, J., Mackessy, S.P., Sixberry, N.M., Stura, E.A., Le Du, M.H., Menez, R., Foo, C.S., Menez, A., Nirthanan, S., and Kini, R.M. (2009). Irditoxin, a novel covalently linked heterodimeric three-finger toxin with high taxon-specific neurotoxicity. FASEB J *23*, 534-545.

Phillips, E., Reeve, A., Bevan, S., and McIntyre, P. (2004). Identification of species-specific determinants of the action of the antagonist capsazepine and the agonist PPAHV on TRPV1. J Biol Chem *279*, 17165-17172.

Phillips, L.R., Milescu, M., Li-Smerin, Y., Mindell, J.A., Kim, J.I., and Swartz, K.J. (2005). Voltage-sensor activation with a tarantula toxin as cargo. Nature *436*, 857-860.

Pignataro, G., Simon, R.P., and Xiong, Z.G. (2007). Prolonged activation of ASIC1a and the time window for neuroprotection in cerebral ischaemia. Brain *130*, 151-158.

Pluzhinikov, K.A., Nol'de, D.E., Tertyshnikova, S.M., Sukhanov, S.V., Sobol, A.G., Torgov, M., Filippov, A.K., Arsen'ev, A.S., and Grishin, E.V. (1994). [Structure-activity study of the basic toxic component of venom from the ant Ectatomma tuberculatum]. Bioorg Khim *20*, 857-871.

Poirot, O., Berta, T., Decosterd, I., and Kellenberger, S. (2006). Distinct ASIC currents are expressed in rat putative nociceptors and are modulated by nerve injury. J Physiol *576*, 215-234.

Portoghese, P.S., Nagase, H., Lipkowski, A.W., Larson, D.L., and Takemori, A.E. (1988). Binaltorphimine-related bivalent ligands and their kappa opioid receptor antagonist selectivity. J Med Chem *31*, 836-841.

Possani, L.D., Martin, B.M., Yatani, A., Mochca-Morales, J., Zamudio, F.Z., Gurrola, G.B., and Brown, A.M. (1992). Isolation and physiological characterization of taicatoxin, a complex toxin with specific effects on calcium channels. Toxicon *30*, 1343-1364.

Price, M.P., McIlwrath, S.L., Xie, J., Cheng, C., Qiao, J., Tarr, D.E., Sluka, K.A., Brennan, T.J., Lewin, G.R., and Welsh, M.J. (2001). The DRASIC cation channel contributes to the detection of cutaneous touch and acid stimuli in mice. Neuron *32*, 1071-1083.

Ramsey, I.S., Delling, M., and Clapham, D.E. (2006). An introduction to TRP channels. Annu Rev Physiol *68*, 619-647.

Rao, J., Lahiri, J., Isaacs, L., Weis, R.M., and Whitesides, G.M. (1998). A trivalent system from vancomycin.D-ala-D-Ala with higher affinity than avidin.biotin. Science *280*, 708-711.

Rosini, M., Budriesi, R., Bixel, M.G., Bolognesi, M.L., Chiarini, A., Hucho, F., Krogsgaard-Larsen, P., Mellor, I.R., Minarini, A., Tumiatti, V.*, et al.* (1999). Design, synthesis, and biological evaluation of symmetrically and unsymmetrically substituted methoctramine-related polyamines as muscular nicotinic receptor noncompetitive antagonists. J Med Chem *42*, 5212-5223.

Rowan, E.G. (2001). What does beta-bungarotoxin do at the neuromuscular junction? Toxicon *39*, 107-118.

Roy, A., Zhou, X., Chong, M.Z., D'Hoedt, D., Foo, C.S., Rajagopalan, N., Nirthanan, S., Bertrand, D., Sivaraman, J., and Kini, R.M. (2010). Structural and functional characterization of a novel homodimeric three-finger neurotoxin from the venom of Ophiophagus hannah (king cobra). J Biol Chem *285*, 8302-8315.

Sajevic, T., Leonardi, A., and Krizaj, I. (2011). Haemostatically active proteins in snake venoms. Toxicon *57*, 627-645.

Schmidt, D., and MacKinnon, R. (2008). Voltage-dependent K+ channel gating and voltage sensor toxin sensitivity depend on the mechanical state of the lipid membrane. Proc Natl Acad Sci U S A *105*, 19276-19281.

Schmidt, J.O. (1982). Biochemistry of insect venoms. Annu Rev Entomol *27*, 339-368.

Schmidt, J.O. (1990). Hymenoptera venoms: striving toward the ultimate defense against vertebrates. In Insect defenses: adaptive mechanisms and strategies of prey and predators, D.L. Evans, and J.O. Schmidt, eds. (Albany, State University of New York Press), pp. 387-419.

Schmidtko, A., Lotsch, J., Freynhagen, R., and Geisslinger, G. (2010). Ziconotide for treatment of severe chronic pain. Lancet *375*, 1569-1577.

Schweitz, H., Bidard, J.N., and Lazdunski, M. (1990). Purification and pharmacological characterization of peptide toxins from the black mamba (Dendroaspis polylepis) venom. Toxicon *28*, 847-856.

Shi, G., Kleinklaus, A.K., Marrion, N.V., and Trimmer, J.S. (1994). Properties of Kv2.1 K+ channels expressed in transfected mammalian cells. J Biol Chem *269*, 23204-23211.

Siemens, J., Zhou, S., Piskorowski, R., Nikai, T., Lumpkin, E.A., Basbaum, A.I., King, D., and Julius, D. (2006). Spider toxins activate the capsaicin receptor to produce inflammatory pain. Nature *444*, 208-212.

Smith, J.A., Amagasu, S.M., Hembrador, J., Axt, S., Chang, R., Church, T., Gee, C., Jacobsen, J.R., Jenkins, T., Kaufman, E.*, et al.* (2006). Evidence for a multivalent interaction of symmetrical, N-linked, lidocaine dimers with voltage-gated Na+ channels. Mol Pharmacol *69*, 921-931.

Sobolevsky, A.I., Rosconi, M.P., and Gouaux, E. (2009). X-ray structure, symmetry and mechanism of an AMPA-subtype glutamate receptor. Nature *462*, 745-756.

Sokolov, S., Kraus, R.L., Scheuer, T., and Catterall, W.A. (2008). Inhibition of sodium channel gating by trapping the domain II voltage sensor with protoxin II. Mol Pharmacol *73*, 1020-1028.

St Pierre, L., Birrell, G.W., Earl, S.T., Wallis, T.P., Gorman, J.J., de Jersey, J., Masci, P.P., and Lavin, M.F. (2007). Diversity of toxic components from the venom of the

evolutionarily distinct black whip snake, Demansia vestigiata. J Proteome Res *6*, 3093-3107.

Strimple, P.D., Tomassoni, A.J., Otten, E.J., and Bahner, D. (1997). Report on envenomation by a Gila monster (Heloderma suspectum) with a discussion of venom apparatus, clinical findings, and treatment. Wilderness Environ Med *8*, 111-116.

Sutherland, S.P., Benson, C.J., Adelman, J.P., and McCleskey, E.W. (2001). Acid-sensing ion channel 3 matches the acid-gated current in cardiac ischemia-sensing neurons. Proceedings of the National Academy of Sciences of the United States of America *98*, 711-716.

Swartz, K.J. (2007). Tarantula toxins interacting with voltage sensors in potassium channels. Toxicon *49*, 213-230.

Swartz, K.J. (2008). Sensing voltage across lipid membranes. Nature *456*, 891-897.

Swartz, K.J., and MacKinnon, R. (1997). Mapping the receptor site for hanatoxin, a gating modifier of voltage-dependent K+ channels. Neuron *18*, 675-682.

Takahashi, H., Kim, J.I., Min, H.J., Sato, K., Swartz, K.J., and Shimada, I. (2000). Solution structure of hanatoxin1, a gating modifier of voltage-dependent K(+) channels: common surface features of gating modifier toxins. J Mol Biol *297*, 771-780.

Terlau, H., and Olivera, B.M. (2004). Conus venoms: a rich source of novel ion channel-targeted peptides. Physiol Rev *84*, 41-68.

Tombola, F., Pathak, M.M., and Isacoff, E.Y. (2006). How does voltage open an ion channel? Annual review of cell and developmental biology *22*, 23-52.

Tominaga, M., Caterina, M.J., Malmberg, A.B., Rosen, T.A., Gilbert, H., Skinner, K., Raumann, B.E., Basbaum, A.I., and Julius, D. (1998). The cloned capsaicin receptor integrates multiple pain-producing stimuli. Neuron *21*, 531-543.

Tominaga, M., and Tominaga, T. (2005). Structure and function of TRPV1. Pflugers Arch *451*, 143-150.

Tsetlin, V., Utkin, Y., and Kasheverov, I. (2009). Polypeptide and peptide toxins, magnifying lenses for binding sites in nicotinic acetylcholine receptors. Biochem Pharmacol *78*, 720-731.

Ueberheide, B.M., Fenyo, D., Alewood, P.F., and Chait, B.T. (2009). Rapid sensitive analysis of cysteine rich peptide venom components. Proceedings of the National Academy of Sciences of the United States of America *106*, 6910-6915.

Undheim, E.A., and King, G.F. (2011). On the venom system of centipedes (Chilopoda), a neglected group of venomous animals. Toxicon *57*, 512-524.

van de Locht, A., Stubbs, M.T., Bode, W., Friedrich, T., Bollschweiler, C., Hoffken, W., and Huber, R. (1996). The ornithodorin-thrombin crystal structure, a key to the TAP enigma? The EMBO journal *15*, 6011-6017.

Vassilevski, A.A., Fedorova, I.M., Maleeva, E.E., Korolkova, Y.V., Efimova, S.S., Samsonova, O.V., Schagina, L.V., Feofanov, A.V., Magazanik, L.G., and Grishin, E.V. (2010). Novel class of spider toxin: active principle from the yellow sac spider Cheiracanthium punctorium venom is a unique two-domain polypeptide. J Biol Chem *285*, 32293-32302.

Vellani, V., Colucci, M., Lattanzi, R., Giannini, E., Negri, L., Melchiorri, P., and McNaughton, P.A. (2006). Sensitization of transient receptor potential vanilloid 1 by the prokineticin receptor agonist Bv8. J Neurosci *26*, 5109-5116.

Venkatachalam, K., and Montell, C. (2007). TRP channels. Annual review of biochemistry *76*, 387-417.

Voets, T., Droogmans, G., Wissenbach, U., Janssens, A., Flockerzi, V., and Nilius, B. (2004). The principle of temperature-dependent gating in cold- and heat-sensitive TRP channels. Nature *430*, 748-754.

Voets, T., Prenen, J., Vriens, J., Watanabe, H., Janssens, A., Wissenbach, U., Bodding, M., Droogmans, G., and Nilius, B. (2002). Molecular determinants of permeation through the cation channel TRPV4. J Biol Chem *277*, 33704-33710.

Waldmann, R., Bassilana, F., de Weille, J., Champigny, G., Heurteaux, C., and Lazdunski, M. (1997a). Molecular cloning of a non-inactivating proton-gated Na+ channel specific for sensory neurons. J Biol Chem *272*, 20975-20978.

Waldmann, R., Champigny, G., Bassilana, F., Heurteaux, C., and Lazdunski, M. (1997b). A proton-gated cation channel involved in acid-sensing. Nature *386*, 173-177.

Walker, C.S., Jensen, S., Ellison, M., Matta, J.A., Lee, W.Y., Imperial, J.S., Duclos, N., Brockie, P.J., Madsen, D.M., Isaac, J.T.*, et al.* (2009). A novel Conus snail polypeptide causes excitotoxicity by blocking desensitization of AMPA receptors. Curr Biol *19*, 900-908.

Wang, S.Y., and Wang, G.K. (2003). Voltage-gated sodium channels as primary targets of diverse lipid-soluble neurotoxins. Cellular signalling *15*, 151-159.

Wemmie, J.A., Chen, J., Askwith, C.C., Hruska-Hageman, A.M., Price, M.P., Nolan, B.C., Yoder, P.G., Lamani, E., Hoshi, T., Freeman, J.H., Jr.*, et al.* (2002). The acid-activated ion channel ASIC contributes to synaptic plasticity, learning, and memory. Neuron *34*, 463-477.

Wemmie, J.A., Price, M.P., and Welsh, M.J. (2006). Acid-sensing ion channels: advances, questions and therapeutic opportunities. Trends Neurosci *29*, 578-586.

Wu, L.J., Duan, B., Mei, Y.D., Gao, J., Chen, J.G., Zhuo, M., Xu, L., Wu, M., and Xu, T.L. (2004). Characterization of acid-sensing ion channels in dorsal horn neurons of rat spinal cord. J Biol Chem *279*, 43716-43724.

Yeh, B.I., Kim, Y.K., Jabbar, W., and Huang, C.L. (2005). Conformational changes of pore helix coupled to gating of TRPV5 by protons. The EMBO journal *24*, 3224-3234.

Yu, L., Sun, C., Song, D., Shen, J., Xu, N., Gunasekera, A., Hajduk, P.J., and Olejniczak, E.T. (2005). Nuclear magnetic resonance structural studies of a potassium channel-charybdotoxin complex. Biochemistry *44*, 15834-15841.

Yu, Y., Chen, Z., Li, W.G., Cao, H., Feng, E.G., Yu, F., Liu, H., Jiang, H., and Xu, T.L. (2010). A nonproton ligand sensor in the acid-sensing ion channel. Neuron *68*, 61-72.

Yuan, C.H., He, Q.Y., Peng, K., Diao, J.B., Jiang, L.P., Tang, X., and Liang, S.P. (2008). Discovery of a distinct superfamily of Kunitz-type toxin (KTT) from tarantulas. PLoS One *3*, e3414.

Zamudio, F.Z., Conde, R., Arevalo, C., Becerril, B., Martin, B.M., Valdivia, H.H., and Possani, L.D. (1997). The mechanism of inhibition of ryanodine receptor channels by imperatoxin I, a heterodimeric protein from the scorpion Pandinus imperator. J Biol Chem *272*, 11886-11894.

Zhu, S., Darbon, H., Dyason, K., Verdonck, F., and Tytgat, J. (2003). Evolutionary origin of inhibitor cystine knot peptides. Faseb J *17*, 1765-1767.

Ziemann, A.E., Allen, J.E., Dahdaleh, N.S., Drebot, II, Coryell, M.W., Wunsch, A.M., Lynch, C.M., Faraci, F.M., Howard, M.A., 3rd, Welsh, M.J.*, et al.* (2009). The amygdala is a chemosensor that detects carbon dioxide and acidosis to elicit fear behavior. Cell *139*, 1012-1021.

CHAPTER 3

A heteromeric Texas coral snake toxin targets acid-sensing ion channels to produce pain

ABSTRACT

Natural products that elicit discomfort or pain represent invaluable tools for probing molecular mechanisms underlying pain sensation(Basbaum et al., 2009). Plant-derived irritants have predominated in this regard, but animal venoms have also evolved to avert predators by targeting neurons and receptors whose activation produces noxious sensations(Bohlen et al., 2010; Chahl and Kirk, 1975; Mebs, 2002; Schmidt, 1982; Siemens et al., 2006). As such, venoms provide a rich and varied source of small molecule and protein pharmacophores(Fry et al., 2009; Terlau and Olivera, 2004) that can be exploited to characterize and manipulate key components of the pain-signaling pathway. With this in mind, we carried out an unbiased *in vitro* screen to identify snake venoms capable of activating somatosensory neurons. Venom from the Texas coral snake (*Micrurus tener tener*), whose bite produces intense and unremitting pain(Morgan et al., 2007), excited a large cohort of sensory neurons. The purified active species (MitTx) consists of a heteromeric complex between Kunitz- and phospholipase A2-like proteins that together function as a potent, persistent, and selective agonist for acid(Abe, 1978)sensing ion channels (ASICs), showing equal or greater efficacy when compared with acidic pH. MitTx is highly selective for the ASIC1 subtype at neutral pH; under more acidic conditions (pH < 6.5), MitTx massively potentiates (>100-fold) proton-evoked activation of ASIC2a channels. These observations raise the possibility that ASIC channels function as coincidence detectors for extracellular protons and other, as yet unidentified, endogenous factors. Purified MitTx elicits robust pain-related behavior in mice via activation of ASIC1 channels on capsaicin-sensitive nerve fibers. These findings reveal a mechanism whereby snake venoms produce pain, and highlight an unexpected contribution of ASIC1 channels to nociception.

RESULTS

To identify novel toxins that activate nociceptors, we screened venoms from a variety of snake species for their ability to depolarize specific subpopulations of somatosensory neurons using calcium imaging as a functional readout. Among these, venom from the Texas coral snake, which elicits intense acute pain associated with local edema and inflammation(Morgan et al., 2007), produced clear and robust activation of most, but not all, neurons cultured from trigeminal ganglia (TG) of newborn (P0-P2) rats (Fig 1a, b). In contrast, coral snake venom had no effect on sympathetic neurons cultured from superior cervical ganglia (not shown).

We next fractionated the crude venom using reversed-phase chromatography (Supplementary Fig. 1) to identify the active component(s). No single fraction excited sensory neurons, but when re-pooled the individual fractions fully reconstituted activity observed with the crude venom, suggesting a requirement for multiple components. Pair-wise analysis of these fractions identified two components (MitTxα and MitTxβ), which could be purified to near-homogeneity with subsequent chromatographic steps, as assessed by gel filtration chromatography, SDS-PAGE, and mass spectrometry (not shown). These two toxins together proved necessary and sufficient to recapitulate activity of the crude venom. Mass spectrometry and N-terminal Edman sequencing showed that both MitTxα and MitTxβ are proteinaceous in nature, and partial amino acid sequences derived from these analyses were used to clone full-length cDNAs from the coral snake venom gland. The deduced amino acid sequences revealed patterns of cysteine residues that classify MitTxα and MitTxβ as Kunitz type and phospholipase A2 (PLA2)-like proteins, respectively (Fig. 1c and Supplementary Fig. 1). Indeed, these families of cysteine-rich disulfide bonded proteins are prevalent components of various

snake venoms(Fry et al., 2009), and in some cases have been shown to form biochemical complexes(Doley and Kini, 2009).

To determine whether MitTxα and MitTxβ form a heteromeric complex, we used isothermal titration calorimetry to detect any such molecular interaction. We observed a substantial exothermic reaction (ΔH = -18.9 ± 1.3 kcal mol^{-1}) upon mixing, resulting from a high affinity binding event (K_d = 12.2 ± 3.1 nM) with 1:1 stoichiometry (n = 1.02 ± 0.05) (Fig. 1d). These biochemical results are consistent with our physiological analysis showing that neither MitTxα nor MitTxβ activated sensory neurons alone, whereas a robust and immediate rise in intracellular calcium was produced when both components were added simultaneously or sequentially (in either order) (Fig. 1e). Moreover, even a brief washout period between sequential applications prevented activation (Fig. 1f), suggesting that only the MitTx α/β complex forms a persistent and productive interaction with its physiological target.

Having defined the molecular nature of the toxin components, we next sought to elucidate its mechanism of action on sensory neurons. As the MitTxβ component lacks critical catalytic residues normally found in the active site of related PLA2 enzymes(Berg et al., 2001) phospholipase activity seemed unlikely to contribute to neuronal excitation. In fact, we failed to detect PLA2 activity associated with any component, together or alone (Supplementary Fig. 1), suggesting that the toxin is not producing neuronal depolarization simply by degrading the plasma membrane (consistent with the observed action on a subset of somatosensory neurons). It is possible that this toxin maintains some lipid-binding character from its PLA2 lineage, which could aid the toxin in effecting neuronal depolarization.

To gain clues as to the cellular mechanism of toxin action, we performed a detailed biophysical analysis of toxin-evoked responses. Whole cell patch clamp recordings showed that purified MitTx α/β complex (hereafter referred to as MitTx) produced robust currents in a subset of trigeminal neurons. These currents were characterized by a linear current-voltage relationship and high permeability to Na^+ versus Cs^+ ions (P_{Na^+}:P_{Cs^+} = 10.1 ± 1.0, Fig. 2a). In searching for potential molecular targets expressed by sensory neurons, we next investigated members of the ASIC family, which exhibit properties consistent with these parameters(Waldmann et al., 1997a; Waldmann et al., 1997b; Wu et al., 2004). We expressed various ASIC subtypes in *Xenopus* oocytes and measured toxin-evoked electrophysiological responses. Figure 2 shows that application of MitTx produced large and sustained membrane currents in oocytes expressing the ASIC1b subtype (Fig. 2b, c). Consistent with our results using cultured neurons, neither MitTxα nor MitTxβ was active on its own, but robust responses were evoked when both components were applied to oocytes, whether pre-mixed or mixed *in situ.* Furthermore, the ENaC/ASIC blocker, amiloride, abolished these responses. When applied at maximal concentration, MitTx elicited responses exceeding those produced by saturating doses of extracellular protons. Whereas protons elicit very transient responses, those evoked by toxin were dramatically prolonged, reflecting both lack of desensitization and slow reversibility after washout (Fig 2c).

Among ASIC subtypes, the most robust toxin-evoked responses were observed with ASIC1a or 1b based on potency (EC_{50} = 9.4 ± 1.3 and 23 ± 3.6 nM, respectively), efficacy (relative to protons), and persistence of action (Fig. 2d and Supplementary Fig. 2). MitTx must interact with an extracellular region of the channel since responses were observed in the outside-out (but not inside-out) configuration when toxin was applied to patches excised from ASIC1a-expressing CHO cells (not shown). Moreover, at least for

ASIC1a, toxin potency (9 nM) is likely limited by the affinity of α/β complex formation (12 nM,Fig. 1d) and not by the toxin-channel interaction itself.

The ASIC3 subtype was also MitTx sensitive, but required ~100-fold higher toxin concentration to achieve half-maximal activation (EC_{50} = 830 ± 250 nM). This lower potency was accompanied by relatively slow activation and fast washout kinetics compared to those observed with ASIC1a or 1b (Supplementary Fig. 2). By comparison, ASIC2a showed very weak activation by toxin, never achieving more than 10% efficacy compared to proton-evoked responses (Fig. 2d, e). Despite this anemic response, the toxin produced a remarkable potentiation of acid-evoked currents, greatly enhancing both potency and efficacy of protons (Fig. 2e, f). Indeed, as the extracellular pH drops below neutrality, the toxin itself becomes an excellent ASIC2a agonist, essentially enhancing the potency of protons by three orders of magnitude. Two remaining ASIC family members, 2b and 4, do not produce proton-activated channels on their own, and we did not observe MitTx-evoked responses in oocytes expressing these subtypes. As a further testament to toxin specificity, MitTx produced neither activation nor persistent inhibition when applied to a diverse range of cloned ion channels, including voltage-gated, ENaC, TRP, P2X, or 5-HT_3 channels (Supplementary Fig. 3). Additionally, MitTx activated the same percentage of trigeminal neurons cultured from wild type or TRPV1/TRPM8/TRPA1 triple knockout mice (Supplementary Fig. 4).

Micrurus tener tener is not the only coral snake species to express ASIC-activating toxins; venom from the Brazilian coral snake (*Micrurus frontalis*) activated a similar cohort of cultured rat trigeminal sensory neurons, or oocytes expressing cloned ASIC1a channels (Supplementary Fig. 5). Interestingly, ASIC1a is also targeted by a peptide toxin from tarantula (PcTx1), but in this case, the toxin serves as a functional antagonist of proton-evoked responses by locking the channel in a desensitized state(Chen et al.,

2006; Escoubas et al., 2000). ASIC1a channels blocked by PcTx1 could not be activated by MitTx, and MitTx-activated channels could not be blocked by PcTx1 (Fig. 2g, h), suggesting physical or functional occlusion of toxin action.

We next used patch clamp recording methods to determine whether MitTx-evoked neuronal responses exhibit properties consistent with an ASIC-mediated mechanism. Sensory neurons show both transient and sustained proton-evoked responses, with the former being mediated primarily by ASIC channels and the latter by capsaicin-sensitive TRPV1 channels(Leffler et al., 2006; Poirot et al., 2006). We found that all MitTx-sensitive neurons exhibited transient responses to extracellular protons (pH 4), toxin responses were blocked by amiloride and eliminated in Na^+-free perfusate, and the relative magnitude of toxin-to-proton evoked responses resembled those observed in transfected mammalian (CHO) cells expressing the cloned rat ASIC1a or 1b channels (Fig. 3a, b). Further evidence that ASIC1 is the predominant target of MitTx came from analysis of electrophysiological responses in TG neurons from newborn ASIC1- or ASIC3-deficient mice(Price et al., 2001; Wemmie et al., 2002). The percentage of toxin-sensitive cells from $ASIC1^{-/-}$ mice was greatly diminished compared to wild type or $ASIC3^{-/-}$ animals (Fig. 3c, d). Using calcium imaging to sample a larger population of neurons, we found that responses to moderate toxin concentrations (20 nM) were completely absent in TG cultures from $ASIC1^{-/-}$ mice, but unperturbed in those from $ASIC3^{-/-}$ animals (Fig. 3e-g). Only at substantially higher toxin concentrations (600 nM; exceeding the EC_{50} for ASIC1 by≥ 30 -fold) did we record a relatively small subset of toxin-sensitive neurons in $ASIC1^{-/-}$ cultures. These residual toxin responses were eliminated when depolarization-evoked calcium influx was suppressed in Na^+-free perfusate (Supplementary Fig. 6), consistent with Ca^{2+}-impermeant ASIC2 and/or 3

subtypes accounting for the activity. Indeed, ASIC3$^{-/-}$ cultures showed a small, but significant diminution in the percentage of neurons responding to 600 nM MitTx (Fig. 3g).

The role of ASIC channels in pain has focused primarily on ASIC3 given its somatosensory neuron-specific pattern of expression(Waldmann et al., 1997a). MitTx provides a novel tool with which to determine whether ASIC1 and ASIC1-expressing neurons also contribute to nociception. Injection of MitTx into the hind paw of wild type mice produced robust nocifensive (pain-related) behavior scored as a characteristic licking response (Fig. 4a). In the same animals, we observed abundant Fos protein expression in superficial laminae of the ipsilateral dorsal spinal cord, demonstrating engagement of nociceptive pathways (Fig. 4b). These responses were diminished in ASIC1-deficient mice, but persisted in ASIC3$^{-/-}$ animals, demonstrating a predominant contribution of ASIC1 channels to toxin-evoked nocifensive behavior.

Are these responses mediated through a well-characterized population of nociceptors? To address this question, we first examined MitTx-sensitive neurons for expression of relevant molecular markers of subpopulations of nociceptors. One third of toxin-sensitive neurons expressed TRPV1, whereas a much smaller group (11%) were labeled by isolectin B4, which in mice marks a population of TRPV1-negative, non-peptidergic C-fibers. The majority (53%) of toxin-sensitive neurons immunostained for the NF200 neurofilament, placing them among the subpopulation of medium-to-large diameter neurons with myelinated axons (Fig. 4c). As many large diameter sensory neurons respond to innocuous mechanical stimulation, these histological results suggest that functional ASIC1 channels are expressed by both nociceptive and non-nociceptive somatosensory neurons. Next, we asked whether MitTx elicits nocifensive responses in mice in which the central terminals of TRPV1-expressing nociceptors have been selectively ablated through spinal (intrathecal) injection of capsaicin(Cavanaugh et al.,

2009). Indeed, these animals showed a complete loss of toxin-evoked behavior and Fos immunoreactivity in the spinal cord (Fig. 4d), demonstrating that the painful effects of MitTx are mediated entirely by a relatively small cohort (less than a third) of ASIC1-expressing nerve fibers.

Bites and stings from venomous creatures produce pain to ward off predators(Chahl and Kirk, 1975; Mebs, 2002; Schmidt, 1982), and thus it stands to reason that some toxins have evolved to target efficiently elements of the pain pathway. In fact, bites from some coral snake species are well known to elicit excruciating pain requiring hospitalization and administration of opiate analgesics(Morgan et al., 2007; Nishioka et al., 1993). Our results show that MitTx has evolved from Kunitz type and PLA2-like protein scaffolds to evoke intense and persistent pain by producing robust and long-lasting activation of ASIC1 channels on the nociceptive terminals of mammalian, avian, or serpentine predators. Just as capsaicin and some spider toxins highlight the importance of TRPV1 in pain sensation, so MitTx implicates ASIC1 channels in this protective sensory modality, further illustrating the power of natural products in identifying key components and therapeutic targets of nociceptive signaling pathways.

In light of its selective expression within somatosensory ganglia and a well-documented contribution to ischemic pain, studies of ASIC channels in nociception have focused primarily on the ASIC3 subtype(Deval et al., 2010; Sutherland et al., 2001; Waldmann et al., 1997a; Wemmie et al., 2006; Yu et al., 2010). The extremely persistent (non-desensitizing) and selective nature of MitTx action has enabled us to functionally isolate ASIC1 channels and reveal their contribution to pain sensation through the activation of TRPV1-expressing neurons. This nociceptor population has been suggested to constitute a 'labeled line' required for acute detection of noxious heat, as well as tissue injury-evoked pain hypersensitivity(Basbaum et al., 2009; Cavanaugh et al., 2009).

Activation of ASIC1 on these nerve fibers may contribute to the non-TRPV1 component of proton-mediated sensitization associated with tissue acidosis and inflammatory pain. ASIC1 is also expressed by non-nociceptive somatosensory neurons, as well as other neural and non-neural tissues(Wemmie et al., 2002; Wemmie et al., 2006; Wu et al., 2004; Ziemann et al., 2009). Thus, MitTx represents a novel class of pharmacological probes with which to elucidate the contributions of ASIC channels to a variety of physiological processes. Finally, it is intriguing that MitTx can potentiate proton efficacy at some ASIC subtypes (most notably ASIC2a) by two or three orders of magnitude.. That is to say, MitTx reveals the fact that protons only activate ASIC2a channels to <10% of maximal open probability, suggesting that protons do not exploit the full potential of ASIC2a as a ligand-gated channel. Although small FMRF-amide-like peptides have been shown to potentiate proton-gated currents through ASIC1 and ASIC3 (primarily by slowing desensitization)(Askwith et al., 2000; Deval et al., 2010), the profound enhancing effects mediated by MitTx hint at the existence of other, more potent physiological modulators for this class of excitatory channels.

METHODS

Toxin Purification

Crude *Micrurus tener tener* venom, pooled from multiple specimens, was provided by the National Natural Toxins Research Center, Texas A&M University-Kingsville, Texas, USA. Lyophilized venom was dissolved in water to 100 mg ml^{-1}, diluted 30-fold into 20% acetonitrile containing 0.1% trifluoroacetic acid (TFA), filtered through 0.1 μm centrifugal filter unit (Millipore) and fractionated by reversed-phase HPLC. Up to 20 mg venom was loaded onto a semi-preparative C18 column (Vydac model 218TP510), and eluted with a 20 min linear gradient (18-36% acetonitrile; 3 ml min^{-1}). Fractions containing

predominantly MitTxα were diluted two-fold with 0.1% TFA, injected onto an analytical PLRP-S column (Varian PL1512-5501), and separated with an 8 minute linear gradient (27-34% acetonitrile; 0.8 mL min^{-1}); MitTxα–containing fractions were again diluted, injected onto an analytical C18 column (Vydac 218TP54), and separated with a 20 minute linear gradient (18-36% acetonitrile; 0.8 mL min^{-1}). MitTxβ fractions from the semi-preparative run were diluted, applied to an analytical C18 column (Vydac 218TP54), and separated with a 7 minute linear gradient (30-36% acetonitrile; 0.8 mL min^{-1}). All HPLC buffers contained 0.1% TFA, and all purifications were performed at room temperature (RT). Purified fractions were lyophilized then dissolved in water, aliquoted, and stored at -80 °C. Protein concentration was determined using calculated extinction coefficient at 280 nm (http://us.expasy.org /tools/protparam.html).

PcTx1 was purified from *Psalmopoeus cambridgei* venom (SpiderPharm Inc.) using two sequential HPLC steps consisting of 114 minute linear gradient (0-54% acetonitrile on a semi-preparative C18 column) followed by the same gradient on an analytical C18 column (as above). *Micrurus frontalis* venom was purchased from Sigma.

Sequence Determination

Toxin masses were determined using a Bruker Apex III ESI-Q-FTICR mass spectrometer, and the N-terminal sequencing was performed on an Applied Biosystems 492 Procise Sequencer previously described(Bohlen et al., 2010). Edman degradation yielding partial sequence (NLNQFRLMIKCTNDRV…) for MitTxβ, but not MitTxα due to modified (pyroglutamic acid) N-terminus. Partial MitTxα sequence was determined *de novo* by MS/MS sequencing analysis. After reduction under acidic conditions (0.1% formic acid, 5mM TCEP for 24 hrs at 37 °C) MitTxα was subjected to CID, HCD, and ETD analyses using an LTQ-Orbitrap mass spectrometer (Thermo Fisher). Data were

analyzed manually, yielding the N-terminal sequence as well as a shorter internal sequence fragment (<Q[L/I]RPAFCYEDPPFFQKCGAFVDSYYF... and …HFFYGQCDV…).

Partial protein sequences were used to clone full-length MitTxα and MitTxβ cDNAs. RNA was extracted from two *M. t. tener* venom glands using TRIZOL reagent (Invitrogen), then isolated by chloroform extraction and isopropanol precipitation. A cDNA library was generated for use in 5' and 3' RACE reactions using SMARTer RACE cDNA Amplification Kit (Clontech). Primers derived from biochemically-determined sequences and, for MitTxβ, taking advantage of conservation in reported *Micrurus* PLA2 sequences, small fragments of MitTxα and MitTxβ sequences were amplified by PCR and then used to design gene-specific 3' and 5'RACE primers. RACE products were sequenced individually after insertion into TOPO vector (Invitrogen), and each sequence fragment was confirmed by multiple sequencing reads and multiple RACE primer sets. The cDNA-derived peptide sequence predicted the observed molecular weight of the purified toxins after consideration of the post-translational modifications (N-terminal cyclization and disulfide bond formation).

Calorimetry

MitTxα and MitTxβ were diluted into ITC buffer [(mM): 150 NaCl, 1 $CaCl_2$, 10 HEPES, adjusted to pH 7.4 with NaOH). Toxin aliquots were diluted with water prior to dilution with ITC buffer to maintain the same dilution factor. Diluted toxin solutions were centrifuged (65,000 × g for 30 min at 4 °C), degassed (5 min at 15 °C), and loaded into a VP-ITC Microcalorimeter (MicroCal). MitTxβ (3 to 10 μM) was titrated into MitTxα (0.3 to 1 μM) following a schedule of one 4μL injection followed by 29 injections of 10μL, each spaced by 5 min. Titrations were conducted at 15 °C. After manual baseline correction,

total heat released per injection was calculated by integrating over the full injection time period. Heat of dilution was estimated by the final titration points and subtracted from baseline. Linear baseline values were confirmed by titration of MitTxβ into buffer. Data were processed and fit to a single-site binding model using Origin v.7 (MicroCal). Reported values are averages of three independent experiments.

Molecular Biology

Full-length (not including UTRs) ASIC1a, 1b, 2a, 3, and 4 were cloned from rat trigeminal ganglion or brain cDNA libraries into pCDNA3 (Invitrogen). The mouse ASIC2b clone was kindly provided by Michael Welsh (University of Iowa, IA), rat ENaC clones were provided by David Pearce (University of California, San Francisco, CA). All constructs were confirmed by DNA sequencing. Other constructs and RNA synthesis have been previously described(Bohlen et al., 2010).

***Xenopus* Oocyte and CHO/HEK Cell Culture**

Xenopus laevis oocytes (Nasco), human embryo kidney 293 (HEK293), and Chinese hamster ovary (CHO-K1) cells were isolated, maintained, transfected, and plated essentially as described(Bohlen et al., 2010). Oocytes were injected with RNA (3–50 ng; 50 nl), and assayed 3–7 days later. CHO culture medium included non-essential amino acids (UCSF Cell Culture Facility). Electrophysiological experiments were conducted 2-20 hours after plating, and imaging experiments were performed 3-4 hours after plating.

Neuronal Cell Culture

Trigeminal ganglia (TG) were dissected from newborn (P0-P2) Sprague-Dawley rats or C57BL/6 mice and cultured as described(Bohlen et al., 2010) for 3-4 hours before calcium imaging or 2-20 hours before electrophysiological recordings. Neurons

dissected from newborn animals were used for all experiments except histology, which used adult neurons due to apparent developmental changes in ASIC subtype expression (see Supplementary Fig 4c). Dorsal root ganglia from adult (4-12 week old) mice were dissected and dissociated as newborn neurons except collagenase P and trypsin incubations were extended to 30 min each. After trituration, cells were centrifuged through a 15% BSA gradient for 5 min at 1000 × g to remove cellular debris. BSA was rinsed from the pellet and cells were resuspended in culture medium. Cells were plated into PDL-coated 384-well plates (Greiner Bio-One) for 14-18 hours before calcium imaging.

Calcium Imaging

Cells were loaded with Fura-2-AM as described(Bohlen et al., 2010). MitTxα, MitTxβ, and PcTx1 solutions were prepared in the presence of 0.1% bovine serum albumin (BSA, Sigma) to minimize toxin adsorption to plasticware. For experiments using low concentrations of MitTxα/β, MitTxα and MitTxβ were first mixed at high concentrations (≥ 1 μM) for ≥ 10 min before dilution.

Electrophysiology

Xenopus oocyte two electrode and mammalian whole-cell recordings were carried out essentially as described(Bohlen et al., 2010). Oocyte extracellular solution contained (mM): 115 NaCl, 2.5 KCl, 1.8 $MgCl_2$, 5 HEPES, and 5 MES adjusted to pH 5-7.4 with NaOH. For pH < 5 citrate was used instead of HEPES/MES. Solutions were applied using gravity-based perfusion over a small-volume oocyte chamber (Automate Scientific), except for toxin-containing solutions, which were pipetted directly onto cells.

Mammalian cell extracellular solution contained (mM): 150 NaCl, 2.8 KCl, 1 $MgCl_2$, 1 $CaCl_2$, 5 HEPES, 5 MES adjusted to pH 7.4 with NaOH, 300-310 mOsmol kg^{-1}. The pipette solution contained (mM): 130 K-gluconate, 15 KCl, 4 NaCl, 0.5 $CaCl_2$, 1 EGTA, 10 HEPES, adjusted to pH 7.2 with KOH, 285 mOsmol kg^{-1}. Solutions were applied from the micro-perfusion system SmartSquirt (Automate Scientific). Toxins were applied in the presence of 0.1 % BSA and MitTxα/β complex was formed at high concentrations as described above.

Fits to the Hill equation were performed using Igor Pro software (Wavemetrics) with four free parameters. Fits in Fig 2d revealed the following values for EC_{50}, n_H, and maximum respectively: 9.4 ± 1.3 nM, 2.4 ± 0.8, and 1.30 ± 0.08 for ASIC1a; 23 ± 1 nM, 3.6 ± 0.7, and 1.35 ± 0.05 for ASIC1b; 36 ± 4 nM, 0.088 ± 0.005, and 2.2 ± 0.5 for ASIC2a; and 830 ± 250 nM, 1.4 ± 0.3, and 1.8 ± 0.3 for ASIC3. Fits in Fig 2f revealed the following values for pH_{50}, n_H, and maximum respectively: 5.98 ± 0.07, 1.3 ± 0.3, and 0.99 ± 0.03 in the presence of toxin and 2.4 ± 0.1, 1.0 ± 0.1, and 1.6 ± 4.1 in the absence of toxin. The baseline parameter was near-zero for all fits.

For permeability experiments from acutely dissociated rat TG neurons, endogenous currents were attenuated by using a minimal ionic composition and by applying rapid voltage ramps (140 ms ramps from -80 mV to +80 mV were applied every 200 ms) to largely desensitize voltage-gated channels; extracellular and intracellular solutions contained (mM): 150 NaCl, 1 $MgCl_2$, 1 $CaCl_2$, 10 HEPES adjusted to pH 7.4 with NaOH. Remaining endogenous currents were negligible in magnitude compared to the very large MitTx-evoked currents, so baseline subtraction was not performed. Dialysis of the intracellular solution was monitored to completion as determined by elimination of K_v channel currents. Cesium wash solution contained 150 mM CsCl instead of NaCl, and pH was titrated with CsOH. P_{Na^+} / P_{Cs^+} was calculated by substituting the observed

reversal potential (V_m) into the Goldman-Hodgkin-Katz voltage equation: $\frac{PNa+}{PCs+} = e^{-Vm*\frac{F}{RT}}$ where F, R, and T have their usual meanings (F/RT = 39.6 V^{-1} at 20 °C). Currents were not corrected for liquid junction potential changes.

Immunohistochemistry

After calcium imaging, adult DRG neurons were fixed with 4% paraformaldehyde (10 min) then washed 3 times in PBS containing 0.1% triton X (PBSTx). Neurons were incubated in blocking solution for 1 hour (10% normal goat serum (NGS) + PBSTx) and then incubated overnight in primary antibody solution (2.5% NGS + PBSTx + primary antibody; rabbit anti-TRPV1, 1:8000 or mouse anti-N5A; Sigma, 1:1000). Cells were washed 3 times with PBSTx before a 2-hour incubation in secondary antibody solution (2.5% NGS + PBSTx, + Alexa-488 or Alexa-594; Invitrogen, 1:1000). For IB4 staining, IB4-FITC (Sigma, 10 μg/mL) was added to the secondary antibody solution. Cells were washed 3 times in PBS before imaging.

For spinal cord Fos immunoreactivity, mice were perfused transcardially with 4% paraformaldehyde 90 min after hindpaw toxin injection (as for behavioral experiments). Frozen spinal cord sections (25 μm) were prepared from lumbar level L4/L5 and immunostained for Fos as described(Caterina et al., 2000).

Behavior

Animal experiments were approved by the UCSF Institutional Animal Care and Use Committee and conducted in accordance with the National Institutes of Health (NIH) Guide for the Care and Use of Laboratory Animals and the recommendations of the International Association for the Study of Pain. Two to five animals were housed per cage and maintained on a 12-h light/dark schedule with ad lib access to food and water.

Injections (20 μL of PBS + 0.1% BSA, with or without 5 μM MitTx) were performed as described(Siemens et al., 2006). For intrathecal capsaicin studies, adult were anesthetized and treated as described(Cavanaugh et al., 2009). Behavioral tests were performed 1 to 5 days after capsaicin injection. Knockout strains were extensively backcrossed to the C57BL/6 wildtype strain. Both behavioral and histological experiments were conducted and scored with the experimenter blind to genotype.

Primer sequences:

MitTxβ Fragment forward: AACCTCTAYCAGTTCATGATTAAATGTACCAACG

MitTxβ Fragment reverse: TCATTGGCAACGTTTGAGGTCGATATTG

MitTxβ 3'RACE: GTTATCTAGCCAGCGACCTCGATTGCAGTGG

MitTxβ 5'RACE: CCACTGCAATCGAGGTCGCTGGCTAGATAAC

MitTxα fragment forward: CCNCCNTTYTTYCARAARTGYGGNGCNTTYGTNG

MitTxα fragment reverse: ACRTCRCAYTGNCCRTARAARAARTG

MitTxα 3'RACE: CCTCCATTCTTTCAAAAATGTGGAGCC

MitTxα 5'RACE: CGCAAGTAATTCTTGACCTGTTGAAGTAGTAGG

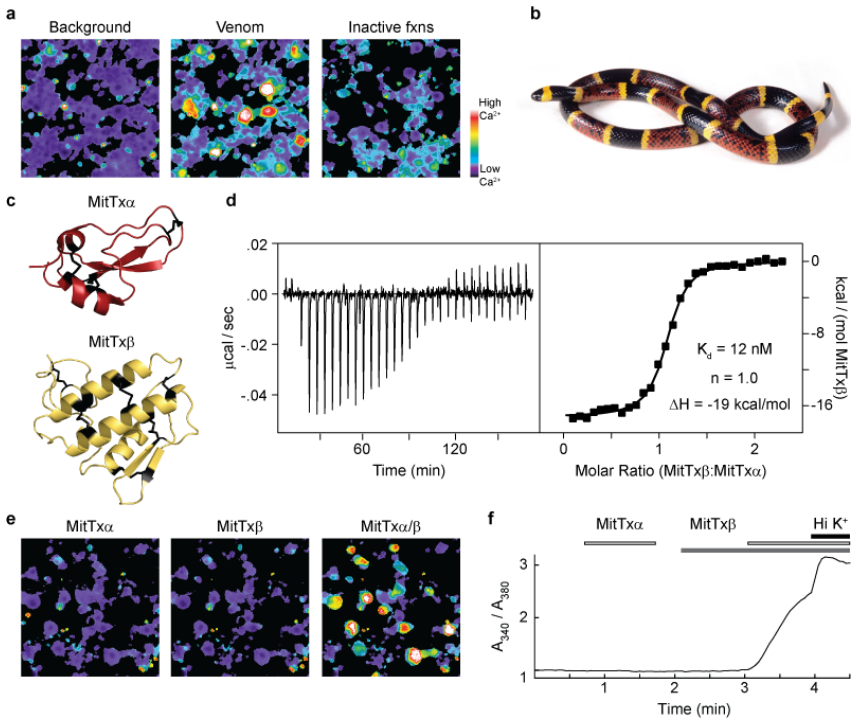

Figure 1

Heteromeric toxin from Texas coral snake activates somatosensory neurons

a, *M. t. tener* venom (0.1 mg ml^{-1}) activates acutely dissociated trigeminal ganglion (TG) neurons as assessed by ratiometric calcium imaging. Pooled venom fractions lacking neuron-specific activity (inactive fxns) produced only weak signals in non-neuronal cells (color bar indicates relative calcium levels). **b,** The Texas coral snake. **c,** Homology-based predicted structural models of MitTx subunits, generated using Prime (Schrodinger)[30]. **d,** Isothermal titration calorimetry reveals formation of high-affinity MitTxα/β complex with 1:1 stoichiometry. **e,** MitTxα and MitTxβ have no effect individually, but recapitulate activity of whole venom when applied together to TG neurons. **f,** Average calcium response from >100 randomly-selected TG neurons that also responded to high extracellular potassium (Hi K^+, 100 mM KCl). Activation by MitTxα/β (300 nM each) only occurs when both toxins are present.

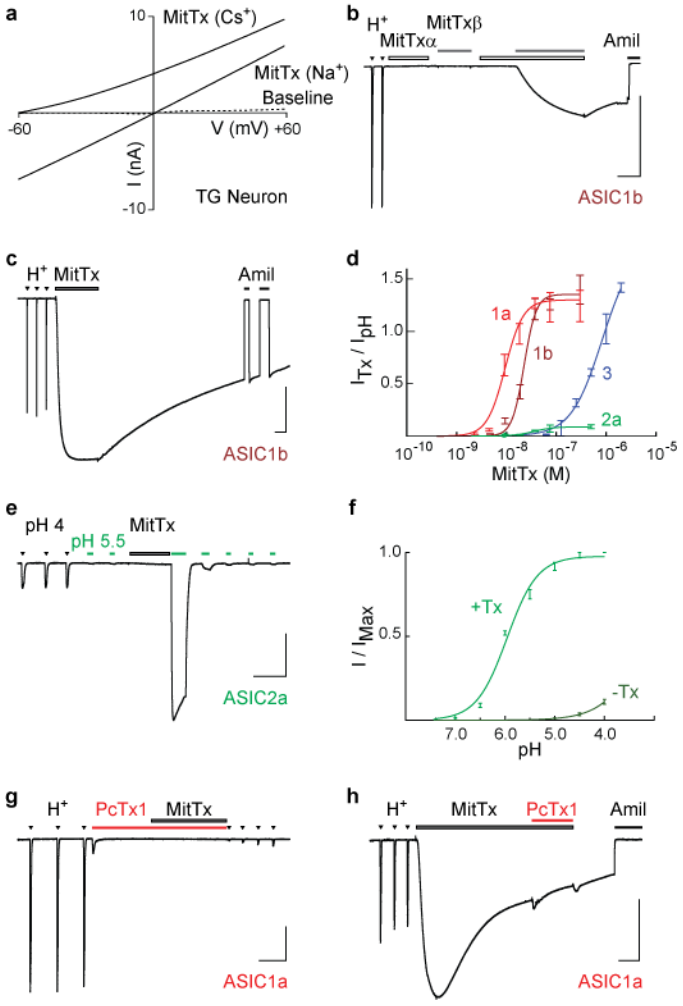
a
10
MitTx (Cs+)
MitTx (Na+)
Baseline
-60
V (mV) +60
I (nA)
-10
TG Neuron
b
H+
MitTxα
MitTxβ
Amil
ASIC1b
c
H+ MitTx
Amil
ASIC1b
d
1.5
1.0
0.5
ITx / IpH
1a
1b
3
2a
10-10 10-9 10-8 10-7 10-6 10-5
MitTx (M)
e
pH 4
pH 5.5
MitTx
ASIC2a
f
1.0
0.5
I / IMax
+Tx
-Tx
7.0 6.0 5.0 4.0
pH
g
H+
PcTx1
MitTx
ASIC1a
h
H+
MitTx
PcTx1
Amil
ASIC1a

Figure 2 MitTx activates ASICs

a, Current-voltage relationships of MitTx (300 nM)-evoked conductances from TG neurons (whole-cell configuration) demonstrate higher permeability for Na^+ over Cs^+. The intracellular solution contained 150 mM Na^+, and a leftward-shift in the reversal potential was observed when the major extracellular cation was changed from 150 mM Na^+ to 150 mM Cs^+. **b,** Voltage clamp recordings show that ASIC1b-expressing oocytes respond to both extracellular acidification (H^+, pH 4) and MitTx, but are insensitive to MitTxα (30 nM) or MitTxβ (300 nM) individually. Toxin-evoked responses were blocked by amiloride (Amil, 1mM). **c,** MitTx (75 nM)-evoked currents are comparable in magnitude to pH 4-evoked currents in ASIC1b-expressing oocytes. Toxin responses are non-desensitizing and persistent compared to transient proton-evoked currents. **d,** Dose-response analysis of toxin-evoked currents normalized to maximal pH 4-evoked response in ASIC-expressing oocytes. Data were fit to the Hill equation. **e,** MitTx (75 nM) is a poor ASIC2a agonist, but dramatically potentiates pH 5.5-evoked responses. **f,** pH dose-response of ASIC2a in the absence (dark green) or presence (light green) of 75 nM MitTx. Data were fit to the Hill equation. **g,** PcTx1 (100 nM) inhibits both pH 6- and MitTx-evoked currents in ASIC1a-expressing oocytes. **h,** MitTx occludes PcTx1 inhibition. Vertical scale bars: 1μA; horizontal bars: 1 min; V_h = -60 mV.

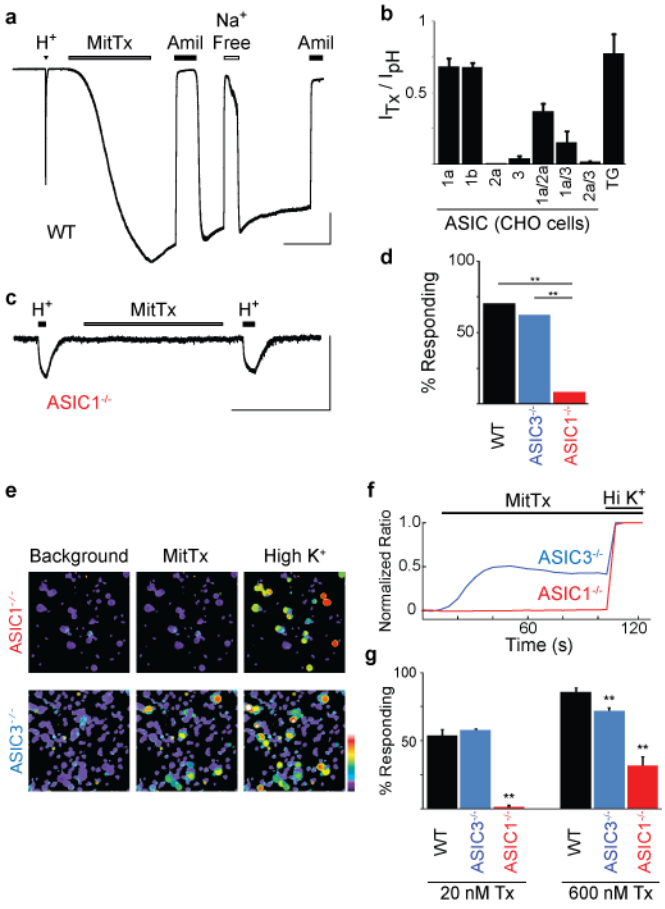
a
H+
MitTx
Amil
Na+ Free
Amil
WT
b
1
0.5
ITx / IpH
1a
1b
2a
3
1a/2a
1a/3
2a/3
TG
ASIC (CHO cells)
c
H+
MitTx
H+
ASIC1-/-
d
100
50
% Responding
**
**
WT
ASIC3-/-
ASIC1-/-
e
Background
MitTx
High K+
ASIC1-/-
ASIC3-/-
f
MitTx
Hi K+
Normalized Ratio
1.0
0.5
0
ASIC3-/-
ASIC1-/-
60
120
Time (s)
g
100
50
% Responding
**
**
**
WT
ASIC3-/-
ASIC1-/-
WT
ASIC3-/-
ASIC1-/-
20 nM Tx
600 nM Tx

Figure 3 ASICs are the neuronal receptor for MitTx

a, Whole-cell recording (V_h = -60 mV) from newborn rat TG neuron shows representative pH 4 (H^+)- and MitTx (75 nM)-evoked responses. Toxin responses were blocked by amiloride (Amil; 1 mM), and eliminated when extracellular Na^+ was replaced with Cs^+ (Na^+ Free). **b,** MitTx (75 nM) activates homo- and heteromeric ASIC family members expressed in CHO cells. MitTx to pH current ratios for ASIC1a or 1b (n = 3-6) resembled profile observed in TG neurons (n = 28). pH 4 was used for all ratios except for measurements of ASIC1a, in which case pH 6 was used to minimize tachyphylaxis. **c,** TG neurons from newborn ASIC1$^{-/-}$ mice lacked MitTx sensitivity. H^+ indicates pH 4. **d,** Percentage of wild type or knockout TG neurons in which toxin-evoked currents were observed by whole cell patch clamp analysis (n = 10-30, **p < 0.01, chi-squared test). **e,** MitTx (20 nM) activates TG neurons from ASIC3$^{-/-}$, but not ASIC1$^{-/-}$ mice. **f,** Average MitTx-evoked calcium response of TG neurons (n > 300) normalized to a high-potassium response (Hi K^+). **g,** Fraction of neurons responding to 20 nM or 600 nM MitTx assessed by calcium imaging (n = 3-4 trials, each with > 100 cells; ** p < 0.01, one-way ANOVA with *post hoc* Tukey's test) Vertical scale bars: 1nA in **a**, 100 pA in **b**. Horizontal scale bars: 1 min. Error bars represent mean ± sem.

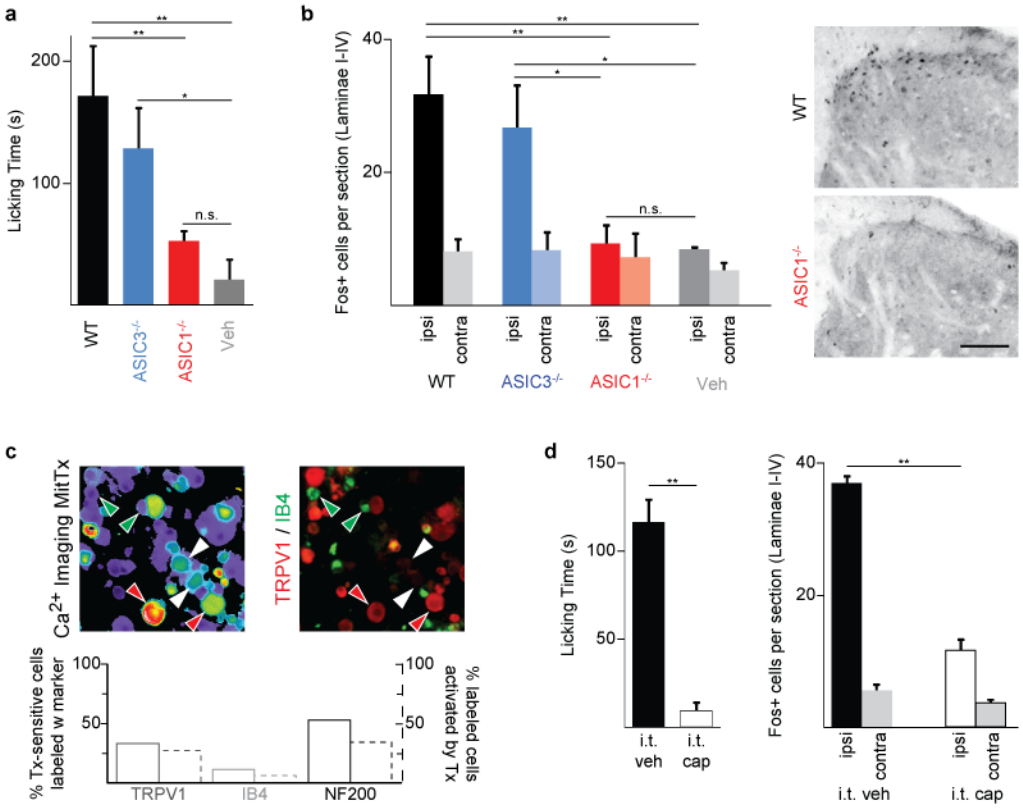
a
Licking Time (s)
200
100
**
**
*
n.s.
WT
ASIC3-/-
ASIC1-/-
Veh
b
Fos+ cells per section (Laminae I-IV)
40
20
**
**
*
*
n.s.
ipsi
contra
WT
ASIC3-/-
ASIC1-/-
Veh
WT
ASIC1-/-
c
Ca2+ Imaging MitTx
TRPV1 / IB4
% Tx-sensitive cells labeled w marker
% labeled cells activated by Tx
100
50
TRPV1
IB4
NF200
d
Licking Time (s)
150
100
50
**
i.t. veh
i.t. cap
Fos+ cells per section (Laminae I-IV)
40
20
**
ipsi
contra
i.t. veh
i.t. cap

Figure 4

MitTx elicits pain behavior via ASIC1- and TRPV1-expressing nociceptors

a, Hind paws of wild-type (WT) or ASIC-knockout mice were injected with MitTx (5 μM in 20 μl PBS with 0.1% BSA) or vehicle alone. Total time spent licking the injected paw was recorded over 15 min. **b,** Quantification and representative images of Fos immunostaining in superficial laminae of spinal cord sections from toxin-injected mice (ipsilateral or contralateral to the injection site). Scale bar: 50 μm. For **a** and **b**, n = 4-7; *p < 0.05; **p < 0.01, one-way ANOVA with *post hoc* Tukey's test. **c,** Adult mouse DRG neurons were tested for toxin-sensitivity using calcium imaging, then stained with antibodies that mark specific subpopulations of cells. Red arrows: Tx-sensitive/TRPV1-positive cells; white arrows: Tx-sensitive/TRPV1-negative cells; green arrows, IB4-positive/Tx-insensitive cells. Percentages were counted for >200 cells per marker and graphed below. **d,** Intrathecal administration of capsaicin (i.t. cap, 10 μg in 5 μl), but not vehicle, eliminates behavioral response and spinal Fos induction after intraplantar toxin injection (as in **a, b**). n = 3–4; **p < 0.001, Student's t-test. Error bars represent mean ± sem.

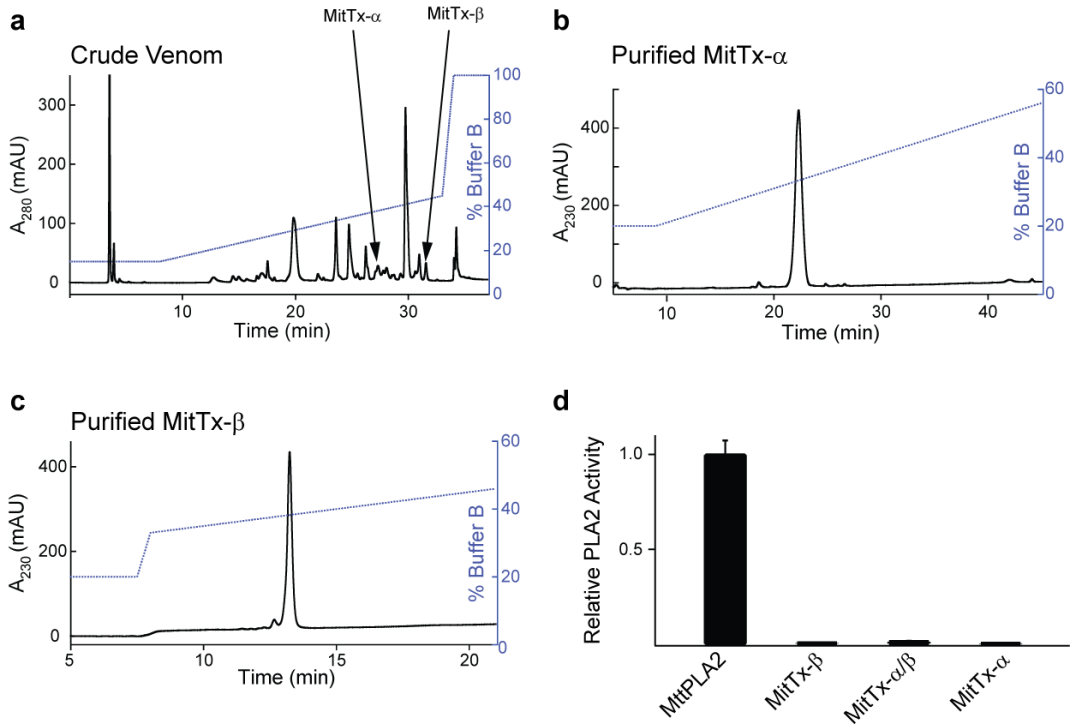

e

```
MitTx-α      <QIRPAFCYEDPPFFQKCGAFVDSYYFNRSRITCVHFFYGQCDVNQNHFTTMSECNRVCHG
Vestiginin-3   KDRPEFC.ELPPDRGTCMGFLQAFYYNPSQKGCLPFMFGGCKANPNNFKTLEECKRTCAA
```

f

PLA2 Active Site

```
MitTx-β      NLNQFRLMIKCTNDRVWADFVDYGCYCVARDSNTPVDDLDRCCQAQKQCYDEAVKVHGCK
Mtt PLA2     NLIHFKNMIECTTKRSWWDFADYGCYCGSGGSGTPVDDLDKCCQVHDDCYGEAEKVHGCW

MitTx-β      PLVMFYSFECRYLASDLDCSGNNTKCRNFVCNCDRTATLCILTATYNRNNHKIDPSRCQ
Mtt PLA2     PKWTLYSYDCS..NGQLTCKDNNTKCKDFVCNCDRTAALCFAKAPYNNKNYNIDLKRCQ
```

Figure 5 Purification and sequence of MitTx subunits

a-c, Reversed-phase C18 chromatogram of crude *M. t. tener* venom (**a**), purified MitTx-α (**b**), or purified MitTx-β (**c**). Buffer B is 90% acetonitrile, 0.1% TFA. **d,** MitTx-β, -α/β, or -α demonstrated minimal PLA2 specific activity relative to a functional phospholipase A2 purified from the same venom (MttPLA2, elution time is 29.5 min in **a**), as measured by the secretory phospholipase A2 assay kit (Cayman Chemical). Bars represent mean ± sem, n≥ 3. **e,** Amino acid sequence of MitTx-α, shown in alignment Vestiginin-3, a *Demansia vestigiata* (Black whip snake) Kunitz type protein of unknown function(St Pierre et al., 2007). <Q denotes pyroglutamate. Vestiginin-3 represents closest BLAST hit in the GenBank database, but there is limited homology with MitTx-α (identical residues are highlighted in red). The cysteine residues characterizing the Kunitz type motif are conserved (highlighted in yellow). **f,** Despite a high degree of sequence identity (highlighted as above) between MitTx-β and MttPLA2, a critical histidine-aspartate pair that participates in the catalytic network across PLA2 enzymes is not conserved in MitTx-β (blue circle).

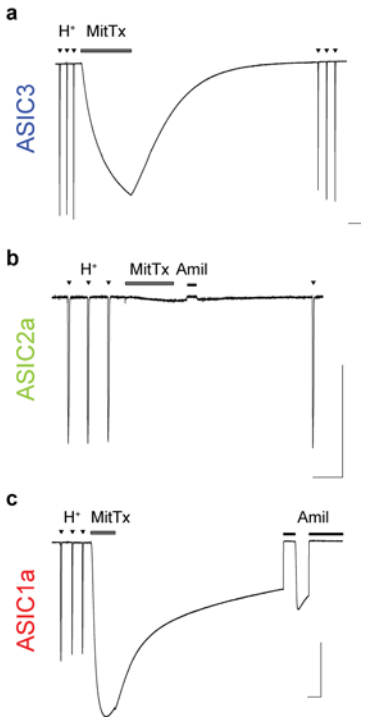

Figure 6 MitTx differentially activates ASIC family members

a, Two-electrode voltage-clamp recording from ASIC3-expressing *Xenopus* oocytes shows that ASIC3, although insensitive to low concentrations of toxin, is activated by MitTx at high concentrations (600nM). Although MitTx-evoked currents approach maximal H^+ (pH 4.0)-evoked currents in magnitude, the current develops slowly compared to ASIC1 and returns to baseline within 10-15 min after washout. **b,** MitTx (75 nM) activation of ASIC2a is detectable and blocked by amiloride (Amil, 1mM), but small relative to H^+ (pH 4.0)-evoked currents. **c,** ASIC1a activation by MitTx (75 nM) is characterized by a fast onset and slow recovery after washout, which follows a similar time course as channel desensitization in continued presence of MitTx (see **Figure 2h**). For ASIC1a, pH 6.0 was used as acid stimulation to minimize acid-induced tachyphylaxis. Vertical scale bars: 1 μA. Horizontal scale bars: 1 min.

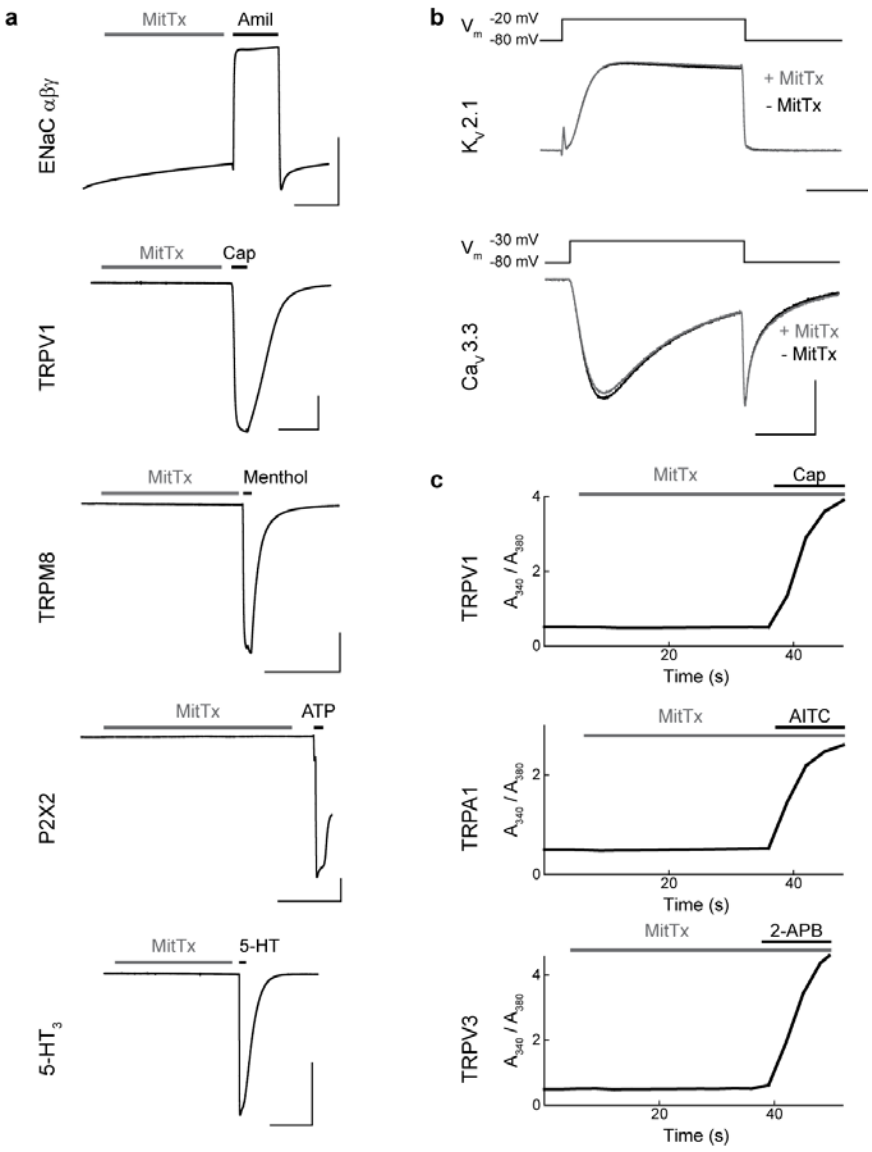
a
MitTx
Amil
ENaC αβγ
MitTx
Cap
TRPV1
MitTx
Menthol
TRPM8
MitTx
ATP
P2X2
MitTx
5-HT
5-HT3
b
Vm -20 mV
-80 mV
+ MitTx
- MitTx
Kv2.1
Vm -30 mV
-80 mV
+ MitTx
- MitTx
Cav3.3
c
MitTx
Cap
TRPV1
A340 / A380
Time (s)
MitTx
AITC
TRPA1
A340 / A380
Time (s)
MitTx
2-APB
TRPV3
A340 / A380
Time (s)

Figure 7 MitTx is specific for ASICs

a, *Xenopus* oocytes expressing various receptors are unaffected by MitTx (300 nM) as assessed by two-electrode voltage-clamp experiments. 10 μM amiloride (Amil), 1 μM capsaicin (Cap), 300 μM Menthol, 1μM ATP, and 3 μM 5-hydroxy-tryptamine (5-HT) were used to verify receptor expression. **b,** Voltage steps (shown above each trace) applied to oocytes expressing voltage-gated channels evoke identical currents in the absence and presence of MitTx (300nM). **c,** Average calcium-imaging response HEK cells transfected with TRP channels in response to MitTx (300 nM), 1 μM capsaicin (Cap), 500 μM allyl-isothiocyanate (AITC), or 2-aminophenyl borate (2-APB). All panels are representative traces of n≥ 3 experiments. Vertical Scale bars: 1 μA. Horizontal scale bars: 1 min in **a**, 100 ms in **b**.

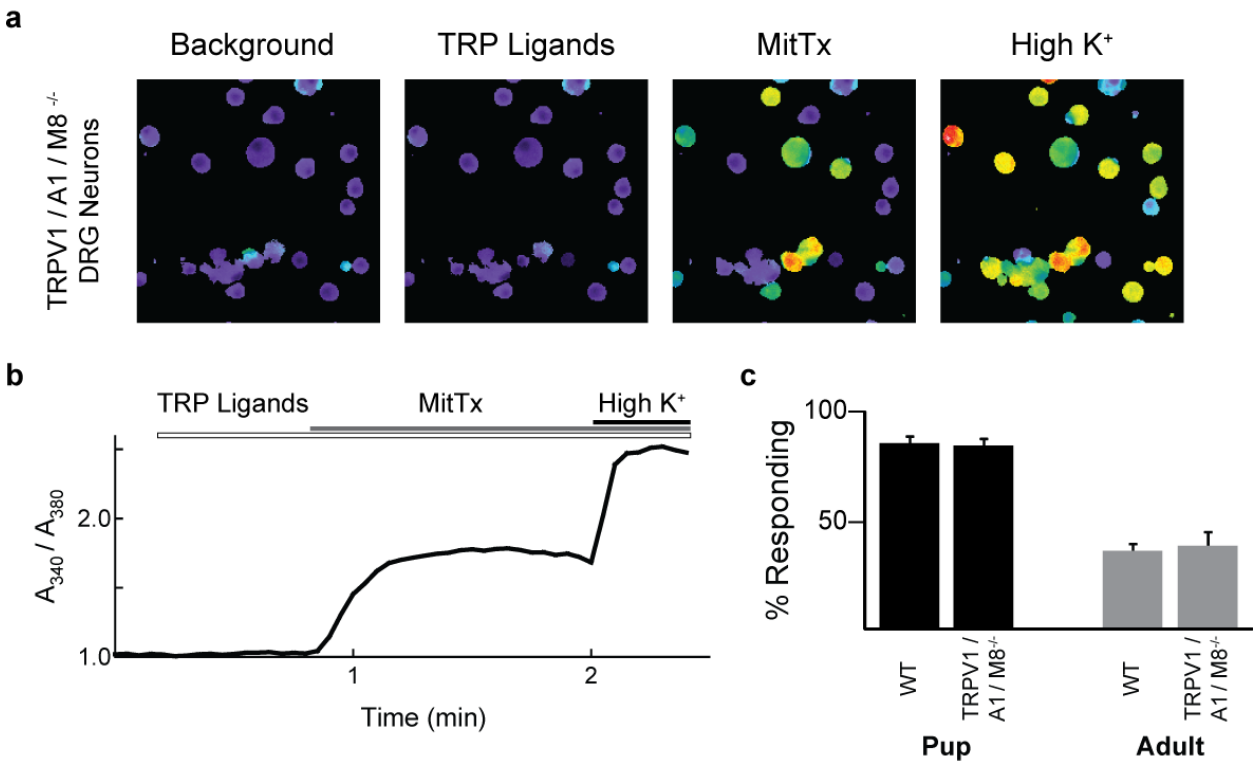

Figure 8 MitTx activates TRPV1/TRPA1/TRPM8 lacking neurons from newborn and adult mice

a, Calcium imaging analysis of DRG neurons isolated from TRPV1 / TRPA1 / TRPM8 triple-knockout mice, which show normal responses to MitTx (300 nM) and no sensitivity to agonists for the knocked-out receptors (5 μM Capsaicin, 500 μM menthol, 1 mM AITC). High extracellular potassium (High K^+) was used to activate all cells. **b,** Average response of all neurons imaged (n > 100 cells). **c,** Percentage of neurons responding in wildtype or triple-knockout animals for cultures isolated from either newborn pups (0-2 days) or adults (8-12 weeks old).

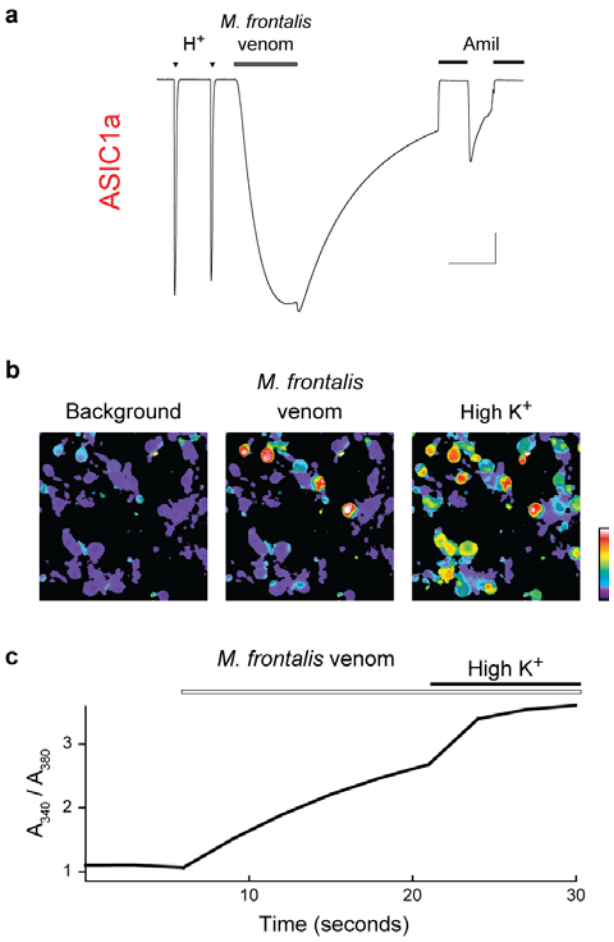

Figure 9 ASIC activation is a conserved feature of coral snake venom

a, Venom from the Brazilian coral snake, *Micrurus frontalis* (0.03 mg ml^{-1}), evokes currents from ASIC1a-expressing *Xenopus* oocytes that are comparable in magnitude to saturating H^+ (pH 6.0) responses, show slow washout rates, and are reversibly blocked by amiloride (Amil, 1mM). Vertical scale bar: 1μA. Horizontal scale bar: 1 min. **b,** *M. frontalis* venom activates a large percentage of TG neurons, similar to *M. t. tener* venom. High extracellular potassium (High K^+) was used to activate all cells. **c,** Average calcium response of all neurons to *M. frontalis* venom shows rapid activation of a large proportion of cells.

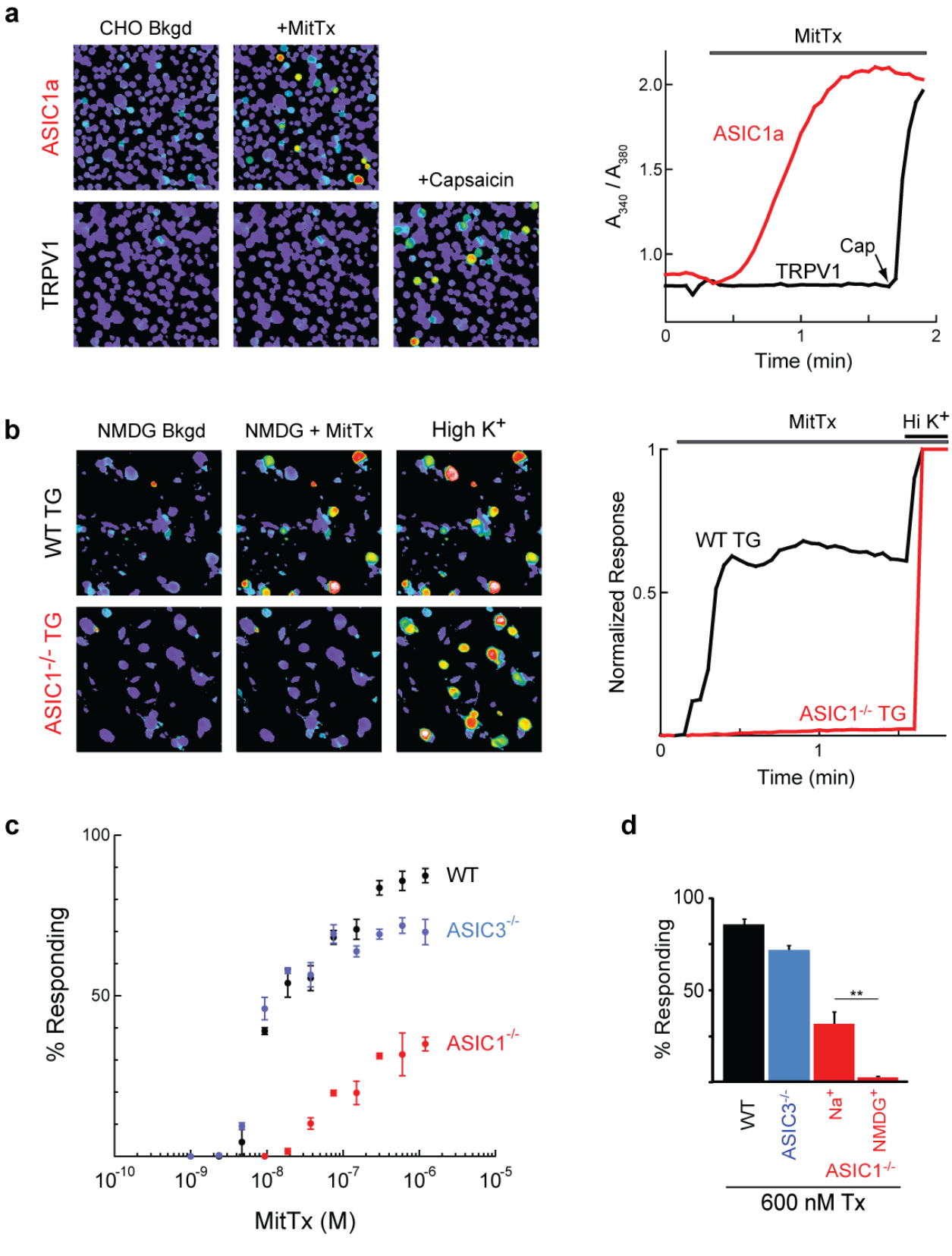
a
CHO Bkgd
+MitTx
+Capsaicin
ASIC1a
TRPV1
MitTx
ASIC1a
Cap
TRPV1
A_{340} / A_{380}
Time (min)
b
NMDG Bkgd
NMDG + MitTx
High K+
WT TG
ASIC1-/- TG
MitTx
Hi K+
WT TG
ASIC1-/- TG
Normalized Response
Time (min)
c
% Responding
WT
ASIC3-/-
ASIC1-/-
MitTx (M)
d
% Responding
WT
ASIC3-/-
Na+
NMDG+
ASIC1-/-
600 nM Tx

Figure 10 Direct MitTx-evoked calcium influx is ASIC1-dependent

a, MitTx (75 nM) elicits calcium influx into ASIC1a-transfected CHO cells (top panels), but not TRPV1-expressing cells (bottom panels). Average signal from all responsive cells (right panel) illustrates relatively slow time course of toxin-evoked responses compared to capsaicin (Cap, 10μM), consistent with a low but significant calcium permeability of ASIC1a. **b,** (Top panels) MitTx-evoked calcium responses in acutely dissociated TG neurons persists when extracellular Na^+ is replaced with $NMDG^+$. Under these conditions, Ca^{2+} represents the only permeant excitatory cation, and the measured calcium response must arise from a calcium-permeable conductance. (Bottom panels) In contrast, $ASIC1^{-/-}$ neurons in the same $NMDG^+$ solution show no calcium response to MitTx (300 nM), but are still excitable by high extracellular potassium (High K^+, 100 mM KCl). (Right panel) average calcium response of all cells in the field. **c,** Dose-response analysis of newborn mouse TG neurons by calcium imaging reveals a multi-phasic response to MitTx within the range of concentrations that activate different ASIC subtypes. $ASIC1^{-/-}$ neurons have a smaller total percentage of responsive cells, and responses are detected only at higher toxin concentrations. In contrast, $ASIC3^{-/-}$ neurons show normal responsiveness at low toxin concentrations, but a smaller percentage is activated at high concentrations of toxin. **d,** At saturating concentrations of MitTx (600 nM), the toxin-evoked calcium response observed in $ASIC1^{-/-}$ neurons can be eliminated by replacement of extracellular Na^+ with $NMDG^+$, consistent with its being mediated by calcium-impermeable ASIC2 and/or 3. Dose response points and bars represent mean ± sem of 3-5 separate applications with ≥ 100 cells counted per trial. $^{**}p < 10^{-5}$, Student's t-test.

ACKNOWLEDGEMENTS

We thank M. Price and M. Welsh for kindly providing ASIC1 and ASIC3 knockout mice; Y. Kelly and J. Poblete for technical assistance; C. Williams for assisting with homology models; F. Findeisen, L. Ma, and D. Minor for assistance with ITC experiments; R. Nicoll and members of the Julius lab for discussion and critical comments. This work was supported by a Ruth Kirschstein NIH predoctoral fellowship (F31NS065597 to C.B.), NIH postdoctoral training grant from the UCSF Cardiovascular Research Institute (A.C.), postdoctoral fellowship from the Canadian Institutes of Health Research (R.S-N.), the Howard Hughes Medical Institute (K.F.M. and A.L.B.), and the NIH (NCRR P41RR001614 to A.L.B., NCRR P40RR018300-09 to E.S., and NINDS R01NS065071 to D.J.).

AUTHOR CONTRIBUTIONS

C.B. and A.C initiated the screen, performed experiments, and analyzed data. R.S-N. and A.I.B. performed and analyzed behavioral experiments and spinal cord histology. K.F.M., A.L.B, S.Z., and D.K. determined partial protein sequences and performed mass spectrometry measurements. E.S. provided snake venom and tissue. C.B., A.C, and D.J. wrote the manuscript with discussion and contribution from all authors. D.J. supervised the project and provided guidance throughout.

FURTHER INFORMATION

GenBank accession numbers for MitTxα, MitTxβ, and MttPLA2 cDNA sequences are JN613325, JN613326, and JN613327 respectively.

REFERENCES

Askwith, C.C., Cheng, C., Ikuma, M., Benson, C., Price, M.P., and Welsh, M.J. (2000). Neuropeptide FF and FMRFamide potentiate acid-evoked currents from sensory neurons and proton-gated DEG/ENaC channels. Neuron *26*, 133-141.

Basbaum, A.I., Bautista, D.M., Scherrer, G., and Julius, D. (2009). Cellular and molecular mechanisms of pain. Cell *139*, 267-284.

Berg, O.G., Gelb, M.H., Tsai, M.D., and Jain, M.K. (2001). Interfacial enzymology: the secreted phospholipase A(2)-paradigm. Chem Rev *101*, 2613-2654.

Bohlen, C.J., Priel, A., Zhou, S., King, D., Siemens, J., and Julius, D. (2010). A bivalent tarantula toxin activates the capsaicin receptor, TRPV1, by targeting the outer pore domain. Cell *141*, 834-845.

Caterina, M.J., Leffler, A., Malmberg, A.B., Martin, W.J., Trafton, J., Petersen-Zeitz, K.R., Koltzenburg, M., Basbaum, A.I., and Julius, D. (2000). Impaired nociception and pain sensation in mice lacking the capsaicin receptor. Science *288*, 306-313.

Cavanaugh, D.J., Lee, H., Lo, L., Shields, S.D., Zylka, M.J., Basbaum, A.I., and Anderson, D.J. (2009). Distinct subsets of unmyelinated primary sensory fibers mediate behavioral responses to noxious thermal and mechanical stimuli. Proceedings of the National Academy of Sciences of the United States of America *106*, 9075-9080.

Chahl, L.A., and Kirk, E.J. (1975). Toxins which produce pain. Pain *1*, 3-49.

Chen, X., Kalbacher, H., and Grunder, S. (2006). Interaction of acid-sensing ion channel (ASIC) 1 with the tarantula toxin psalmotoxin 1 is state dependent. J Gen Physiol *127*, 267-276.

Deval, E., Gasull, X., Noel, J., Salinas, M., Baron, A., Diochot, S., and Lingueglia, E. (2010). Acid-sensing ion channels (ASICs): pharmacology and implication in pain. Pharmacol Ther *128*, 549-558.

Doley, R., and Kini, R.M. (2009). Protein complexes in snake venom. Cell Mol Life Sci *66*, 2851-2871.

Escoubas, P., De Weille, J.R., Lecoq, A., Diochot, S., Waldmann, R., Champigny, G., Moinier, D., Menez, A., and Lazdunski, M. (2000). Isolation of a tarantula toxin specific for a class of proton-gated Na+ channels. J Biol Chem *275*, 25116-25121.

Fry, B.G., Roelants, K., Champagne, D.E., Scheib, H., Tyndall, J.D., King, G.F., Nevalainen, T.J., Norman, J.A., Lewis, R.J., Norton, R.S.*, et al.* (2009). The toxicogenomic multiverse: convergent recruitment of proteins into animal venoms. Annu Rev Genomics Hum Genet *10*, 483-511.

Jacobson, M.P., Pincus, D.L., Rapp, C.S., Day, T.J., Honig, B., Shaw, D.E., and Friesner, R.A. (2004). A hierarchical approach to all-atom protein loop prediction. Proteins *55*, 351-367.

Leffler, A., Monter, B., and Koltzenburg, M. (2006). The role of the capsaicin receptor TRPV1 and acid-sensing ion channels (ASICS) in proton sensitivity of subpopulations of primary nociceptive neurons in rats and mice. Neuroscience *139*, 699-709.

Mebs, D. (2002). Venomous and poisonous animals : a handbook for biologists, and toxicologists and toxinologists, Physicians and pharmacists (Boca Raton, Fla., CRC Press).

Morgan, D.L., Borys, D.J., Stanford, R., Kjar, D., and Tobleman, W. (2007). Texas coral snake (Micrurus tener) bites. South Med J *100*, 152-156.

Nishioka, S.A., Silveira, P.V., and Menzes, L.B. (1993). Coral snake bite and severe local pain. Ann Trop Med Parasitol *87*, 429-431.

Poirot, O., Berta, T., Decosterd, I., and Kellenberger, S. (2006). Distinct ASIC currents are expressed in rat putative nociceptors and are modulated by nerve injury. J Physiol *576*, 215-234.

Price, M.P., McIlwrath, S.L., Xie, J., Cheng, C., Qiao, J., Tarr, D.E., Sluka, K.A., Brennan, T.J., Lewin, G.R., and Welsh, M.J. (2001). The DRASIC cation channel contributes to the detection of cutaneous touch and acid stimuli in mice. Neuron *32*, 1071-1083.

Schmidt, J.O. (1982). Biochemistry of insect venoms. Annu Rev Entomol *27*, 339-368.

Siemens, J., Zhou, S., Piskorowski, R., Nikai, T., Lumpkin, E.A., Basbaum, A.I., King, D., and Julius, D. (2006). Spider toxins activate the capsaicin receptor to produce inflammatory pain. Nature *444*, 208-212.

St Pierre, L., Birrell, G.W., Earl, S.T., Wallis, T.P., Gorman, J.J., de Jersey, J., Masci, P.P., and Lavin, M.F. (2007). Diversity of toxic components from the venom of the evolutionarily distinct black whip snake, Demansia vestigiata. J Proteome Res *6*, 3093-3107.

Sutherland, S.P., Benson, C.J., Adelman, J.P., and McCleskey, E.W. (2001). Acid-sensing ion channel 3 matches the acid-gated current in cardiac ischemia-sensing neurons. Proceedings of the National Academy of Sciences of the United States of America *98*, 711-716.

Terlau, H., and Olivera, B.M. (2004). Conus venoms: a rich source of novel ion channel-targeted peptides. Physiol Rev *84*, 41-68.

Waldmann, R., Bassilana, F., de Weille, J., Champigny, G., Heurteaux, C., and Lazdunski, M. (1997a). Molecular cloning of a non-inactivating proton-gated Na+ channel specific for sensory neurons. J Biol Chem *272*, 20975-20978.

Waldmann, R., Champigny, G., Bassilana, F., Heurteaux, C., and Lazdunski, M. (1997b). A proton-gated cation channel involved in acid-sensing. Nature *386*, 173-177.

Wemmie, J.A., Chen, J., Askwith, C.C., Hruska-Hageman, A.M., Price, M.P., Nolan, B.C., Yoder, P.G., Lamani, E., Hoshi, T., Freeman, J.H., Jr.*, et al.* (2002). The acid-

activated ion channel ASIC contributes to synaptic plasticity, learning, and memory. Neuron *34*, 463-477.

Wemmie, J.A., Price, M.P., and Welsh, M.J. (2006). Acid-sensing ion channels: advances, questions and therapeutic opportunities. Trends Neurosci *29*, 578-586.

Wu, L.J., Duan, B., Mei, Y.D., Gao, J., Chen, J.G., Zhuo, M., Xu, L., Wu, M., and Xu, T.L. (2004). Characterization of acid-sensing ion channels in dorsal horn neurons of rat spinal cord. J Biol Chem *279*, 43716-43724.

Yu, Y., Chen, Z., Li, W.G., Cao, H., Feng, E.G., Yu, F., Liu, H., Jiang, H., and Xu, T.L. (2010). A nonproton ligand sensor in the acid-sensing ion channel. Neuron *68*, 61-72.

Ziemann, A.E., Allen, J.E., Dahdaleh, N.S., Drebot, II, Coryell, M.W., Wunsch, A.M., Lynch, C.M., Faraci, F.M., Howard, M.A., 3rd, Welsh, M.J.*, et al.* (2009). The amygdala is a chemosensor that detects carbon dioxide and acidosis to elicit fear behavior. Cell *139*, 1012-1021.

Publishing Agreement

It is the policy of the University to encourage the distribution of all theses, dissertations, and manuscripts. Copies of all UCSF theses, dissertations, and manuscripts will be routed to the library via the Graduate Division. The library will make all theses, dissertations, and manuscripts accessible to the public and will preserve these to the best of their abilities, in perpetuity.

Please sign the following statement:

I hereby grant permission to the Graduate Division of the University of California, San Francisco to release copies of my thesis, dissertation, or manuscript to the Campus Library to provide access and preservation, in whole or in part, in perpetuity.

Author Signature

1-17-2012

Date